

Diplomarbeit in Physik

**Discovery potential of  
MSUGRA-Supersymmetry in the  
 $\mu$ +Jet+MET channel at CMS**

Holger Pieta

September 15, 2008

Prof. Dr. Thomas Hebbeker  
III. Physikalisches Institut A  
Fakultät für Mathematik, Informatik und Naturwissenschaften  
Rheinisch-Westfälische Technische Hochschule Aachen



# Abstract

In this thesis a study is presented, investigating the discovery potential for supersymmetry in the  $\mu$ +jets+ $\cancel{E}_T$  channel during the early data taking of the CMS detector at LHC.

Supersymmetry predicts a new particle for each one present in the standard model, differing in spin by half a unit. As these supersymmetric particles, called *sparticles*, have not been observed so far, this symmetry must be broken and the masses of the new particles must be higher than their standard model counterparts. Assuming the unification of masses and couplings at very high energies and the involvement of gravity in the breaking mechanism, *minimal supergravity* makes strong predictions about the mass spectrum, production mechanisms and decay channels of the sparticles. For most regions of the allowed parameter space, it predicts a decay of sparticles via a cascade to lighter particles, hence multiple jets and leptons are expected. Assuming conserved R-parity, at the end of the cascade a stable heavy particle, usually assumed to be the lightest neutralino, will escape undetected, resulting in large missing energy. The potential of separating such events from the standard model background in the CMS detector has been evaluated using the full detector simulation, taking into account the effects of systematic uncertainties. The separation has been carried out both by conventional rectangular cuts as well as using the multivariate analysis technique *Boosted Decision Trees* (BDTs).

Some regions in the parameter space just beyond the existing limits from TEVATRON and LEP are shown to be observable within  $100 \text{ pb}^{-1}$  of integrated luminosity. Larger regions further away from existing limits are reachable within  $1 \text{ fb}^{-1}$ . Regions with high sparticle masses generally need more integrated luminosity or better controlled systematics to be observed. The use of BDTs increases the discovery mass range, however they require strictly controlled systematic uncertainties.



# Contents

|   |            |
|---|------------|
| <b>Abstract</b>   | <b>iii</b> |
| <b>1 Introduction</b>                                     | <b>1</b>   |
| <b>2 Theoretical foundations</b>                          | <b>3</b>   |
| 2.1 The Standard Model . . . . .                          | 3          |
| 2.1.1 Local gauge theories . . . . .                      | 4          |
| 2.1.2 Quantum chromodynamics . . . . .                    | 5          |
| 2.1.3 Electroweak interactions in the GSW-Model . . . . . | 6          |
| 2.1.4 Higgs boson . . . . .                               | 7          |
| 2.2 Beyond the Standard Model . . . . .                   | 7          |
| 2.2.1 Deficits of the standard model . . . . .            | 7          |
| 2.2.2 Supersymmetry - Introduction . . . . .              | 9          |
| 2.2.3 New particles . . . . .                             | 10         |
| 2.2.4 Solving problems . . . . .                          | 11         |
| 2.2.5 Symmetry breaking . . . . .                         | 11         |
| 2.2.6 Supergravity . . . . .                              | 12         |
| 2.2.7 Phenomenology . . . . .                             | 13         |
| 2.2.8 Benchmark points . . . . .                          | 14         |
| 2.2.9 Previous searches . . . . .                         | 16         |
| <b>3 Experimental setup</b>                               | <b>17</b>  |
| 3.1 The Large Hadron Collider (LHC) . . . . .             | 17         |
| 3.1.1 Collider physics . . . . .                          | 17         |
| 3.1.2 LHC design . . . . .                                | 18         |
| 3.2 The Compact Muon Solenoid (CMS) . . . . .             | 21         |
| 3.2.1 The inner tracker . . . . .                         | 22         |
| 3.2.2 Calorimeter . . . . .                               | 24         |
| 3.2.3 Solenoid . . . . .                                  | 27         |
| 3.2.4 Muon system . . . . .                               | 28         |
| 3.2.5 Trigger . . . . .                                   | 32         |
| 3.2.6 Luminosity monitoring . . . . .                     | 33         |
| 3.3 Computing on the Grid . . . . .                       | 33         |
| 3.4 Reconstruction . . . . .                              | 34         |
| 3.4.1 Muons . . . . .                                     | 34         |
| 3.4.2 Jets and missing transverse energy . . . . .        | 35         |
| <b>4 Analyses</b>   | <b>37</b>  |
| 4.1 Common aspects . . . . .                              | 37         |
| 4.1.1 Monte Carlo samples . . . . .                       | 37         |
| 4.1.2 Systematic uncertainties . . . . .                  | 39         |
| 4.1.3 Statistical interpretation . . . . .                | 40         |

|          |   |           |
|----------|---|-----------|
| 4.1.4    | Preselection . . . . .  | 42        |
| 4.2      | Conventional Analysis: Rectangular cuts . . . . .               | 46        |
| 4.2.1    | Optimization strategy . . . . .                                 | 46        |
| 4.2.2    | Results . . . . .   | 48        |
| 4.3      | Boosted decision trees . . . . .                                | 55        |
| 4.3.1    | Training . . . . .  | 56        |
| 4.3.2    | Boosting . . . . .  | 57        |
| 4.3.3    | Pruning . . . . .   | 58        |
| 4.3.4    | Workflow . . . . .  | 58        |
| 4.3.5    | Results . . . . .   | 59        |
| 4.4      | Comparison of analysis techniques . . . . .                     | 62        |
| 4.4.1    | Study without systematic uncertainties . . . . .                | 62        |
| <b>5</b> | <b>Conclusion</b>   | <b>65</b> |
| <b>A</b> | <b>Preselection distributions</b>                               | <b>67</b> |
| <b>B</b> | <b>BDT Response distributions</b>                               | <b>71</b> |
| <b>C</b> | <b>Expected events and significances for BDT based analysis</b> | <b>75</b> |
| <b>D</b> | <b>Parameters of low mass benchmark points</b>                  | <b>85</b> |
| <b>E</b> | <b>Background samples</b>                                       | <b>87</b> |
|          | <b>Bibliography</b>   | <b>91</b> |

# 1 Introduction

Curiosity is one of mankind's main driving force, urging him to poke around in everything he can get his hands on. To really understand a complex system's inner workings, it soon proved to be helpful to understand every single ingredient of it. Closely examining a small part of complex system usually exposes it to be a complex system itself, again containing many interacting components. Even the ancient Greeks suspected matter to be constructed from tiny particles, which they called atoms, meaning indivisible. However it took some thousand years to the first direct experimental observation of these atoms. And soon after, the atoms itself again showed to possess a substructure. Following this path deeper and deeper finally revealed the elementary particles, which we at the moment assume to be indivisible. While there are no experimental hints to further substructures, some theories predict them. Each step further down proved to be a step closer to a general understanding, as the number of fundamental particles decreased every time.

To our current knowledge twelve elementary fermionic particles constitute matter. Between these particles four fundamental forces are known to interact via mediating bosonic particles: Gravity, weak, electromagnetic and strong. All but gravity can be described by gauge theories, all together called the *standard model*. The gauge groups of this model reflect fundamental degrees of freedom and symmetries. Identifying these underlying symmetries and incorporating them in the theories allows to develop a model of great predictive power, nevertheless there is a huge number of free parameters left, which have to be determined by measurements. The standard model is hence commonly regarded as an *effective theory*, which describes the universe, but does not explain it. Moreover there are some puzzling inconsistencies, e.g. the origin of the boson masses. Many of these problems can be solved by extending the standard model by new particles. For example the boson masses can be explained via the Higgs-mechanism, which also predicts a new boson. A number of inconsistencies can be solved by not only adding one new particle, but actually more than doubling the number of particles. As these new particles add a fermion-boson symmetry to the standard model, the new model is commonly called *supersymmetry*.

The Higgs boson is experimentally limited to not be heavier than a few hundred GeV. The supersymmetric particles are usually expected, albeit this is not necessary, to be lighter than about 1 TeV. All these new particles, especially the Higgs boson, are the main motivation to study the high center of mass energies, which will be reachable at the LHC.

As the supersymmetric particles have not been observed so far, the symmetry must be broken and the supersymmetric particles must be heavier than their standard model counterparts. Broken supersymmetry adds a huge number of new free parameters, however they can be reduced by making certain assumptions like coupling unification at very high energies. Accomplished by a breaking mechanism, which includes gravity, this restricted model is called *minimal supergravity* (mSUGRA). If R-parity is conserved, supersymmetric particles can only be produced and annihilated in pairs. This leads to a stable lightest supersymmetric particle (LSP). As this particle is still rather heavy, it is a good candidate for cold dark matter and leads to a distinctive signature in the detector: It escapes undetected and hence shows as a large missing energy. Since the rest frame along the

beam axis is not known at a hadron collider, only the missing transverse energy (MET or  $\cancel{E}_T$ ) can be used. Produced supersymmetric quarks and gluons usually decay via a cascade of lighter particles, which results in many leptons and jets.

In this study the potential of one of the LHC experiments, the Compact Muon Solenoid (CMS), to observe these events is evaluated. As this detector is optimized to detect muons, which are also easy to identify, the channel  $\mu$ +jets+MET is used. This study has been performed using the full detector simulation and incorporating the most important backgrounds and systematic uncertainties.

After an introduction to the standard model in the first chapter, supersymmetry is described. Its fundamental characteristics and phenomenological traits are shown in the second part of this chapter. Since this study relies on the simulation of the detector, the second chapter introduces the experimental setup, hence mainly LHC and CMS. In the last chapter, two analyses are described and compared, one using conventional rectangular cuts and one relying on a multivariate analysis system: Boosted decision trees.



## 2 Theoretical foundations

### 2.1 The Standard Model

After decades of ample research, the knowledge about elementary particles and their interactions finally converged into one model of our universe. Brought into existence in the early 1970s, mostly by Glashow, Salam and Weinberg, it has been challenged and tested thoroughly and yet remains compatible with all experimental data, hence we speak of the *Standard Model of electroweak interaction* [1, 2, 3]. Extended to describe the strong force, it is most referred to as the *Standard Model*.

Following the ideas of a quantum field theory, it describes most observable phenomena as a function of fields spread over space. Some states of these fields, commonly known as *matter*, act as point-like spin-1/2 particles, called *fermions* (see Table 2.1). These particles are called point-like, as they are not built from other particles, thus do not possess a substructure.

The *Quarks*, to be recognized by a non-integer charge, cannot be found alone, only in groups of at least two, called *hadrons*. Groups of two are called *mesons*, groups of three *baryons*. Two groups of three quarks are widely known: *uud*, called *Proton*, and *udd*, called *Neutron*. All other combinations form a widespread zoo of particles, which are formed in processes of sufficiently high energy and will decay after a short time.

The remaining six fermions, called *leptons*, form two groups of different character: First the charged ones, of which only one is found in everyday matter, the *electron*; the two others will decay. Three uncharged particles are known as *Neutrinos*, which are able to pass most matter with hardly any interaction and possess the surprising trait to be able to transform into each other, which is called *mixing*. This mixing has also been observed for quarks.

There are four kinds of interactions between those particles: Gravitational, weak, electromagnetic and strong. Only gravitation affects them all, but is of so low strength, it can be neglected in most matters of particle physics. To be affected by the electromagnetic force, particles need to carry a charge; for strong interactions a color charge is needed. The weak interaction affects all fermions, except for right handed neutrinos. On higher

|                      | Family | 1               | 2                | 3                |
|----------------------|--------|-----------------|------------------|------------------|
| up-type<br>Quarks    | Name   | Up (u)          | Charm (c)        | Top (t)          |
|                      | Mass   | $\approx 2$ MeV | 1.25 GeV         | 172.5 GeV        |
| down-type<br>Quarks  | Name   | Down (d)        | Strange (s)      | Bottom (b)       |
|                      | Mass   | $\approx 5$ MeV | $\approx 95$ MeV | 4.2 GeV          |
| charged<br>Leptons   | Name   | Electron (e)    | Muon ( $\mu$ )   | Tau ( $\tau$ )   |
|                      | Mass   | 511 MeV         | 106 MeV          | 1.78 GeV         |
| uncharged<br>Leptons | Name   | e-Neutrino      | $\mu$ -Neutrino  | $\tau$ -Neutrino |
|                      | Mass   | $< 2$ eV        | $< 2$ eV         | $< 2$ eV         |

**Table 2.1:** *Fermions in the Standard Model*

| Force           | Relative strength | Range [m]  | Carrier             |
|-----------------|-------------------|------------|---------------------|
| Gravity         | $10^{-40}$        | $\infty$   | Graviton            |
| Weak force      | $10^{-2}$         | $10^{-13}$ | $W^\pm, Z^0$        |
| Electromagnetic | $10^{-2}$         | $\infty$   | Photon ( $\gamma$ ) |
| Strong force    | 1                 | $10^{-15}$ | 8 Gluons            |

**Table 2.2:** Range and strength of fundamental forces and their carriers.

energy scales electromagnetic and weak interaction can be unified to the *electroweak* interaction. While strong and weak interactions are limited to very small distances, gravity and electromagnetic force are carried over unlimited distances (see Table 2.2). The forces, except for gravity, can be described by local gauge theories, wherein the interactions are mediated by *gauge bosons*, fundamental spin-1 particles. Gravity may be mediated by a spin-2 boson, the *graviton*, but there have been no direct observations of this particle.

All four interactions are encountered in everyday life:

- The strong force binds quarks to nucleons and nucleons to nuclei.
- The electromagnetic force binds electrons to nuclei, thus forming atoms; it also forms atoms to molecules and macroscopic bodies.
- The weak force is responsible for radioactive decays, i.e.  $\beta$ -decay.
- The gravitation clusters matter to planets, stars, galaxies,...

The structure of weak interactions suggests the pairing of one charged lepton and one neutrino into a family. Likewise two quarks are paired into one family. Each of these families possesses a separate, additive quantum number, which is however violation by mixing. While the fermion masses are used as free parameters in the standard model, the introducing of mass terms for the bosons violates gauge invariance. This is no problem for the massless photon and gluon, but W and Z-bosons do possess a mass. One solution to this dilemma is the 'Higgs-mechanism', which introduces a new fundamental spin-0 particle. The discovery of the Higgs-boson is one of the main goals of the LHC.

### 2.1.1 Local gauge theories

In the standard model, fundamental particles are described by space and time dependent fields  $\Psi(x)$ , where  $x$  denotes both space and time.

Many considerations in physics are based on symmetries. For example: The outcome of an experiment should not change, if its location in space or time is varied. Mathematically speaking: The equations of motion should not change under certain unitary transformations. A transformation is unitary, if the adjoint operator  $U^\dagger$  of a transformation  $U$  equals the inverse operator  $U^{-1}$ .

In Quantum electrodynamics (QED) the consideration of global symmetry introduces charges and currents, but the forces are still missing. One way to add forces is making the symmetry local. The transformation

$$\Psi(x) \rightarrow \Psi'(x) = U\Psi(x) \quad (2.1)$$

must then become a function of space and time, thus

$$\Psi(x) \rightarrow \Psi'(x) = U(x)\Psi(x) \quad (2.2)$$

To keep the above Lagrangian invariant under local transformations, an additional vector field  $A_\mu(x)$  must be introduced. The fields will then transform like

$$\Psi \rightarrow \Psi' = e^{i\alpha\chi(x)}\Psi, \quad A_\mu \rightarrow A'_\mu = A_\mu - \partial_\mu\chi(x) \quad (2.3)$$

With an arbitrary constant  $\alpha$  and a scalar, space-time dependent function  $\chi(x)$ . These additional vector fields will manifest as spin 1 bosons, which is the photon for QED.

These transformations can be collected in *symmetry groups*. The symmetry group

$$SU(3)_C \times SU(2)_L \times U(1)_Y \quad (2.4)$$

describes strong and electroweak interactions in the standard model. In  $SU(2)_L \times U(1)_Y$  the electromagnetic and weak force are combined to one *electroweak* interaction.

### 2.1.2 Quantum chromodynamics

Building mesons and baryons from sets of quarks is a good explanation for their large variety, but there is a problem. The  $\Delta^{++}$  resonance is the lightest spin 3/2 particle, thus may contain three up quarks in equal spin state:  $|\Delta^{++}\rangle = |uuu\rangle |\uparrow\uparrow\uparrow\rangle$ . These three bound fermions must then be in the same state, thus will violate the Pauli-principle. To solve this problem, an additional quantum number is introduced, which needs at least three different states: The color. The three states are then called *Red* (R), *Green* (G) and *Blue* (B). As this additional degree of freedom is not observed in hadrons, they must be color-singlets, thus the colors of the quarks must add up to *white*; either by color plus anticolor or by the sum of all colors. If (anti-)quarks carry (anti-)color, the two simplest allowed combinations are:  $|q\bar{q}\rangle$  and  $|qqq\rangle$ . In particular, single quarks cannot be observed as free particles.

Assuming a process generates either lepton or quark pairs. The relative probability for both cases depends to the number of lepton and quark states. As the number of quark states is proportional to the number of different colors a quark can carry, one can measure the number of colors. Experimental evidence restrict this number to three [4]. With three colors, the system can be described by the gauge group  $SU(3)_C$ . If one looks at the color as a conserved charge, which is the source of a field with the gluons as its quanta, the strong interaction can be described in a local gauge theory (Discovered by Gross and Wilczek in 1973). To keep the equations of motion invariant under the eight rotating transformations of  $SU(3)_C$ , eight additional vector fields  $G_j^\mu$  have to be introduced, whose particles are the eight colored gluons.

At the PETRA collider first evidence for gluons was found in three jet events in 1979 [5], as a radiated massless gluon manifests itself as an additional jet.

Gluons interacting with a quark may flip its spin as well as change its color, thus the gluons must carry a spin and they must carry color. But, as a colored particle, the gluons itself will then be affected by the strong force. This results in a increasing strong coupling constant  $\alpha_S$  with increasing distance. In contrast, coupling constants of the electroweak interaction decrease with increasing distance. This explains first the *asymptotic freedom*, quarks behave like free particles on small distances, and second the *confinement*: During the separation of two colored particles, the number and interactions of the gluons binding both particles will increase, storing more and more energy. Eventually the energy will be high enough to generate additional colored particles. The initial and the additional particles will form colorless hadrons, so that there are no free colored particles and no additional interactions.

| Particle | Charge | Weak isospin |       | Weak hypercharge |
|----------|--------|--------------|-------|------------------|
|          | $Q$    | $T$          | $T_3$ | $Y$              |
| $\nu_L$  | 0      | 1/2          | 1/2   | -1/2             |
| $\nu_R$  | 0      | 0            | 0     | 0                |
| $l_L$    | -1     | 1/2          | -1/2  | -1/2             |
| $l_R$    | -1     | 0            | 0     | -1               |
| $q_L^u$  | 2/3    | 1/2          | 1/2   | 1/6              |
| $q_L^d$  | -1/3   | 1/2          | -1/2  | 1/6              |
| $q_R^u$  | 2/3    | 0            | 0     | 2/3              |
| $q_R^d$  | -1/3   | 0            | 0     | -1/3             |

**Table 2.3:** Charge, isospin and hypercharge of fermions

### 2.1.3 Electroweak interactions in the GSW-Model

The gauge group  $U(1)$  is not sufficient to describe conversions of charged to uncharged leptons, which will be the case, if a W boson is part of the interaction. The next complex gauge group  $SU(2)$  is able to do this, but will for itself describe only massless bosons. Even if there was no direct observation of the mass of the W and the Z-boson, there would be a good reason for massive bosons: The short range of the weak force.

Introducing an additional scalar field with a non-zero ground state will lead to a spontaneously broken symmetry. This leads to the three gauge bosons acquiring mass via the *Higgs-mechanism*. Gauge bosons in  $SU(2)$  groups couple to weak isospin, thus we can assign left-handed fermions to doublets, weak isospin 1/2, and right-handed fermions to singlets, weak isospin 0, see Table 2.3. So these bosons will couple only to left-handed and not to right-handed fermions, which is observed in experiments with W-bosons. Two of these three gauge bosons,  $W_{1,2}$ , can be linearly combined to the  $W^\pm$ -bosons:

$$W^\pm = \frac{1}{\sqrt{2}}(W_1 \mp iW_2) \quad (2.5)$$

For the third,  $W_3$ , it is not that simple: On the one hand it possess a mass, acquired via the Higgs-mechanism, so it can not be the photon; on the other hand it couples only to left-handed fermions, but the Z-boson couples to all fermions.

In the sixties Glashow, Weinberg and Salam<sup>1</sup> [1, 2, 3] introduced an additional  $U(1)$  gauge symmetry, thus the model  $SU(2) \times U(1)$  acquires a new massless boson: the  $B$ . This boson couples to particles carrying the *weak hypercharge*  $Y$ ; The electromagnetic charge is  $Q = T_3 + Y$ . Linear combinations of  $B$  and  $W^3$  show the observed features of the  $\gamma$  and the Z-boson:

$$\gamma = \cos\Theta_W \cdot B + \sin\Theta_W \cdot W^3 \quad (2.6)$$

$$Z = -\sin\Theta_W \cdot B + \cos\Theta_W \cdot W^3 \quad (2.7)$$

The angle  $\Theta_W$  is called *weak mixing angle* or *Weinberg angle*. It does not only determine the boson mixing, but shows up also in the mass terms  $m_W = m_Z \cos \Theta_W$  and the coupling constants  $g$  and  $g'$ :

$$\cos \Theta_W = \frac{g}{\sqrt{g^2 + g'^2}}, \quad \sin \Theta_W = \frac{g'}{\sqrt{g^2 + g'^2}} \quad (2.8)$$

---

<sup>1</sup>hence the name *GSW-model*

with  $g = e/\sin \Theta_W$ . Here  $g$  is the coupling constant for  $SU(2)$  and  $g'$  for  $U(1)$ . As the two gauge groups are independent, the coupling constants may (and, as seen in the above equations, actually do) differ.

### 2.1.4 Higgs boson

Adding four additional scalar fields  $\phi_i$  will in the end lead to massive gauge bosons and fermions. Three of the four new fields are absorbed by the boson masses, leaving one which shows as a new particle, the Higgs-boson. The Higgs has not been observed so far, but especially at LEP [6, 7] upper and lower limits have been determined:

$$114 \text{ GeV} \leq m_H \leq 196 \text{ GeV} \quad (2.9)$$

## 2.2 Beyond the Standard Model

The Standard Model is rather successful in describing physics at moderate energy scales. Nevertheless it poses some open questions on higher energy scales and for more complex systems, like the universe itself.

One major problem is the still missing explanation for *dark matter*: Measurements show a vast difference between the amount of visible matter in the universe and the amount of matter needed to explain observed gravitational effects (see eg. [8]).

Additionally, calculations of the  $W_L W_L$  scattering amplitude show a violation of the unitarity bound at center of mass energies of around 1.7 TeV. The Higgs mechanism provides a solution for this problem, but only if the Higgs boson is lighter than about 1 TeV [9]. Otherwise something else must happen, i.e. new gauge bosons with masses of below 1 TeV have to contribute.

As shown in Fig. 2.1(a) the high energy extrapolations of the three coupling constants of the standard model will *not* meet at one point. While there is no a priori reason for them to meet, it would be a sign for a unified underlying theory explaining all interactions. Such theories are called *Grand Unified Theories* (GUT).

While there are many symmetries in the standard model, one very interesting is missing: The bosonic force carriers and the fermionic matter particles do not form a converging boson-fermion-symmetry. Without this symmetry a *fine tuning* or *hierarchy problem* occurs. Detailed descriptions and calculations regarding these topics can be found in [10].

### 2.2.1 Deficits of the standard model

#### Cold dark matter

Measurements of the orbital speed of stars in galaxies can only be explained, if most matter of the galaxies is located outside the central bulge. As this matter does not emit light, it is called 'Dark matter'. This dark matter must be cold, thus moving with non-relativistic speed, otherwise structure formation in the early universe cannot be explained.

Measurements by the Wilkinson Microwave Anisotropy Probe (WMAP)[11] show only around 4% of the total energy density of the universe to be ordinary baryonic matter. Another 23% is *dark matter*; the rest is energy, most of it *dark energy*.

One way to explain this dark matter is by introducing a stable, uncharged and only weakly interacting massive particle (a *WIMP*).

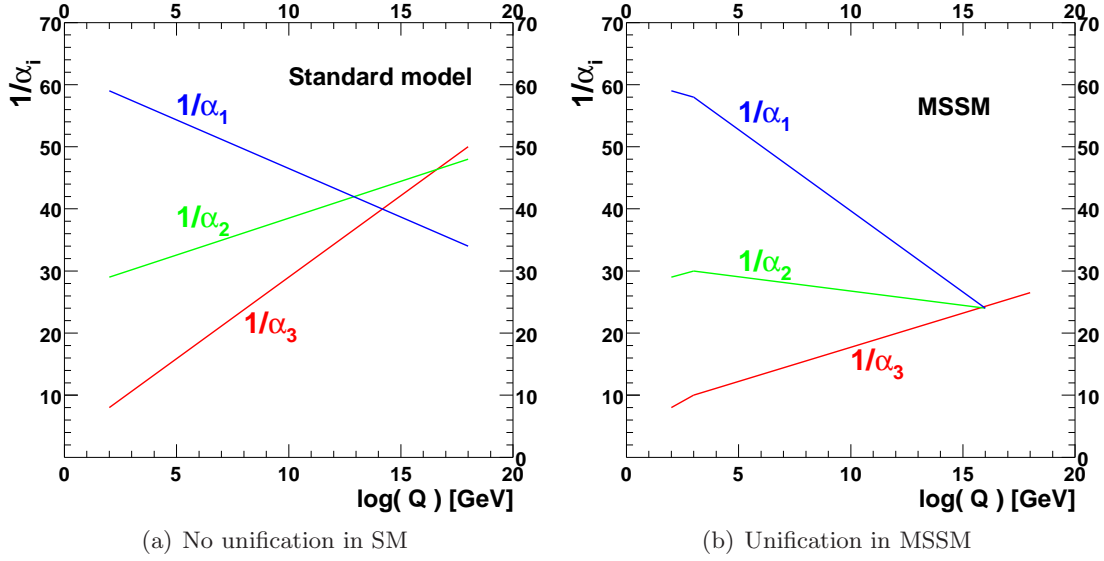


**Figure 2.1:** Unification of coupling constants: There is no point in SM, where all three constants meet. In MSSM unification can be reached. The plots are adapted from [12]

### Gauge coupling unification

Around a charge, even in vacuum, a polarization cloud will form. The higher the momentum transfer during an interaction, the deeper the cloud will be probed, lessening its effect. Thus the coupling constant  $\alpha_i$  depends on the momentum transfer  $Q^2$ :

$$\frac{1}{\alpha_i(Q^2)} = \frac{1}{\alpha_i(Q_0^2)} + \frac{b_i}{2\pi} \log \frac{Q^2}{Q_0^2} \quad (2.10)$$

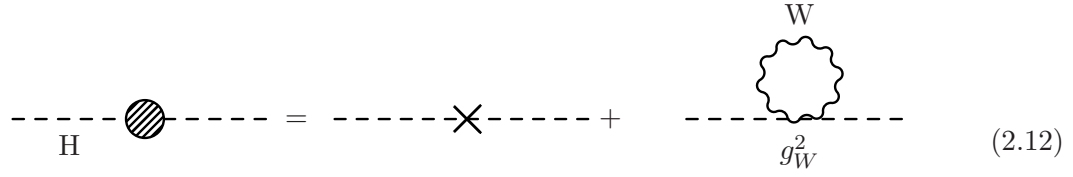
The parameter  $b_i$  is determined by the processes generating the polarization, here for the standard model [10]:

$$\begin{aligned} b_1 &= 0 - \frac{4}{3}N_F - \frac{1}{10}N_H \\ b_2 &= \frac{22}{3} - \frac{4}{3}N_F - \frac{1}{6}N_H \\ b_3 &= 11 - \frac{4}{3}N_F + 0 \end{aligned} \quad (2.11)$$

with the number of families  $N_F$  and the number of Higgs multiplets  $N_H = 1$  in the standard model. As shown in Fig. 2.1(a), the  $\alpha_i$  will not meet in one point. If additional interacting particles with the right attributes are added, the running coupling constants will get a kink at the energy scale defined by the new particle's masses, because then there will be more processes. Properly chosen values for the masses and other parameters will cause all coupling constants to meet at one point, as shown in Fig. 2.1(b).

### Hierarchy problem

As one can see in equation 2.12, the measurable Higgs mass  $m_H$  has two contributions: The fundamental mass parameter  $m_0$  and radiative boson corrections, in this example the W:  $\delta m_W^2$ .



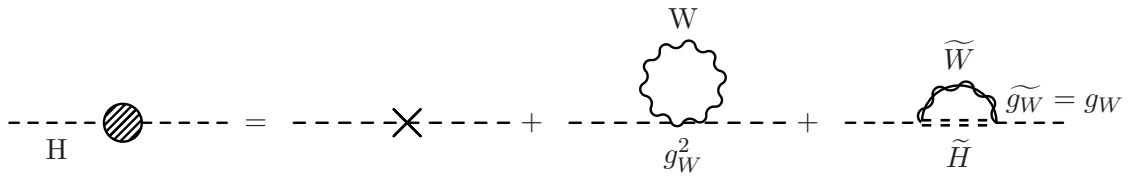
$$\begin{array}{c}
 \text{--- H ---} \text{ (with a shaded circle loop)} \text{ ---} = \text{---} \text{ (with an X)} \text{ ---} + \text{---} \text{ (with a W loop)} \text{ ---} \\
 m_H^2 = m_0^2 + \delta m_W^2
 \end{array} \quad (2.12)$$

The corrections depend on the scale  $\Lambda$  and the boson mass:

$$\delta m_W^2 \approx -g_W^2 \int_0^\Lambda \frac{d^4 k}{k^2} \approx -g_W^2 (\Lambda^2 + m_W^2) \quad (2.13)$$

Using the Planck scale, thus  $\Lambda \approx M_{Pl}$ , one gets a correction of the order of  $10^{36} \text{ GeV}^2$ . Thus the mass parameter must be of the same order of magnitude to cancel this effect. To get a Higgs mass of the order of 100 GeV, this cancelation must be accurate for 32 orders of magnitude, which is highly unlikely.

If there were fermions with roughly the same characteristics as the bosons, additional fermionic loops would be added:



$$\begin{array}{c}
 \text{--- H ---} \text{ (with a shaded circle loop)} \text{ ---} = \text{---} \text{ (with an X)} \text{ ---} + \text{---} \text{ (with a W loop)} \text{ ---} + \text{---} \text{ (with a fermion loop)} \text{ ---} \\
 m_H^2 = m_0^2 + \delta m_W^2 + \delta m_{\widetilde{W}}^2
 \end{array} \quad (2.14)$$

These loops will stabilize the value of  $m_H$ , as they introduce an opposite sign:

$$\delta m_{\widetilde{W}}^2 \approx +\widetilde{g}_W^2 \int \frac{d^3 k}{k^2} \approx +\widetilde{g}_W^2 (\Lambda^2 + m_{\widetilde{W}}^2) \quad (2.15)$$

Of course this will only work, if  $g_W^2 \approx \widetilde{g}_W^2$  and  $m_{\widetilde{W}}$  of the same order of  $m_W$ . Otherwise some fine tuning is again necessary, which is known as the *little hierarchy problem*.

### 2.2.2 Supersymmetry - Introduction

Looking at the standard model particles, it is obvious that there is no symmetry between the bosonic force carriers and the fermionic matter particles. Thus one has to extend the standard model to construct this symmetry, by doubling the particle content. This idea came up first in the 1970ies [13]. For each standard model particle one new particle with exactly the same attributes is added, only the spin has to be changed by 1/2 unit. Mathematically speaking, there is an operator  $Q$ , which transforms fermions to bosons and vice versa:

$$Q|Fermion\rangle = |Boson\rangle \quad Q|Boson\rangle = |Fermion\rangle \quad (2.16)$$



| Standard model  | Supersymmetry  |
|---|--|
| Leptons: $\begin{pmatrix} e \\ \nu_e \end{pmatrix} \begin{pmatrix} \mu \\ \nu_\mu \end{pmatrix} \begin{pmatrix} \tau \\ \nu_\tau \end{pmatrix}$ | Sleptons: $\begin{pmatrix} \tilde{e} \\ \tilde{\nu}_e \end{pmatrix} \begin{pmatrix} \tilde{\mu} \\ \tilde{\nu}_\mu \end{pmatrix} \begin{pmatrix} \tilde{\tau} \\ \tilde{\nu}_\tau \end{pmatrix}$ |
| Quarks: $\begin{pmatrix} u \\ d' \end{pmatrix} \begin{pmatrix} c \\ s' \end{pmatrix} \begin{pmatrix} t \\ b' \end{pmatrix}$                     | Squarks: $\begin{pmatrix} \tilde{u} \\ \tilde{d}' \end{pmatrix} \begin{pmatrix} \tilde{c} \\ \tilde{s}' \end{pmatrix} \begin{pmatrix} \tilde{t} \\ \tilde{b}' \end{pmatrix}$                     |

Table 2.4: Fermions and sfermions

Such operators must be anticommuting spinors carrying spin 1/2, thus *supersymmetry* is a spacetime symmetry [10]. For a realistic theory involving chiral fermions, the Haag-Lopuszanski-Sohnius extension [14] of the Coleman-Mandula theorem [15] requires the following relations:

$$\begin{aligned} \{Q, Q^\dagger\} &= P^\mu \\ \{Q, Q\} &= \{Q^\dagger, Q^\dagger\} = 0 \\ [P^\mu, Q] &= [P^\mu, Q^\dagger] = 0 \end{aligned} \tag{2.17}$$

One aspect of this algebra are so called *supermultiplets*, in which the particle states are grouped. As  $Q$  and  $Q^\dagger$  commute with most symmetry transformations, all states in one supermultiplet possess equal masses and quantum numbers, with the exception of spin. Each of these supermultiplets contains equal numbers of bosonic and fermionic degrees of freedom.

### 2.2.3 New particles

The simplest supermultiplet contains one spin 1/2 fermion (resulting in two fermionic states) and two scalars. It is called *matter supermultiplet* (or *chiral multiplet*), as it contains the standard model matter fermions. The next simplest supermultiplet contains one spin 1 boson. Bosons in renormalizable theories are massless (at least before symmetry breaking), thus resulting in two states, too. The superpartner is then a massless spin 1/2 fermion. These supermultiplets are called *gauge multiplets*. Assuming a spin 2 graviton (also massless, thus only 2 states), one additional supermultiplet contains this particle and one spin 3/2 fermion. Finally there is one additional particle state (particles with spin  $> 0$  yield two states) for each state in the standard model, effectively doubling the number of particles. The Higgs boson, as a scalar, may belong to a chiral supermultiplet, but if one assumes only one of these, gauge anomalies in the electroweak gauge symmetry will occur. Additionally the supersymmetric Higgs-mechanism gives mass only to fermions in one spin state. To solve this problem, two chiral supermultiplets are required, resulting in eight degrees of freedom. Three of them are absorbed by the  $Z$  and  $W^\pm$  bosons, leaving five which will manifest as actual Higgs bosons.

Each fermion in the standard model is accompanied by a supersymmetric *sfermion*, called *squark*, *slepton*, *sneutrino*, *selectron*, *smuon*, *stau* and so on (see Table 2.4). The gauge boson counterparts are called *gauginos*. Actually not the well known  $\gamma$ ,  $Z^0$  or  $W^\pm$  bosons get a supersymmetric partner, but the fundamental bosons  $B$  and  $W^{1,2,3}$ , which are then called *binos* and *winos* and mix to the observable particles. Additionally the four supersymmetric *higgsinos* of the two Higgs supermultiplets will mix in, resulting in the *charginos* and *neutralinos* (see Table 2.5). The remaining four gauge eigenstates of the Higgs supermultiplets mix to the five observable Higgs particles. The eight gluon fields get one counterpart each, the *gluinos*.

Of course there may be even more supermultiplets realized by nature, but to keep things



|              |               | Electroweak (+Higgs)   | Strong                                    |
|--------------|---------------|--|---|
| Gauge bosons | fundamental   | $B, W^1, W^2, W^3$   | $g^1, \dots, g^8$                         |
|              | mix to called | $\underbrace{\gamma, Z^0, W^\pm}_{\text{gauge bosons}}$  | gluon                                     |
| Gauginos     | fundamental   | $\widetilde{B}, \widetilde{W}^3, \widetilde{H}_u^0, \widetilde{H}_d^0$   | $\widetilde{g}^1, \dots, \widetilde{g}^8$ |
|              | mix to called | $\underbrace{\widetilde{\chi}_{1,2,3,4}^0}_{\text{neutralinos}}$ $\underbrace{\widetilde{W}^{1,2}, \widetilde{H}_u^\pm, \widetilde{H}_d^\pm}_{\text{charginos}}$ | gluino                                    |

**Table 2.5:** Gauge bosons, gauginos and part of the Higgs sector

|             | Standard model | Supersymmetry   |
|-------------|----------------|---|
| fundamental | $H$            | $H_u^0, H_d^0, H_u^\pm, H_d^\pm$                          |
| mix to      |                | $\underbrace{h^0, H^0, A^0, H^\pm}_{\text{Higgs bosons}}$ |

**Table 2.6:** In the standard model four Higgs fields with one observable particle are sufficient; in the MMSM four additional fields are necessary, resulting in four more particles.

simple one usually restricts to the minimal number of supermultiplets for a coherent theory. This is then called *Minimal Supersymmetric Standard Model* (MSSM).

### 2.2.4 Solving problems

For all the above mentioned problems (cold dark matter, coupling unification, hierarchy problem) supersymmetry provides a solution. One may assign a new multiplicative quantum number, the *R-parity*, to each particle: +1 for particles and -1 for sparticles. If R-parity is conserved, sparticles can only be produced or annihilated in pairs. Thus the *lightest supersymmetric particle* (LSP) is stable and may be a good candidate for cold dark matter, as long as it is uncharged, only weakly interacting and massive (see section 2.2.5).

Equation 2.11 will change in the presence of new particles [10]:

$$\begin{aligned}
 b_1 &= 0 - 2N_F - \frac{3}{10}N_H \\
 b_2 &= 6 - 2N_F - \frac{1}{2}N_H \\
 b_3 &= 9 - 2N_F - 0
 \end{aligned} \tag{2.18}$$

with two supersymmetric Higgs doublets  $N_H = 2$ . Thus the evolution of the coupling constants will change, leading to one common point at high energies (see Fig. 2.1(b)). Above this energy, the couplings can not be separated.

Also, the fermionic supersymmetric gauge particles will do the job of the unknown fermions in equation 2.14, canceling the divergence and thus bringing the measurable Higgs mass and the fundamental Higgs mass parameter to one scale.

### 2.2.5 Symmetry breaking

Obviously supersymmetric theories have one serious drawback: No sparticle has been observed so far. Thus the symmetry must be broken, sparticle masses are not equal to the masses of their corresponding particles. The breaking is usually introduced by additional

terms in the Lagrangian, which parametrise the effects of a broken supersymmetry without actually explaining why it is broken. If this breaking is *hard*, i.e. all couplings and masses are to be freely chosen, the hierarchy problem will most likely reappear. Consequently the breaking must be *soft*: Couplings in broken and unbroken supersymmetry must be equal. Then the supersymmetric Lagrangian can be separated in two: One contains the gauge and Yukawa interactions, preserving supersymmetric invariance; the second contains the breaking terms.

$$\mathcal{L} = \mathcal{L}_{SUSY} + \mathcal{L}_{Soft} \quad (2.19)$$

These breaking terms may spoil the solution for the hierarchy problem, if the sparticle masses are too high. Detailed calculations restrict the sparticle masses to less than about 1TeV, otherwise fine tuning is again necessary.

In an unbroken supersymmetry all attributes are determined, thus there are no new free parameters besides the 19 of the standard model. Breaking will lead to more free parameters; in the MSSM there are 105 new parameters: eight in the gaugino-Higgsino sector, 21 masses, 36 mixing angles and 40 CP-violating phases in the squark-slepton sector [10]. Luckily most of these parameters are somewhat restricted by phenomenology and may be further restricted by additional assumptions (i.e. supergravity).

### 2.2.6 Supergravity

As shown in section 2.1.1, making a symmetry local introduces new forces. Similarly making supersymmetry local may add new forces. To make supersymmetry a local symmetry not just one but two new field must be introduced: First a field carrying spin 3/2: the *gravitino*. And secondly a spin 2 field: the *graviton*. While a globally broken supersymmetry leads to a massless goldstino, graviton and gravitino, in a locally broken supersymmetry, the gravitino absorbs the goldstino and thus acquires mass; much like the Higgs-mechanism in the standard model, thus often called *superHiggs-mechanism*.

Albeit the theory now includes gravity, it is still no full quantum theory of gravity, as it is still not renormalizable. One promising idea for a full quantum theory of gravity is *string theory*, but this is beyond the scope of this work.

To avoid gauge anomalies, the breaking must take place in a *hidden sector*. Its effect must then be transmitted to the visible sector. This can either be done by gauge forces or by gravity, which is called *Gauge mediated supersymmetry breaking* (GMSB) or *Supergravity* respectively.

While MSSM is a low energy effective theory, including gravity allows to consider energies close to the Planck-scale. This *minimal supergravity* (mSUGRA) allows to reduce the number of free parameters by assuming various unifications at high energies: Scalar mass, gaugino mass and trilinear couplings. Then there are, with respect to the Standard Model, only five additional free parameters left:

- $m_0$ : Unified scalar mass
- $m_{1/2}$ : Unified gaugino mass
- $A_0$ : Unified trilinear coupling
- $\tan\beta$ : Ratio of Higgs field vacuum expectation values
- $sign(\mu)$ : Sign of the unified Higgsino mass term



**Chargino/Neutralino/Slepton** Basically there are two processes for the production of charginos, neutralinos or sleptons, which may reduce the cross section by interference:

$$(2.23)$$

Additionally there may be chargino/neutralino+squark production:

$$(2.24)$$

## Decay

The decay modes available for each sparticle again depend on the mass hierarchy, but usually the following general observations apply:

- *Gluginos* As a gluino interacts strongly, there is just one way:  $\tilde{g} \rightarrow q + \tilde{q}$ . If the squarks are heavier than the gluino, this decay will take place via a virtual squark decaying into quark plus chargino/neutralino.
- *Squarks* If the squark is heavier than the gluino,  $\tilde{q} \rightarrow q + \tilde{g}$  will be the dominant decay mode. Otherwise the squark dominantly radiates a chargino/neutralino:  $\tilde{q} \rightarrow q + \tilde{\chi}$ .
- *Charginos/Neutralinos* Heavier charginos/neutralinos will dominantly decay into slepton and lepton:  $\tilde{\chi} \rightarrow \tilde{l} + l$ . Otherwise the decay into neutralino/chargino plus gauge boson  $\tilde{\chi} \rightarrow \tilde{\chi} + Z^0/W^\pm$  will be dominant.
- *Sleptons* A slepton will decay into a lepton and a chargino/neutralino:  $\tilde{l} \rightarrow l + \tilde{\chi}^0/\tilde{\chi}^\pm$

Differences between charged/uncharged or particle/antiparticle are not denoted explicitly, as they are determined by charge and color conservation. Some of these decay modes may be kinematically forbidden. If all are forbidden, they will take place by one of the decay products being virtual, thus a three body decay will take place.

These decay modes may, in combination, lead to decay chains with distinctive signatures. Like shown in Fig. 2.2, the sparticles will cascade down the mass hierarchy, potentially resulting in some jets, few leptons, and a substantial amount of missing energy.

### 2.2.8 Benchmark points

While five instead of 105 free parameters are a significant improvement, these are still too many to allow a complete scan of the parameter space in each analysis. To make things even worse, the experimental signatures may vary significantly even for small changes of the parameters. This makes it hard to compare various analysis approaches or experiments, thus one has to decide on a limited number of parameter sets, called *Benchmark points*, which are then used by all participants. The CMS community has chosen some *low*

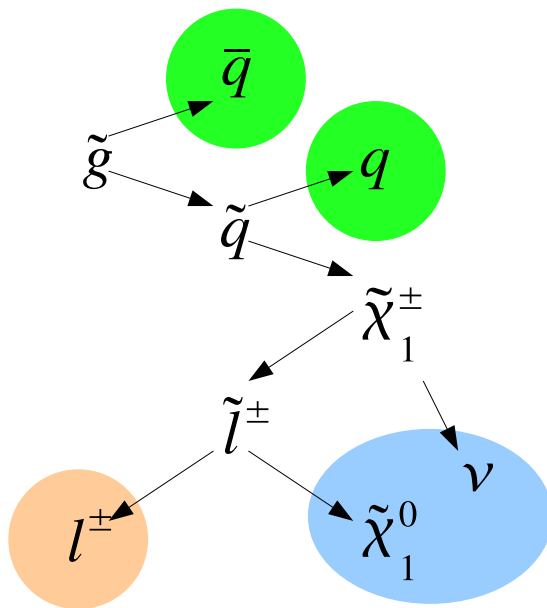


**Figure 2.2:** Typical supersymmetric decay chain. Particles shaded in green are visible as jets, red are leptons and blue shows missing energy.

mass points (LM) with fairly light sparticles and some *high mass points* with quite heavy sparticles [18]. As the cross section drops for increasing sparticle masses, it is unlikely to detect the high mass points within the first years of LHC running. Thus in this analysis only some of the low mass points will be looked at. Table 2.7 summarizes the parameters of the used LM points; Fig. 2.3 shows them in the  $m_0$ - $m_{1/2}$  plane.

| LM point | $m_0$ | $m_{1/2}$ | $\tan\beta$ | $A_0$ | $\text{sign}(\mu)$ |
|----------|-------|-----------|-------------|-------|--------------------|
| LM1      | 60    | 250       | 10          | 0     | +                  |
| LM2      | 185   | 350       | 35          | 0     | +                  |
| LM4      | 210   | 285       | 10          | 0     | +                  |
| LM5      | 230   | 360       | 10          | 0     | +                  |
| LM6      | 85    | 400       | 10          | 0     | +                  |
| LM8      | 500   | 300       | 10          | -300  | +                  |
| LM9      | 1450  | 175       | 50          | 0     | +                  |
| LM10     | 3000  | 500       | 10          | 0     | +                  |
| LM9p     | 1450  | 218       | 50          | 0     | +                  |

**Table 2.7:** *mSUGRA* parameters of the CMS benchmark points LMx.

With the exception of LM9 and LM10, all these points have a mass hierarchy like

$$m_{\tilde{\chi}} \lesssim m_{\tilde{l}} < m_{\tilde{q}} \lesssim m_{\tilde{g}} \quad (2.25)$$

thus the occurrence of the above decay chains is expected. Consequently, an analysis using at least one lepton, some jets and missing energy is expected to be a good choice. The LM10 parameter set leads to heavy squarks and sleptons of about 3 TeV, thus a direct production of charginos or neutralinos is expected. This will result in some leptons, but only very few jets in case of a gluino decaying via a virtual squark. LM10 and LM9, with

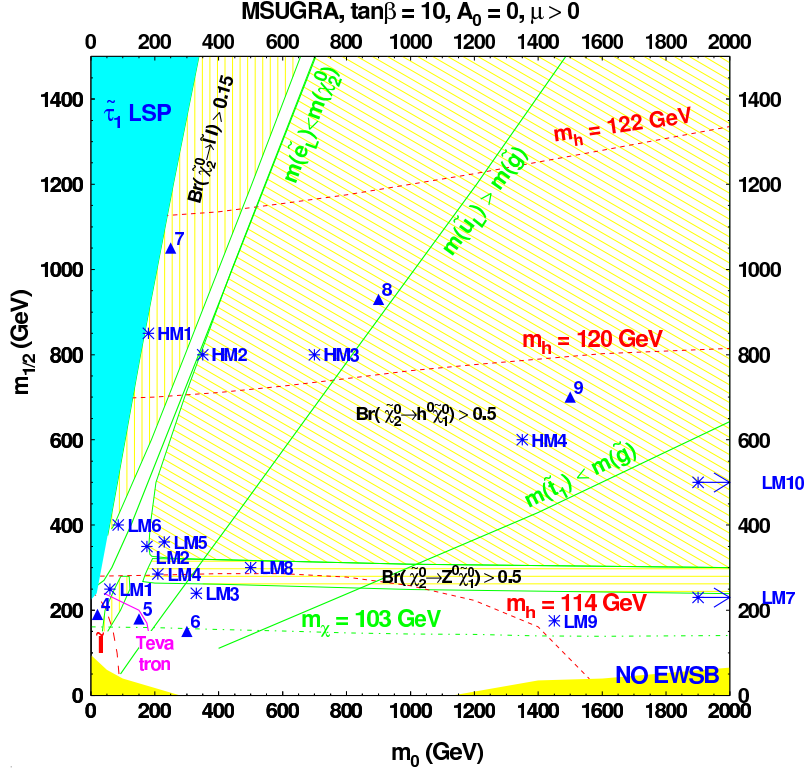


**Figure 2.3:** CMS  $m$ SUGRA benchmark points in the  $m_0$ - $m_{1/2}$ -plane: Low mass (LM) and high mass (HM) points [18].

intermediate squark and slepton masses, are thus used to evaluate the performance of the present analysis in case of non-optimal parameters chosen by nature.

LM1, LM2 and LM6 are compatible with WMAP cold dark matter limits, with LM1 just beyond the Tevatron reach. The others are not, but can be made compatible by giving up some Higgs unification assumptions.

During the definition of these points, a top mass of 175 GeV has been used. Later on, with a top mass of 172.5 GeV, it showed that there is not electroweak symmetry breaking for LM7 and LM9 using the spectrum calculator ISASUGRA [19]. Increasing  $m_{1/2}$  to about 500 GeV solves this problem for LM7, but then LM7 and LM10 are roughly the same, hence LM7 has been dropped entirely. LM9 can be repaired by increasing  $m_{1/2}$  to about 300 GeV, which is then called LM9p. Additionally LM9 showed to be very sensitive to the top mass, which is taken into account with LM9t175 with a top mass of 175 GeV.

## 2.2.9 Previous searches

Searches for R-parity conserving  $m$ SUGRA have been performed at LEP [20] as well as TEVATRON [21]. None of these searches discovered supersymmetry so far, hence lower limits on the sparticle masses have been set:

- $m_{\tilde{q}} \geq 379$  GeV and  $m_{\tilde{g}} \geq 308$  for  $\tan \beta = 3$ ,  $A_0 = 0$  and  $\mu < 0$  [22]
- $m_{\chi^\pm} \geq 127$  GeV for  $\tan \beta = 3$ ,  $A_0 = 0$  and  $\mu < 0$  [23]

Previous studies of the CMS discovery potential [24] in the  $\mu + \text{Jet} + \cancel{E}_T$  channel showed very high significances. However they are not easily comparable, as they used different background samples and methods.

## 3 Experimental setup

### 3.1 The Large Hadron Collider (LHC)

#### 3.1.1 Collider physics

As shown in the previous chapter, new physics is expected to manifest in new particles with masses of the order of 1 TeV. To produce these particles directly, an accelerator with center of mass energy  $\sqrt{s}$  of at least the mass of the particles is needed. Otherwise the particles can only participate in the interaction through virtual effects. Then the probability of such an interaction drops quickly with increasing difference between  $\sqrt{s}$  and the particle mass. Thus an accelerator with  $\sqrt{s}$  as high as possible is desirable. Unfortunately the energy loss via synchrotron radiation per revolution of a given particle with mass  $m$  and energy  $E$  in an accelerator with radius  $R$  is proportional to  $E^4/(m^4R)$ . This makes it very hard to build an electron ring collider with a center of mass energy higher than 200 GeV, which have been achieved at the *Large Electron Positron Collider* (LEP).

Pointlike particles, e.g. electrons, provide a very clean experimental environment. Thus it is obvious to use heavier leptons like the muon as colliding particles to reduce the energy loss per revolution. While there are some ideas how to accomplish this (i.e. [25]), practical challenges like the production of a sufficient number of muons are not solved yet. The muon production rate must be high enough to compensate for the decay of the unstable muons.

Protons however are easy to produce in vast numbers, just by ionizing hydrogen, and they are heavy enough to reduce the synchrotron radiation energy loss, allowing very high energies. However, they have the drawback of not being elementary particles: The effective center of mass energy of a given interaction depends on the energy fractions  $x_a$  and  $x_b$  carried by the interacting partons:

$$\sqrt{s'} = \sqrt{x_a x_b s} \quad (3.1)$$

Additionally, the proton remnants not taking part in the interaction may be scattered into the detector, creating background. The momentum carried by these remnants can not be measured, because they escape predominantly close to the beam. Consequently the rest frame of the hard scattering process is not known. As the proton momentum transverse to the beam axis is very small, the transverse energy balance can be measured. Invisible particles like the LSP can be detected indirectly, as they escape undetected and spoil the energy balance.

The expected event rate depends on the cross section and the *luminosity* delivered by the accelerator:

$$\frac{N_{events}}{t} = \mathcal{L} \cdot \sigma \quad (3.2)$$

The number and types of possible interactions for a given combination of two partons  $i$  and  $j$  determines the partonic cross section  $\hat{\sigma}_{ij}$ . The sum of these partonic cross sections, weighted by the probability to find each combination, is the total cross section. This probability can be described by *Parton Density Functions* (PDF)  $f_i(x_i, Q^2)$ , which are



equal to the probability to find a given parton  $i$  with momentum fraction  $x_i$  at an energy scale  $Q$ :

$$\sigma_{total} = \sum_{i,j} \int dx_i \int dx_j f_i(x_i, Q^2) f_j(x_j, Q^2) \hat{\sigma}_{ij} \quad (3.3)$$

All this leads to a non-trivial energy dependence as shown in Fig. 3.1: While the total cross section will be fairly similar for LHC and Tevatron, the cross section of interesting processes will be much higher at LHC.

As the cross section of interesting processes is usually rather small compared to the total pp cross section, a high luminosity has to be reached in order to gain a sufficient event rate. Assuming a gaussian proton density distribution of the beam, with widths  $\sigma_x$  and  $\sigma_y$  along the x- and y-axes, the luminosity can be approximated by:

$$\mathcal{L} = \frac{n_B N_B^2 f}{4\pi\sigma_x\sigma_y} \quad (3.4)$$

Here  $n_B$  is the number of bunches per beam,  $N_B$  the number of protons per bunch and  $f$  the revolution frequency. While  $f$  is fixed by the speed of light and the accelerator dimensions, all other parameters must be optimized to gain the highest luminosity possible. Increasing the luminosity will yield a higher probability to get an interesting process per bunch crossing, but will also increase the number of background interactions.

### 3.1.2 LHC design

The LHC is a superconducting proton-proton collider build in the former LEP tunnel at CERN. At design conditions it will reach a center of mass energy of 14 TeV and a luminosity of  $\mathcal{L} = 10^{-34} \text{ cm}^{-2} \text{ s}^{-1}$ . After being accelerated in the 27 km tunnel, 2808 bunches of  $1.15 \cdot 10^{11}$  protons each will collide in two of the four experiments: ATLAS<sup>1</sup> and CMS<sup>2</sup>. Additionally low luminosity runs at  $10^{-32} \text{ cm}^{-2} \text{ s}^{-1}$  will provide collisions for the b-physics experiment LHCb and the elastic scattering experiment TOTEM<sup>3</sup>. Heavy ion physics will be investigated at ALICE<sup>4</sup> during special runs, when lead ions are accelerated and collide with a center of mass energy of 1150 TeV.

These luminosities are high enough to provide a sufficient rate of *hard interactions*, in which the physics processes interesting for most experiments take place. At the same time the probability for *soft interactions* is orders of magnitude higher than for hard interactions, thus around 20 of these soft interactions are expected per bunch crossing. As these soft interactions are considered unwanted background by most experiments, the detector must be able to separate these *pile-up events* from the hard interactions.

Dipoles are used to hold the beams on track, which must generate a field of 8.4 T. At a pp collider, both beams need different magnet field polarities in these dipoles. Thus the beams run in separated vacuum pipes with separated dipole fields. Only in approximately 130 m long sections at the interaction regions both beams will share one beam pipe. Sustained fields of this strength can only be generated by superconducting magnets, thus all 1232 dipoles are cooled down to 1.9 K using superfluid helium.

A collider designed to guide and accelerate beams of a certain energy is usually not suitable for much lower energies. Consequently, the LHC main ring must be supplied with preaccelerated protons (see Fig. 3.2). The protons are produced by ionizing hydrogen in a

---

<sup>1</sup>Now regarded as a proper name, formerly: A Toroidal LHC Apparatus

<sup>2</sup>Compact Muon Solenoid

<sup>3</sup>Total and Elastic Measurement; located at CMS

<sup>4</sup>A Large Ion Collider Experiment



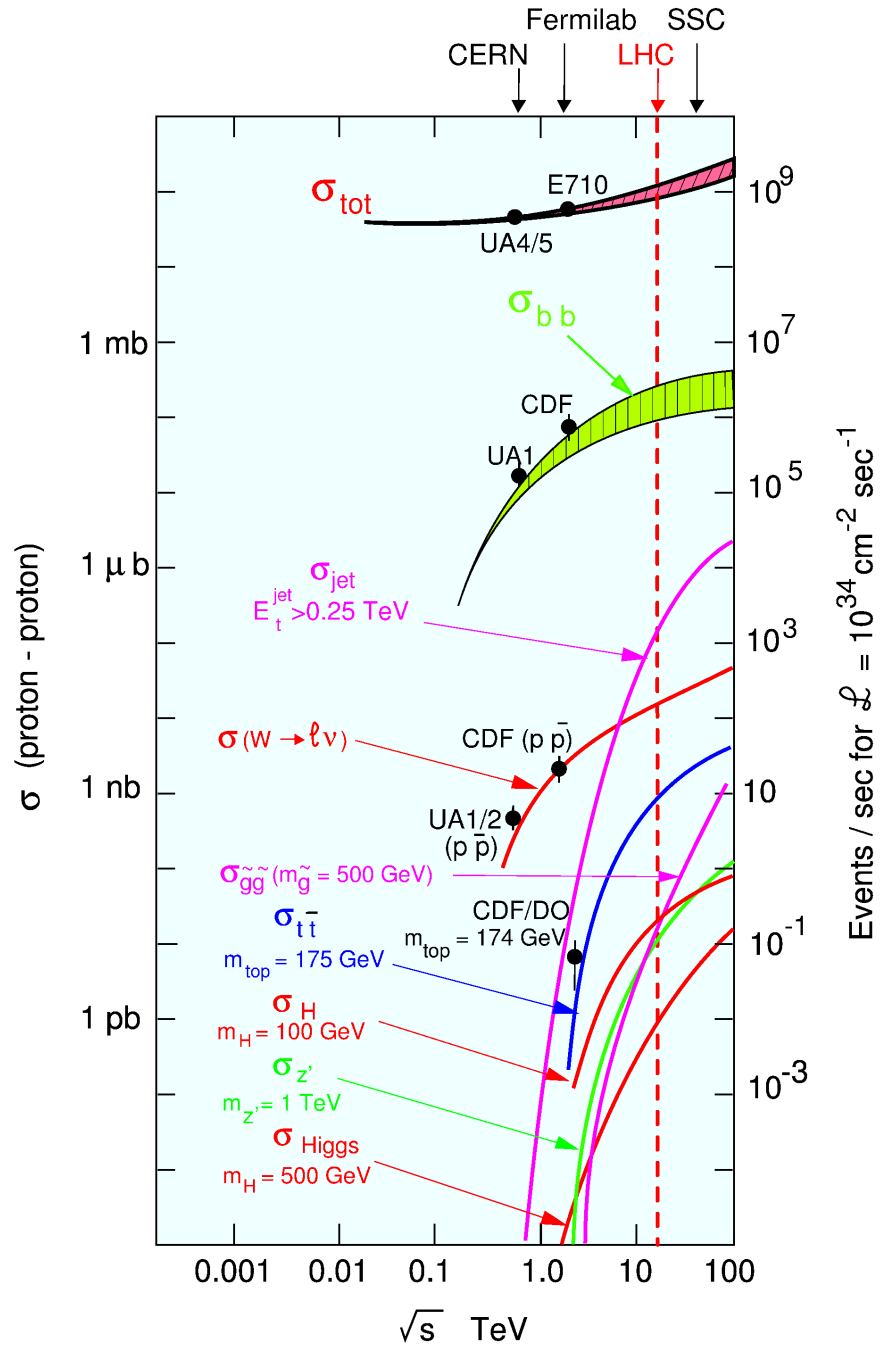
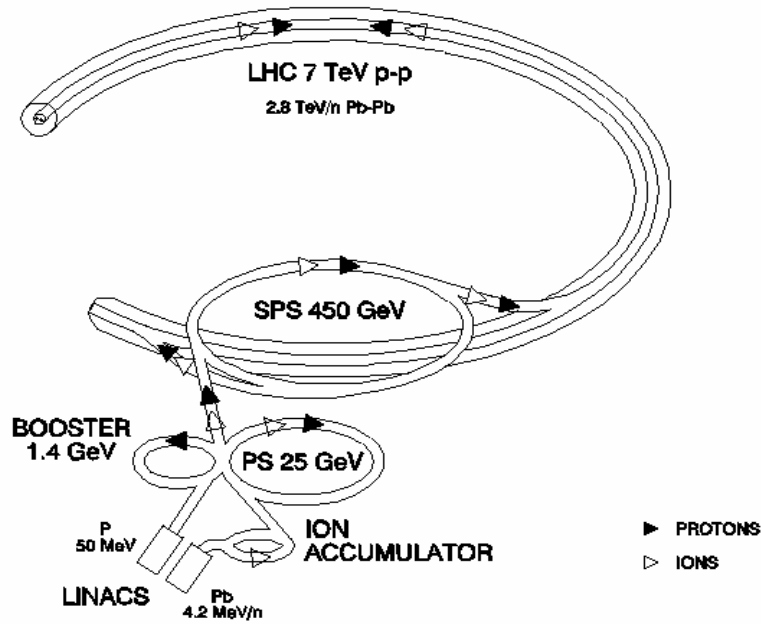


Figure 3.1: Cross sections and event rates at  $pp$ -colliders as a function of center of mass energy [26].



**Figure 3.2:** The injector chain for LHC delivers protons with 450 GeV energy to the main ring.

plasmatron and then accelerating them in the *Linac2* proton linear accelerator to 50 MeV. Each of the four rings of the *Proton Synchrotron Booster* (PSB) is then filled with one 30  $\mu\text{s}$  bunch delivered by *Linac2*. After accelerating the protons to 1.4 GeV the bunches are compressed to 190 ns. Six of these bunches, grouped into two batches, are then sent to the *Proton Synchrotron* (PS). Still at 1.4 GeV the bunches are split in three, then accelerated to 25 GeV and again split in two, resulting in batches of 72 bunches. These bunches are now spaced by the desired 25 ns. After compression and rotation these bunches are 4 ns long and are then fed into the *Super Proton Synchrotron* (SPS) every 3.6 seconds. Four PS cycles are necessary to fill the SPS for one supercycle, then the protons are accelerated to 450 GeV. It takes around 9 minutes to execute 24 SPS supercycles to fill both LHC rings with 2808 bunches in total, plus some additional overhead in form of pilot bunches and setup; around 15 minutes per filling are expected. Ramping up the energy will take about 20 minutes; routine testing between two runs maybe 30 minutes. Thus the LHC turnaround time is expected to be little more than one hour.

Residual gas scattering and mainly the interactions themselves will reduce luminosity over time with an expected lifetime of 15 h, resulting in 6 to 12 hours of data taking. Assuming 200 days of data taking per year and the above estimates for run length and turnaround time, something like 80 to 120  $\text{fb}^{-1}$  integrated luminosity per year are expected under design conditions.

Because of the unexpected tendency of some dipoles to quench at fields lower than 8.4 T, the first run end of 2008 will be at 10 TeV center of mass energy. This run will yield a integrated luminosity of the order of 10  $\text{pb}^{-1}$ , which is not sufficient to observe supersymmetry. Mid of 2009, after additional checkouts and commissioning runs with at first 75 ns and later 25 ns bunch spacing will follow, yielding 2.5  $\text{fb}^{-1}$  at a peak luminosity of  $10^{33} \text{ cm}^{-2} \text{ s}^{-1}$ .

Detailed discussions of the facts and figures presented in this section can be found in [27, 28, 29].

## 3.2 The Compact Muon Solenoid (CMS)

A general purpose detector like the *Compact Muon Solenoid* (CMS) at a collider usually looks at collisions, where the center of mass system is approximately at rest in the laboratory frame. Consequently the reaction products leave the interaction point in all directions, suggesting a spherical detector layout. The beams have to pass the detector and the location of the interaction along the beam axis can be determined with a precision up to a few centimeters. Thus the detectors are usually built as cylinders closed by caps at both ends. This allows to add magnets to measure the momentum of charged particles, following a curved path in the field.

The vast variety of produced particles at very different energies cannot be measured precisely using only one type of detector. Therefore a number of different detector components are layered concentrically, each of them measuring different quantities or particle types.

The CMS concept was first proposed in the LHC workshop 1990 in Aachen [30], suggesting a high field solenoid and a good muon system in a fairly compact form. After years of research, development, planning and construction all over the world, the detector is now approaching its completion. As shown in Fig. 3.3, the final design basically consists of four elements, listed from the inside out:

- A silicon inner tracker: Pixel vertex detector and strip tracker.
- Calorimeter: Lead tungstate crystal electromagnetic calorimeter and a brass/scintillator sampling hadronic calorimeter.
- A 3.8 Tesla superconducting solenoid.
- Muon system based on Drift Tubes (DT, barrel), Cathode Strip Chambers (CSC, endcap) and Resistive Plate Chambers (RPC).

All these components together reach a total length of 21 meters and a diameter of 15 meters, resulting in a total weight of 12500 tons. To ease maintenance the detector is divided into five wheels and three endcap discs on each end. The central wheel supports the magnet and most components mounted inside the magnet. Two wheels on each side can be moved on air pads to allow access to the central structures. The detector is closed on each sides by three discs, the innermost supporting the endcaps of the calorimeter.

The magnet allows the measurement of the particle momentum transverse to the beam axis via the track curvature and protects the calorimeter against the vast amount of very low energetic particles. It is placed outside of the calorimeter to avoid a degradation of energy measurements in the calorimeter. The direction and track curvature of charged particles inside the magnet is measured by the silicon strip tracker and the silicon pixel vertex detector, which also provides precise measurements of the interaction vertex. The calorimeter measures the energy and the flight direction of all electromagnetically or strongly interacting particles. All detectable particles passing calorimeters and magnet, which should be mostly muons, will be measured by the muon systems. The muon system again works as a tracker, measuring direction and curvature of the tracks, using the field in the iron return yokes interleaved with the muon chambers.

The following sections provide an overview of the various subsystems, a detailed description can be found in the recently published CMS detector paper [32].

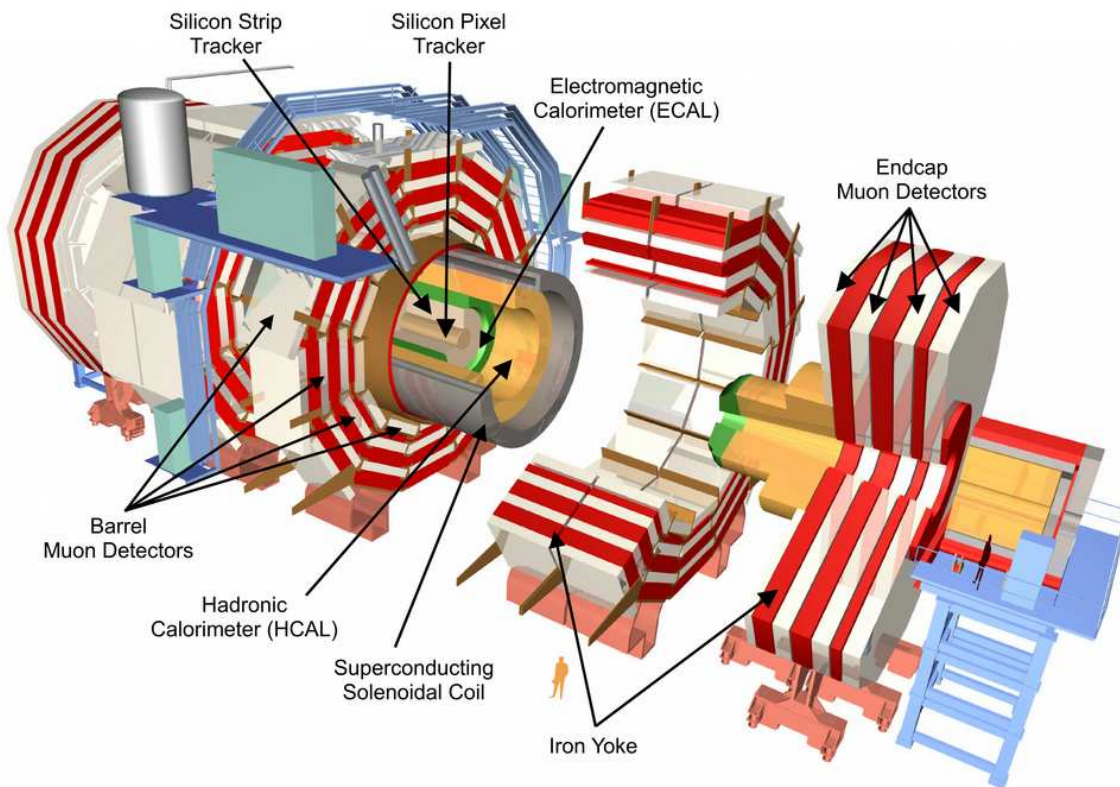


Figure 3.3: Perspective view of the CMS detector [31]

### 3.2.1 The inner tracker

At design luminosity 20 overlapping inelastic interactions will produce around 1000 particles every 25ns. Thus the innermost tracking detector needs a high spatial resolution and fast response to identify vertex positions. Precise measurement of the vertex position is important due to two reasons: First to detect and exclude particles coming from additional interactions. And secondly, eventually even more important, an event may contain secondary vertices. Some particles, usually b or c quarks and  $\tau$  leptons, may travel some millimeters before decaying. To detect these secondary vertices a detector close to the interaction point with an excellent spatial resolution is necessary. Close to the interaction point the particle flux will be high, requiring an intrinsically radiation hard detector.

For a good momentum resolution by measuring the track curvature in the magnetic field, both a good spatial resolution and a long lever arm is necessary. Hence the CMS inner tracker consists of a pixel detector close to the beam and a strip detector, which offers the lever arm without being unaffordable.

More details concerning the inner tracker are given below and can be found in [33].

#### Silicon pixel detector

The silicon pixel detector in CMS, which offers a good spatial resolution, is used for vertex detection. It also provides the seeds for the track finding algorithms. Using pixels of  $100 \times 150 \mu\text{m}^2$  a resolution of  $10 \mu\text{m}$  in  $\phi$  direction and  $17 \mu\text{m}$  along the beam can be achieved. The charges generated by a passing particle in one pixel will also drift into neighboring pixels because of the high magnetic field. This allows to interpolate the hit

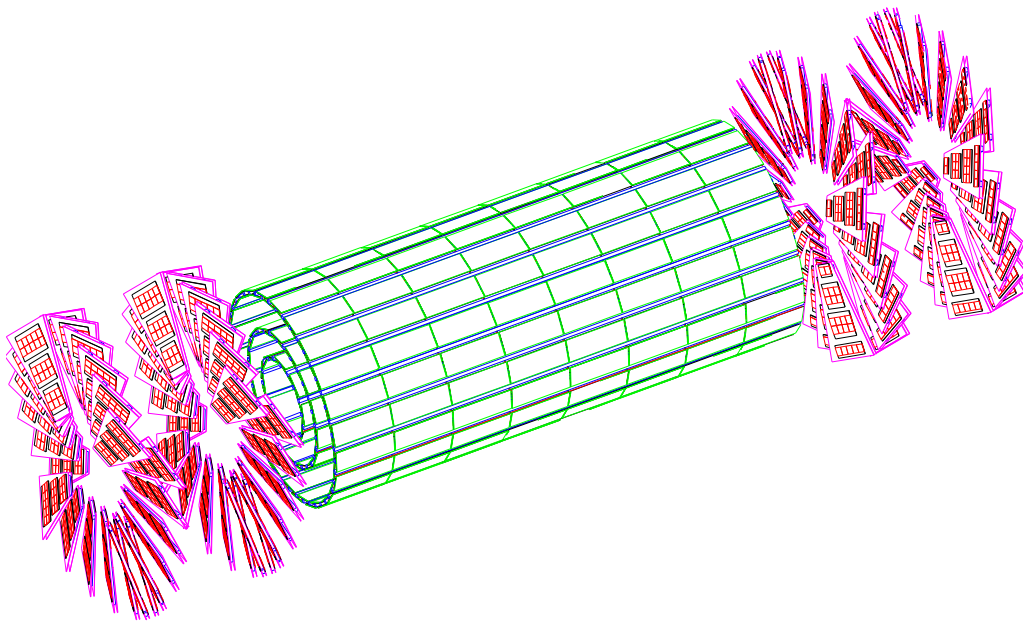


**Figure 3.4:** Barrel and endcaps of the CMS pixel detector, the innermost part of the inner tracking system [33].

position by weighting the pixels. Thus a resolution better than the pixel size is possible.

The 1440 modules are arranged in three concentric barrel layers and two endcaps on each side (see Fig. 3.4). Mounted 4.4 to 10 cm from the beam axis, the barrel layers cover an acceptance range up to pseudorapidity  $|\eta| \approx 1.5$ . Complemented by two disks on each side, located 34.5 and 46.5 cm along the beam axis from the nominal interaction point, the forward pixel detector provides at least two hits per track up to  $|\eta| = 2.5$ .

To minimize the amount of material in a particle path, to keep radiation sensitive electronics away from the interaction point and to maintain the pulse height information, the analogue signal is transmitted by lasers through optical fibers to the readout electronics. Cooling the silicon down to  $-10^\circ\text{C}$  will help to minimize the radiation damage.

### Silicon strip detector

Track finding algorithms need about five hits to work reliably. But adding more layers of silicon pixel detectors would just be too expensive. As the stream of particles will spread out with growing distance to the interaction point, it is possible to change from pixels to strips. The solenoid field only allows the measurement of the transverse momentum component. Silicon strip detectors with their strips along the beam axis provide such measurement at a moderate cost. Using common lithographic processing, sensors with strips up to 12 cm long and a strip pitch of 80 to 120  $\mu\text{m}$  can be made.

In total 24244 of these sensors form nearly 200  $\text{m}^2$  of active area, thus they form the largest silicon detector ever build. To guarantee a sufficient number of hits up to  $|\eta| = 2.5$ , these modules are mounted in ten barrel layers (see Fig. 3.5). Both ends are closed by twelve discs in the endcaps on each side. All this covers a cylinder of 5.4 m length, reaching from 0.2 m from the beam at the innermost layer to 1.2 m at the outermost layer. Four layers contain double sided *stereo modules*: Two modules are mounted back to back with a slight angle, allowing a position measurement along the strips.

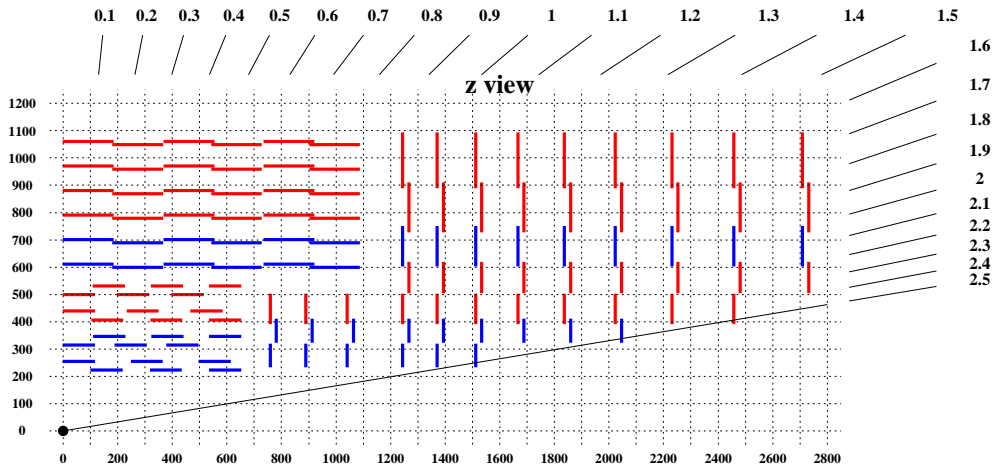


**Figure 3.5:** Pseudorapidity coverage of the silicon strip tracker: Double sided stereo layers are shown in blue, single sided layers in red [34].

Charge sharing between adjacent strips allows a resolution of about  $15 \mu\text{m}$  for the inner modules with a strip width of  $61 \mu\text{m}$ .

In combination pixel and strip detector form the inner tracker with around 40 million channels. Assuming proper alignment, a transverse momentum resolution of

$$\frac{\Delta p_T}{p_T} = 0.15 p_T [\text{TeV}] \oplus 0.5\% \quad (3.5)$$

is expected to be reachable. Isolated muons should be reconstructed with an efficiency of about 99% [32].

### 3.2.2 Calorimeter

The inner tracker inside the magnet field can only measure the momentum of charged particles. Uncharged particles, like photons, leave no track at all in the tracker. Consequently the next layer of the CMS detector just outside the tracker is the calorimeter.

To guarantee a good energy resolution the particle must be completely absorbed, thus the calorimeter needs a certain thickness. Light electromagnetic particles like electrons and photons can be stopped easily, but heavier hadrons like protons or neutrons travel a much longer distance through any material. In both cases materials made from heavy elements are preferred: They provide a huge number of hull electrons per volume and heavy nuclei to interact with electrons and photons. Hadrons will be absorbed by nuclear interactions with the large nuclei.

Materials providing good energy resolution, subdivided into cells small enough for a good angular resolution, tend to be very costly. Furthermore the nuclear interaction length for hadrons is much longer than the radiation length for electrons or photons, making very thick layers of material necessary. Thus the CMS calorimeter consists of two layers: Inside a relatively thin crystal electromagnetic calorimeter (ECAL) and outside a thick hadronic sampling calorimeter (HCAL).

Detailed descriptions of the calorimeter are given below and can be found in [35].



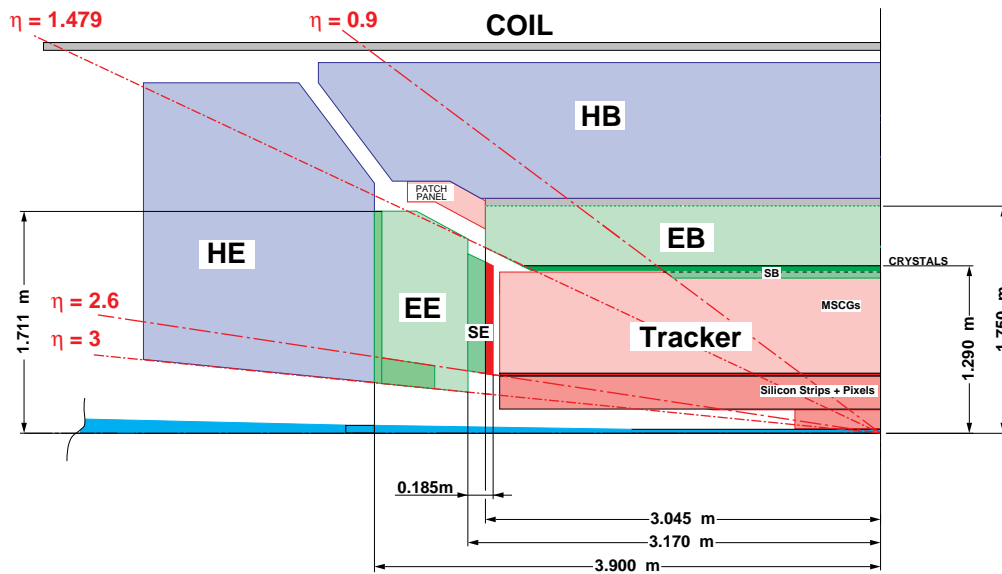


Figure 3.6: Schematics of one quadrant of the tracker and calorimeter of CMS [35].

### Electromagnetic calorimeter

Electromagnetic calorimeters at LHC must fulfill various competing requirements: They must be fast, finely grained, radiation hard and small, but nevertheless provide a good energy resolution. In CMS this is made possible by a ECAL built from scintillating lead tungstate crystals ( $\text{PbWO}_4$ ). It is divided into a barrel section and two endcaps (see Fig. 3.6). The barrel consists of 61200 crystals, read out by avalanche photodiodes (APD); one endcap contains 7324 crystals with vacuum phototriodes (VPT) used as photodetectors. APDs, in contrast to common photo multipliers, are not affected by the magnetic field.

Lead tungstate is the material of choice because of two characteristics:

- Short radiation length of 0.89 cm: After traveling one radiation length, the energy of electrons drops to  $1/e$  on average.
- Small Moliere radius of 2.2 cm: On average 95% of the absorbed energy is contained within one Moliere radius, providing a good angular resolution.

The scintillation time is quite comparable to the LHC bunch distance in time, 80% of the light is emitted within 25ns. The crystal light yield and diode gain are strongly temperature dependent, requiring a temperature constant within  $0.05K$ . Both radiation damage and recovery increase with the temperature, balancing at  $18^\circ C$  for an optimal life time. Consequently an effective thermal screen between tracker and ECAL is necessary.

The ECAL barrel (EB) covers a pseudorapidity range up to  $|\eta| \approx 1.5$  (see Fig. 3.6). Holding a crystal volume of a little over  $8 \text{ m}^3$ , it weighs 67.4 tons. The crystal length of 23 cm equals about 25 radiation lengths.

The ECAL endcaps (EE) are located 3.15 m away from the interaction point, extending the ECAL reach to  $|\eta| = 3$ . Each endcap contains  $1.45 \text{ m}^3$  of active volume with a mass of 12 tons. Test beam measurements of fully equipped ECAL modules showed an energy resolution of [32]:

$$\left(\frac{\sigma}{E}\right)^2 = \left(\frac{2.8\%}{\sqrt{E}}\right)^2 + \left(\frac{0.12}{E}\right)^2 + (0.3\%)^2 \quad (3.6)$$

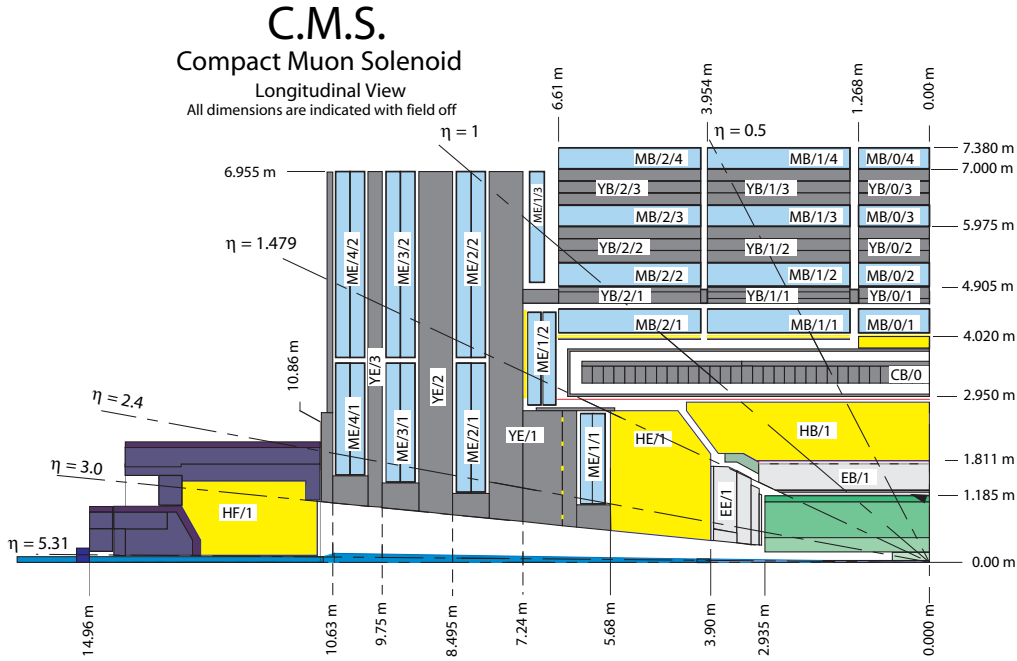


**Figure 3.7:** Schematic view of one quadrant on the CMS detector showing tracker, calorimeters and muon system [36].

The three contributions are:

- Stochastic fluctuation of the light yield, light collection and absorption in the ECAL crystals and all material inside of the ECAL.
- Noise: Electronic, digitization and pileup.
- Constant term: Non-uniformity of light collection and calibration errors.

A preshower detector at the inner surface of the ECAL endcaps improves the spatial resolution, however it will not be installed from the beginning.

### Hadronic calorimeter

The HCAL of CMS consists of four distinctive parts: The usual barrel (HB) and endcap (HE) sections (see Fig. 3.6), two *very forward calorimeters* (HF) and an *outer hadronic calorimeter* (HO) (see yellow areas in Fig. 3.7).

The barrel and endcaps are sampling calorimeters made from absorber-scintillator sandwiches. One layer of high density absorber material is followed by one layer of scintillator to measure the shower developing in the absorber. As the HB and HE are placed inside the solenoid, the absorber materials must be non-magnetic: Brass from old russian artillery shells has been used. Being stored in underground bunkers for decades, the inner radioactivity of the brass has declined. This radioactivity would otherwise increase the inner background of the calorimeter. The barrel section contains, from inside out, one steel support layer, 14 brass plates and then again a steel support layer. This adds up to five to ten nuclear interaction lengths, depending on the angle of incident. Between each two absorber layers one 3.7 mm thick plastic scintillator is placed, which is read out by wavelength-shifting fibers. The last scintillator after the outermost absorber is 9 mm



thick to detect showers, which develop late in the absorbers. The first scintillator before the innermost absorber uses the ECAL and its support structures as an absorber. The scintillator layers are subdivided in 72 sections along the  $\phi$  direction and 16 sectors along the  $\eta$  direction, providing a segmentation of  $(\Delta\phi, \Delta\eta) = (0.087, 0.087)$ . The HB covers the rapidity region up to  $|\eta| = 1.3$ .

Each endcap contains 17 absorber-scintillator layers, each with 7.9 mm brass and 3.7 mm plastic scintillator. Again a 9 mm inner scintillator uses the ECAL as an absorber. Both ECAL and HCAL add up to about ten nuclear interaction length. The granularity decreases from  $(\Delta\phi, \Delta\eta) = (0.087, 0.087)$  to  $(\Delta\phi, \Delta\eta) = (0.17, 0.17)$  for  $1.3 < |\eta| < 3$ .

Especially in the very center of the HB, about just seven interaction length will lead to a high fraction of shower energy leaving the HCAL. Thus additional scintillators, forming the HO, are placed outside the magnet, using the solenoid and the first layer of the return yoke iron as a *tail catcher*. This extends the total thickness of the calorimeter to at least 11.8 nuclear interaction lengths. The HO scintillators are subdivided into tiles which roughly match the granularity of the HB.

The HCAL including HO is expected to reach a resolution of [37]:

$$\frac{\Delta E}{E} = \frac{100\%}{\sqrt{E}} + 4.5\% \quad (3.7)$$

The very forward calorimeters, covering  $3 < |\eta| < 5.2$ , will be exposed to large particle fluxes. Consequently radiation hardness was the main design goal, even more important than energy resolution. The HF consists of quartz fibers embedded in a steel absorber, providing about ten nuclear interaction lengths. As the fibers measure the Cherenkov radiation of passing particles, they are sensitive mostly to the electromagnetic fraction of the showers. They will help measuring missing energy.

### 3.2.3 Solenoid

At a physicist's point of view, the magnet of a detector should be as large and strong as possible:

- A longer magnet generates a more homogeneous field.
- A magnet with a greater diameter allows to put more detector components inside the field. Hence the coil will not deteriorate the energy measurement, albeit some detector types are affected by B-fields.
- A stronger magnet allows better momentum measurements.

As a magnet's price will grow nonlinear with size and strength, a compromise has to be made. The CMS solenoid is 12.5 meters long with a free inner diameter of 5.9 meters. It generates a field of 3.8 T using four layers of superconducting coils.

A solenoid provides a very homogeneous field in its inner volume. This allows a precise momentum measurement in the inner tracker. The field outside of the solenoid will be guided by iron return yokes, which allows the muons system to not only identify muons but provide a momentum measurement. The longitudinal field causes no deviation of a particle's trajectory along the beam axis, improving the vertex measurement along the beam axis. The drawback of a solenoid field is its strong inhomogeneity in the endcap region, affecting the performance of the muon endcaps.

Assuming the full coil thickness of around 30 cm to be solid copper, a magnet of this size and strength would need about 100 MW of energy to be delivered electrically and

removed as heat. Consequently superconducting materials must be chosen, regardless of their price and the engineering problems they impose. The NbTi coil must be cooled below 9.8 K to stay superconducting. Long tests at an operating temperature of about 4.5 K has been successful. In case of catastrophic failures the 2.6 GJ stored energy can be dissipated in about 200 seconds using a resistor block located outside the cavern. During normal shutdown the energy will be dissipated slowly within a few hours.

### 3.2.4 Muon system

There are various reasons why muons merit a certain attention. Most new physics processes are expected to be fairly lepton rich, i.e. standard model Higgs ( $H \rightarrow ZZ \rightarrow lll$ ), heavy gauge bosons ( $W' \rightarrow l\nu$ ,  $Z' \rightarrow ll$ ) and last but not least supersymmetry. Muons are very easy to identify in contrast to electrons: They are the only particles passing fairly unaffected through the whole detector but nevertheless leave ionized tracks.

Located outside the magnet, interleaving the return yoke, the muon system must cover a very large area. The area to be covered is increased even more by the CMS muon system's important feature to provide not only a muon identification, but several hits for momentum measurement. Hence the detector technology must be inexpensive, reliable and robust, but nevertheless precise and fast. Following the general design of the detector, the muon system consists of the cylindrical barrel section and two endcaps (see Fig. 3.7). In the barrel section a small muon flux, low neutron background and the uniform field, which is mainly enclosed in the return yoke, allows the use of drift tubes (DT). All this is not the case in the endcaps, thus technology insensitive to the field must be used: Cathode strip chambers (CSC). In both barrel and endcaps resistive plate chambers (RPC) complement the muon measurement, as they provide an excellent timing measurement, albeit their lower spatial resolution. The RPCs, but also the DTs and CSCs are used for the muon trigger system. The barrel DTs and RPCs cover a pseudorapidity range of  $|\eta| \leq 1.2$ . Slightly overlapping are the endcap CSCs covering  $0.9 < |\eta| < 2.4$ , while the endcap RPCs stop at  $|\eta| = 2.1$ .

Overall they provide a detection area of about 25000 m<sup>2</sup>.

Detailed descriptions of the muon system are given below and can be found in [36].

#### Drift tubes

The barrel section consists of four concentric *stations*, called *Muon Barrel* 1 to 4 (MB1 to MB4, see Fig. 3.8). Each station is subdivided into five wheels along the beam axis, numbered  $-2$  to  $2$ , and 12 sectors along the  $\phi$  angle. One unit addressed by wheel, station and sector is a *chamber*. The chambers of MB1 to MB3 contain three *superlayers* (SL), the inner and outer one measuring the  $\phi$ -position of a particle, the one in the middle measuring the  $z$ -position. The chambers in MB4 contain only two SL provide no  $z$ -position measurement. All SL are build from four layers of  $11.5 \times 42$  mm<sup>2</sup> drift tube cells, which are not stacked exactly on top of each other, but shifted by half a cell. This allows to reduce ambiguities and avoids uninterrupted lines of dead material pointing to the interaction point.

The active elements of one cell consist of the central wire, two cathodes at the I-beams and two field forming stripes near the anode wire on the plates (see Fig. 3.9).

The maximal drift time of around 380 ns corresponds to about 15 bunch crossings. One hit inside a cell can be located with a precision of better than 250  $\mu$ m with more than 99% efficiency. One chamber allows a precision in  $\phi$  of better than 100  $\mu$ m with eight hits.

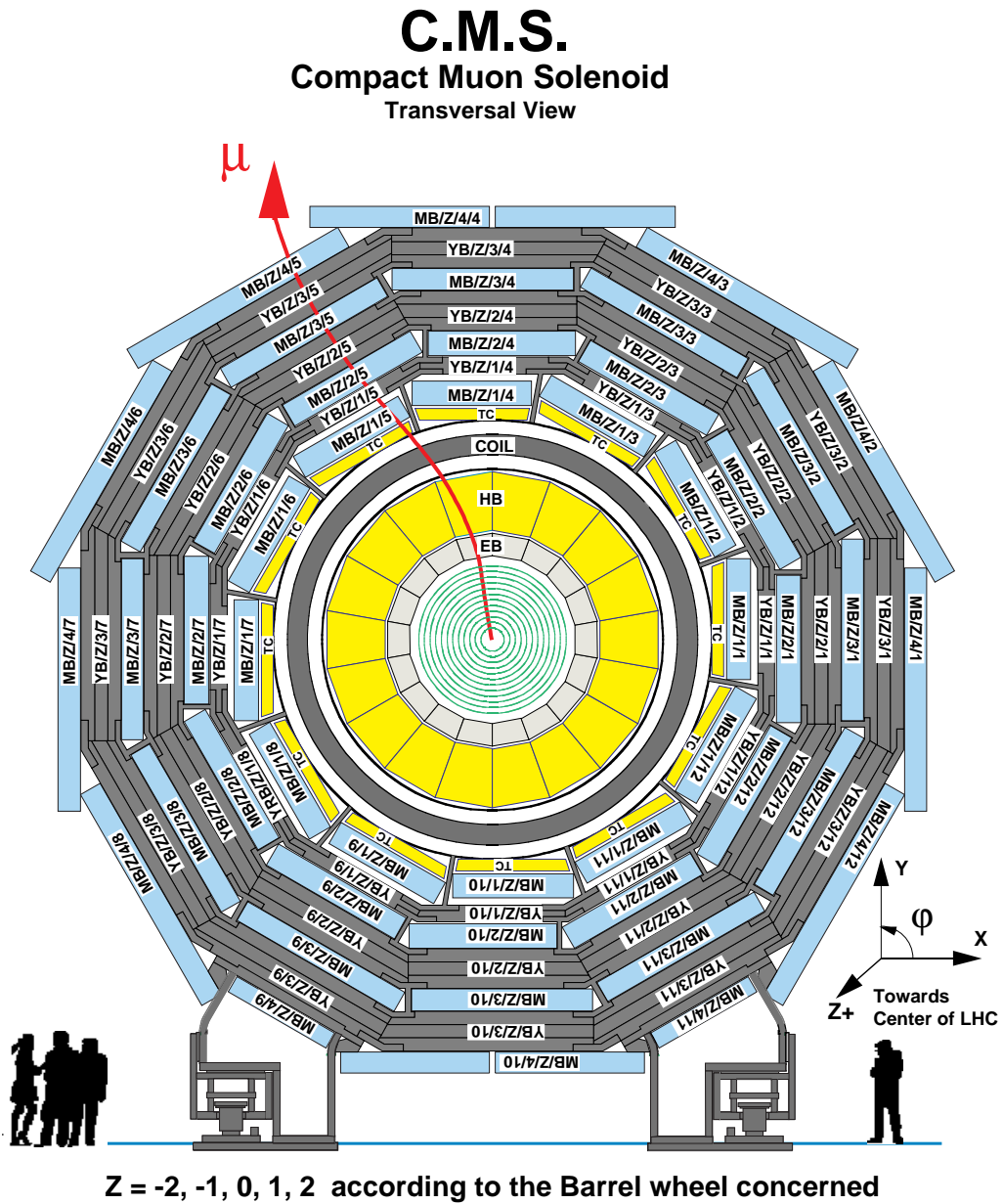


Figure 3.8: Transverse view of the CMS detector [36]. From the center outwards: Tracker, ECAL, HCAL, solenoid and the interleaved muon barrels and return yoke barrels.

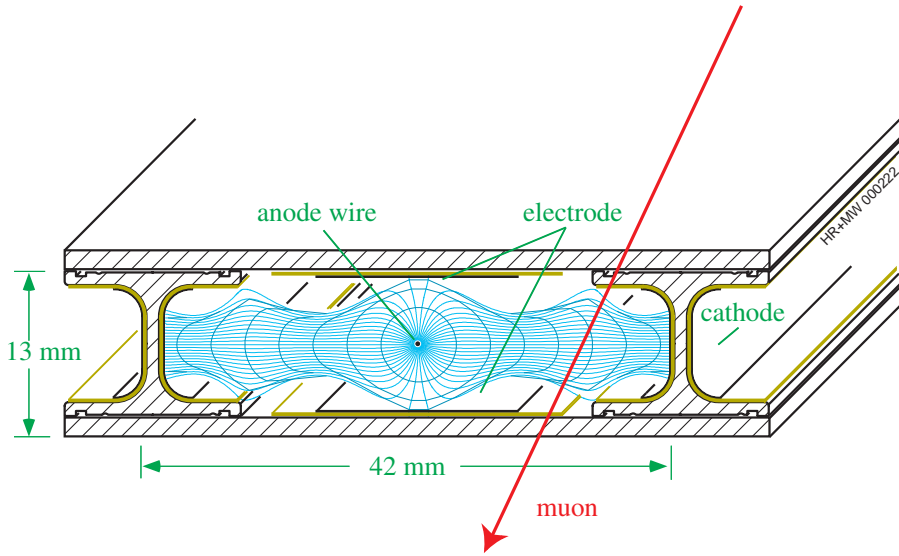


Figure 3.9: Cross section of a drift tube cell showing the field [38].

### Cathode Strip Chambers

The DT measurements rely on a well known magnetic field over distances of the order of cm. The strong and highly non-uniform fields in the endcap regions would deform the fields in the DT, degrading the spatial resolution. Moreover the high particle flux and high background would lead to many hits in one chamber, making it hard to separate them. Consequently a different technology must be used in the endcaps: *Cathode Strip Chambers* (CSC).

The CSCs in each endcap are mounted in four discs perpendicular to the beam, called *Muon Endcap* 1 to 4 (ME1 to ME4) (see Fig. 3.7). The chambers are arranged with overlaps to avoid dead regions.

Each chamber consists of six anode wire planes, interleaved among seven cathode panels. Each wire plane contains about 1000 wires with 3.2 mm distance, hence forming a multi-wire proportional chamber together with the cathode panels. The wires are aligned along the  $\phi$ -direction. They provide a measurement of the radial coordinate with a precision of a few millimeters and precise time measurements to assign the muons to bunch crossings. All cathode panels are divided into strips aligned perpendicular to the wires, hence along the radial coordinate. They are between 8.4 mm wide near to beam and 16 mm at the outer edge, covering a constant  $\Delta\phi$  width. By weighting the charge distributed over several strips, a precision of about 150  $\mu\text{m}$  along the  $\phi$  direction is achieved (see Fig. 3.10).

### Resistive Plate Chambers

The RPCs are complementary to the other muon detectors, adding redundancy. They provide a reasonable position measurement along the  $\phi$ -direction, but a timing measurement with a precision of the order of a few nanoseconds, allowing to assign muons to bunch crossings. This makes them very useful for triggering purposes.

In the barrel the two innermost muon DT stations are sandwiched by two RPCs, the two outer stations carry only one RPC. This allows a momentum measurement even for low energy muons absorbed in the iron return yoke before they reach the outer stations.

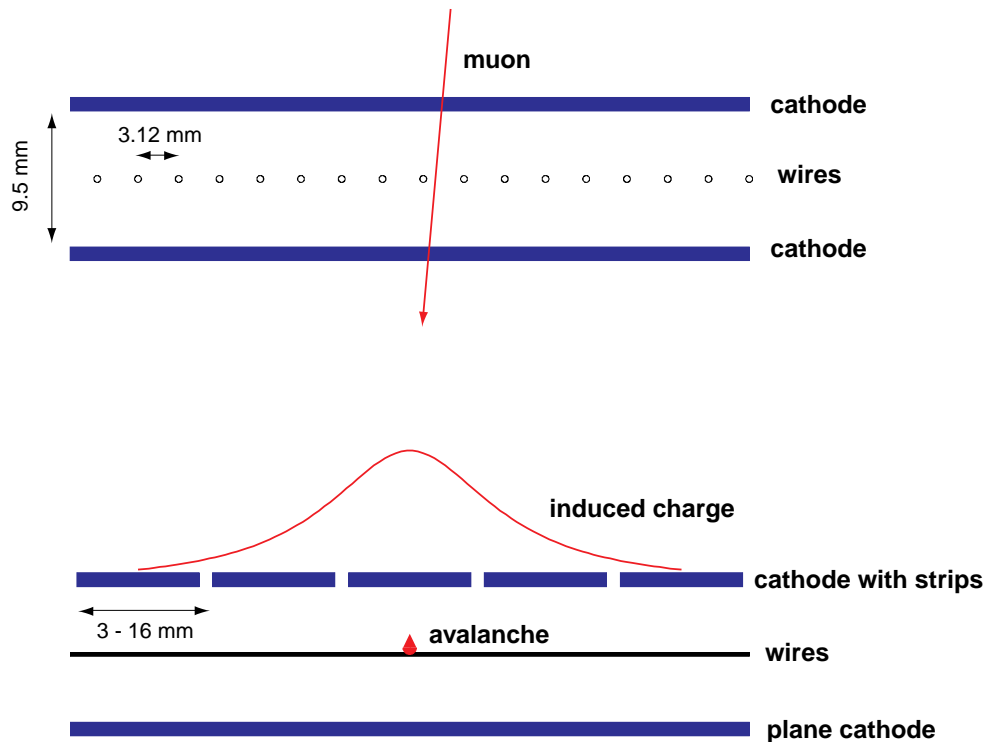


**Figure 3.10:** Position measurement with wires and strips in a CSC [36].

Each endcap muon station carries one RPC, however they stop at  $|\eta| < 2.1$ .

One RPC consists of two bakelite plates held 2 mm apart by a plastic spacer mesh. To apply a voltage of about 10 kV the bakelite plates are painted with a conductive graphite paint. They are read out by aluminium strips isolated from the graphite paint by a PET film.

The RPCs are driven in the fast *avalanche* mode. However they are less sensitive in this mode and provide small signals, which must be amplified by front end electronics. *Double gap RPCs*, where one RPC gap is mounted on each side of the readout strips, increase sensitivity and signal strength.

Much like for the CSCs, the signal in adjacent strips is weighted to gain a spatial resolution better than the strip width.

## Performance

For muons up to about  $p_T = 200$  GeV the transverse momentum resolution of the muon system alone is deteriorated by multiple scattering in the material before the first muon station [39]. The momentum resolution in this region is consequently dominated by the inner tracker, which provides a resolution of the order of 1%. For muons with a higher momentum, the combined reconstruction in both inner tracker and muon system provides a resolution of the order of 10% up to a muon  $p_T$  of about 1 TeV. In the endcaps the resolution is a bit lower, but still in the same order of magnitude.

The reconstruction efficiency of combined muons is typically between 95% and 99%, with some drops at transition regions in the barrel and between barrel and endcap.

| Trigger                                      | Threshold (GeV)  |
|--|------------------|
| Single, double electron/photon               | 22, 11           |
| Single, double muon                          | 14, 3            |
| Single, double tau                           | 100, 66          |
| 1-, 2-, 3-, 4-Jets                           | 150, 100, 70, 50 |
| Transverse energy sum ( $H_T$ )              | 300              |
| Missing transverse energy ( $\cancel{E}_T$ ) | 60               |
| $H_T$ and $\cancel{E}_T$                     | 200, 40          |
| Jet and $\cancel{E}_T$                       | 100, 40          |
| Tau and $\cancel{E}_T$                       | 60, 40           |
| Muon and $\cancel{E}_T$                      | 5, 30            |
| Electron/photon and $\cancel{E}_T$           | 15, 30           |
| Muon and jet                                 | 7, 100           |
| Electron/Photon and jet                      | 15, 100          |
| Muon and tau                                 | 7, 40            |
| Electron/Photon and tau                      | 15, 52           |
| Electron/photon and muon                     | 15,7             |

**Table 3.1:** Level 1 trigger thresholds at design luminosity [18].

### 3.2.5 Trigger

With CMS running under design conditions, more than  $10^8$  channels will generate data every 25 ns. Even after zero-suppression of the order of 1 MB per bunch crossing would have to be read out at 40 MHz, resulting in about 40 TB per second. No computer or storage system known today is able to swallow such a data rate, most of which is considered dispensable, because no interesting interaction occurred. Hence a trigger system must be deployed, which is able to sort the data and only send such events to the storage systems, which appear to contain interesting physics.

For CMS, this trigger is divided into two levels: The level 1 trigger (L1) is based on custom hardware pipeline processors without dead time, it provides a decision every 25 ns. Applying the thresholds shown in Table 3.1, the L1 trigger reduces the event rate to about 30 kHz. The second level trigger, called *High Level Trigger* (HLT), is based on about 1000 off-the-shelf PCs and reduces the event rate to about 100 Hz. Usual tape archives are able to manage the resulting data rate of about 100 MB/s.

The L1 trigger basically searches for localized clusters of energy in the calorimeter and for groups of hits in the muon systems, which can be grouped to tracks. If the number and energy or momentum of these clusters and tracks exceed a certain threshold, the event is accepted.

In the HLT software algorithms, much like the ones used in the offline reconstruction, look at the whole detector to determine the number and type of particles found in the events. There are various *trigger paths*, which can accept or reject the events based on leptons, jets, missing transverse energy, etc including correlations and topological information. In this analysis the muon based triggers shown in Table 3.2 are used. Isolation on trigger level is divided in calorimeter and track isolation. A muon is considered isolated, if the energy in a cone<sup>5</sup> of  $\Delta R < 0.24$  is below a certain threshold. This threshold is  $\eta$  dependent: The transverse energy  $E_T$  must be lower than 2 to 4 GeV in the calorimeter and the transverse momentum  $p_T$  must be lower than 0.8 to 1.2 GeV for tracks.

<sup>5</sup>  $\Delta R = \sqrt{\Delta\phi^2 + \Delta\eta^2}$



| Trigger name   | Description                 | $p_T$ threshold |
|----------------|-----------------------------|-----------------|
| HLT1MuonIso    | at least one isolated muon  | 11 GeV          |
| HLT2MuonIso    | at least two isolated muons | 3 GeV           |
| HLT2MuonNonIso | at least two muons          | 3 GeV           |

**Table 3.2:** Muon high level trigger used in this analysis.

### 3.2.6 Luminosity monitoring

The integrated luminosity determines the number of events. There are two methods to measure the luminosity. First, by determining the beam parameters and calculating the luminosity with equation 3.4. As it is rather difficult to measure the beam parameters at the interaction point, an uncertainty of less than 10% is not expected. Secondly, by measuring the event rate of a well known process, which is easy to identify. As long as the cross section of this process is theoretically well known, it is possible to determine the luminosity using equation 3.2.

The TOTEM [40] project aims to precisely measure the total cross section and the elastic and inelastic rates. Then the luminosity can be calculated using

$$N_{inel} + N_{el} = \sigma_{tot} \cdot \int \mathcal{L} dt \quad (3.8)$$

The optical theorem relates the total cross section  $\sigma_{tot}$  to the imaginary part of the forward scattering amplitude. The latter is related to the differential elastic event rate per momentum transfer  $t$ :

$$\sigma_{tot} = \left( \frac{dN_{el}}{dt} \right)_{t=0} \frac{16\pi}{N_{el} + N_{inel}} \frac{1}{1 + \rho^2} \quad (3.9)$$

with the ratio  $\rho$  between the real and imaginary part of the forward scattering amplitude.

TOTEM measures  $dN_{el}/dt$  and  $N_{el}$  with its *roman pots* and  $N_{inel}$  using its forward inelastic detector and the CMS forward HCAL.

## 3.3 Computing on the Grid

After the startup of LHC, several thousand physicists all over the world want to work on several Petabytes of data. Additionally, huge amount of processing power will, and already is, needed for Monte-Carlo simulation. It is just not feasible to aggregate the required amount of storage capacity, computing power and maintenance man power at one site. Hence it has been agreed to distribute the computing system geographically. Along with the necessary high speed connections between all site, this is then called *LHC Computing Grid* (LCG). As the operations on one recorded event are quite independent of all other operations on all other recorded events, it is comparatively simple to parallelize the computing.

To meet the special requirement of high energy physics, the LCG consists of several hierarchical layers, called *tiers*. Each data delivered by the detectors is first stored on tape at the topmost tier T0 located at CERN. Fast reconstruction for calibration and monitoring purposes is performed also on the T0. After dividing the data into streams, depending on the high level trigger decision, a stream is sent to six T1 centers located around the world. After full reconstruction, the T1s distribute the data to a high number

of T2s, which are usually located at single institutes. On these T2s the ordinary user may run his analyses.

The T2s are also used for Monte-Carlo event generation and detector simulation. The simulated data, delivered in a format much like the detector data, is then fed back into the T0 to run down the same path as measured data.

As the particular data sets, a user wants to access, are not necessarily located at his home institute, a set of software tools is used, called *middleware*. Its basic task is to take the users programs, pack them and send them to a computer in the grid with direct access to the desired data. After successful computation, the output of the programs is then fetched back and sent to the submitting user.

## 3.4 Reconstruction

The output of a detector on its basic level consists of electric signals in wires. Even after digitalization and storing in a computer readable format, this is not suitable for physics analyses. Hence these data must be fed through sophisticated algorithms, which try to construct the physical objects back from the detector data. This procedure is hence called *reconstruction*.

In this study three types of objects are used: Muons, jets and missing transverse energy.

### 3.4.1 Muons

Muons are fairly straight forward to identify: They are the only particles passing the whole detector and hence generate signals in the muon system. To measure the momentum of a muon, the curvature of the muon's flight path due to the solenoids field is used. A muon passing a detector component will leave a trail of ionization events, which are called hits. These hits can then be combined to form a track, showing the flight direction of the muon.

In this study only *global muons* are used, whose tracks show hits in both the muon system and the inner tracker.

At first the data of the various strips and wires of the DTs, CSCs and RPCs are used to define points in space, where a muon most likely has passed. Looking at the most separated layers of each chamber, pairs of hits are combined to track segment candidates. If enough hits in the inner layers can be well fitted to one track segment candidate, the candidate is kept and promoted to a track segment.

The track segments of the innermost chambers are then projected outwards to the next chambers using a Kalman-filter technique [41]. Material effects of the return yoke between the chamber are taken into account using GEANE [42]. If a suitable track segment, in the DTs, or suitable hits, in the CSCs, are found, both are combined to a new track. At this point the RPC hits are also used, despite their low spatial resolution. This new track is then again projected to the next chamber, refitted and then again projected to the last chamber. If nothing suitable is found in one chamber, it is just skipped and the next chamber is used. The last fit over all chambers forms the *standalone muon*.

To obtain a global muon, the standalone muon track is extrapolated to the inner tracker. Taking material effects into account, this defines a region of interest in the inner tracker. In this region pairs of hits in different tracker layers are combined to form track seed. These seeds are then used to build tracks in the region of interest. All tracks in the region of interest are now refitted together with the hits of the original standalone track. The best fitting track is then used as the global track.



### 3.4.2 Jets and missing transverse energy

Both jets and missing transverse energy,  $\cancel{E}_T$ , are constructed from *calorimeter towers*. All ECAL cells covering one HCAL cell together with this very cell are combined to a calotower, showing the energy deposit in this fraction of the calorimeter. To provide a precise energy measurement, both calorimeters must be calibrated.

The light yield of the ECAL crystals varies over about 15% among all barrel crystals [32]. Moreover the endcap VPT signal yield varies by almost 25%. Measurements performed during assembly reduce these variations to less than 5% in the barrel and 10% in the endcap. To achieve a uniform response over all cells, intercalibration methods must be performed. During the assembly cosmic muons have been used to provide a first intercalibration, which has been controlled by test-beam measurements. Well understood physics events like  $W \rightarrow e\nu$  or  $Z \rightarrow ee$  will be used during data taking to improve the intercalibration. The light yield, which is affected by irradiation, will be monitored using a laser system.

The HCAL cells have been intercalibrated using radiative sources to check the scintillators and charge injectors to check the electronics [39]. Additional test-beam measurements have been performed to determine the energy scale. The calibration will be monitored using a UV laser system and radiative sources.

The absolute energy scale for both calorimeters depends on the reconstruction purpose, for which the data will be used, e.g. electrons, photons or jets. The jet calibration will be described in section 3.4.2.

#### Jets

A hadronizing particle will usually lead to a bunch of particles, all going in roughly the same direction, which is called *Jet*. If they hit the calorimeter, they will cause a fairly broad area of calorimeters cells to light up. For most analyses, not the calorimeter hits itself, but the hadronizing particle is the interesting object. To reclaim as much information about the primary particle as possible, the calorimeter hits must be regrouped. While there are many algorithms suitable for this task, the *iterative cone* algorithm is used in this study.

The highest energetic calotower is used as a seed, yielding direction and energy of the first iteration. All calotowers in a  $\Delta R \leq 0.5$  cone are then grouped with the seed to form a proto-jet. The weighted average of  $\eta$  and  $\phi$  of this proto-jet is then used as the direction for the next iteration. This is repeated until the energy changes by less than 1% and the direction changes by  $\Delta R < 0.01$ . All calotowers assigned to this now final jet are then removed from the list of calotowers and the process is started over until no calotower exceeding the seed threshold is left.

#### Missing transverse energy

To reconstruct the missing transverse energy, the transverse energy of all calorimeter towers are added up:

$$\vec{\cancel{E}}_T = - \sum \vec{E}_T^{tower} \quad (3.10)$$

The scalar sum of the transverse energy may also be used:

$$E_T^{sum} = \sum |\vec{E}_T^{tower}| \quad (3.11)$$

Both variables are calculated with taking muons into account. To get the  $\cancel{E}_T$  generated by invisible particles alone, one must regard the muons and their energy deposit in the calorimeter.

#### Jet energy scale corrections

Both the detector as well as the clustering algorithms tend to lose a certain fraction of a jet's energy. On the other hand, the pile-up events usually add energy to each jet. To make things worse, both effects are  $\eta$  dependent. Hence the jet energy must be corrected to really represent the underlying physics.

Here the so called  $L2+L3$  corrections are used. The goal of the relative L2 correction is to gain a flat jet response versus  $\eta$ , thus account for the above mentioned  $\eta$  dependence. To accomplish this, correction factors for various eta and jet  $p_T$  regions are determined by comparing calorimeter jets to associated generator jets. Finally these factors are planned to be derived from jet balance in dijet events. After leveling out the response versus  $\eta$ , the L3 correction aims at adjusting the absolute jet energy in a control region,  $|\eta| \leq 1.3$ . Hence a  $p_T$  dependent correction function is determined by again comparing the calorimeter jets to matched generator jets. When real data will be available, the function parameters will be determined by balancing  $\gamma/Z$ +jets events.

The corrections determined for the jets are then used to correct the  $\cancel{E}_T$ , too. The  $\cancel{E}_T$  is divided into clustered and unclustered energy. The former is the energy in calorimeters assigned to a jet, the latter everything left. The clustered energy is then corrected using the above jet correction. Additionally muons must be added to the energy contributing to the  $\cancel{E}_T$ , as they are nearly invisible for the calorimeters.

## 4 Analyses

This study aims at evaluating the potential of CMS to discover supersymmetry. New physics involving new particles, i.e. supersymmetry, usually manifests in a tiny change of the total cross section, because there are new processes made possible by the new particles. As one can see in Fig. 3.1 the cross sections of supersymmetric processes (pink, at about 10 pb) are about ten orders of magnitude lower than the total cross section. Fortunately these new processes usually generate events with different signatures than the Standard Model. By carefully choosing requirements, called cuts, to be fulfilled by events, it is possible to choose a signature, which prefers the new physics events. Then one may count the events passing the cuts and compare the number of measured events with the number of events expected from the Standard Model.

In this study two approaches are used to choose the requirements: A conventional cut based analysis, and a multivariate analysis based on *Boosted Decision Trees* (BDT).

Both analyses require detailed knowledge of both the new physics, the Standard Model and the detector response. To gain this information Monte Carlo simulations of the elementary physics processes and the detector are carried out.

Aspects common to both analyses will be discussed in the next section, including Monte Carlo samples, systematic uncertainties, statistical methods and common preselection cuts. Next both analyses are presented separately in more detail, followed by a comparison of both methods.

The first round of data taking will be at a center of mass energy of only 10 TeV. As the collected luminosity of about  $10 \text{ pb}^{-1}$  is not sufficient for a discovery of most fractions of the mSUGRA parameter space, all following studies look at events with a center of mass energy of 14 TeV.

### 4.1 Common aspects

#### 4.1.1 Monte Carlo samples

##### Signal

After choosing the mSUGRA parameters, the sparticle masses and decays are computed using the SUSY-HIT package [43]. It utilizes SOFTSUSY [44] for mass spectrum calculations and SDECAY/HDECAY [45, 46] to calculate decay widths and branching fractions. The obtained mass spectra can be found in appendix D. These data are then passed to PYTHIA [47], which generates the events. These events are then put through the CMS simulation and reconstruction chain.

For each used LM point, about  $10^5$  events have been produced.

Using the mass spectrum, PROSPINO2 [48] is used to calculate leading- (LO) and next-to-leading order (NLO) cross sections.

### Standard model background

On a very basic level of understanding, supersymmetry manifests itself through decaying heavy particles. Consequently the main backgrounds are Standard Model processes involving heavy particles or high energies. Most of the considered backgrounds would not result in many jets on their own, but at a hadron collider additional jets are likely produced by initial and final state gluon radiation (ISR/FSR). ALPGEN [49], which is used to produce  $W/Z$ +jets and  $t\bar{t}$  events, takes this effect into account by generating events according to the leading order matrix elements up to high jet multiplicities. All backgrounds generated with ALPGEN are grouped into subsamples depending on the number of additional jets. With the exception of the sample with the highest jet multiplicity, all of these samples are *exclusive*, hence they contain exactly the stated number of additional jets. The samples with the highest jet multiplicities are *inclusive*, containing also events with more than the stated number of jets.

QCD-multijet, Drell-Yan and boson pair events are produced with PYTHIA, which approximates the production of additional jets via a parton shower algorithm and is expected to underestimate the number of additional jets with high momentum. The following backgrounds are considered in this study:

- Pair production of the heaviest quark, hence  $t\bar{t}$ , is fairly abundant with a cross section of 833 pb (NLO+NLL<sup>1</sup>) [50]. Even worse, its signature is very much like supersymmetry: Occasional leptons, some jets and missing energy. The number of jets is increased even more by ISR/FSR jets, of which up to four are simulated by ALPGEN.
- W bosons are produced even more frequently, because of a cross section of about 66 nb (NLO). Vector boson cross sections are calculated using MCFM [51]. If the boson decays leptonically, the lepton and the neutrino fulfill part of the requirements of the  $\mu$ +jets+ $\cancel{E}_T$  channel. To produce a significant amount of missing energy, the boson must be fairly off shell, which reduces the probability to get such an event. Jets can be produced by ISR/FSR, which may even increase the amount of missing energy by boosting the boson transverse to the beam. To take a detailed look at these highly boosted bosons, the samples with up to five additional jets are again divided into four subsamples with increasing transverse momentum of the boson up to 1.6 TeV.
- Z bosons are a bit rarer with a cross section of 6.6 nb (NLO). There will be either charged leptons ( $Z \rightarrow ll$ ) or missing energy ( $Z \rightarrow \nu\nu$ ), hence to have both, either must be somehow faked by secondary physics or detector effects. The samples are subdivided like the W boson samples.
- Off-shell Drell-Yan processes may result in significant amounts of missing energy, hence four samples with boson masses higher than 200, 500, 1000 and 1500 GeV are also used. These four samples have a combined cross section of about 1.8 pb (LO), because only decays into muon-pairs are considered. Bosons with masses below 200 GeV are contained in the Z+jets samples.
- Pair production of vector bosons, here WW, WZ and ZZ, will increase the number of muons, amount of missing energy and eventually the number of jets compared

---

<sup>1</sup>Next-to-leading-logarithmic

to single boson production. With a cross section of about 108 pb (LO), they are frequent enough to be considered.

- Multijet events (often called *QCD-events*) are caused by the production of light quarks and gluons. As there is a very limited number of highly energetic isolated leptons or neutrinos, these events are usually not expected to fulfill the signature requirements. Particularly missing transverse energy may be faked by jet or muon miss-measurement. The probability to fake missing transverse energy increases with the amount of transverse energy in the event. As the cross section falls steeply with the amount of transverse energy, the events are divided into 21 samples with increasing transverse momentum  $\hat{p}_T$  of the produced partons. Although the probability for a large misreconstructed  $\cancel{E}_T$  is rather small, it may still be a problem because of the extremely high cross section of such events of the order of millibarn.

Both generators used will only calculate the LO cross section of the simulated processes. Higher order calculations like [50] or using MCFM for W- and Z-production usually return only the total cross section without subdivision into jet or  $p_T$  samples. By comparing total LO and NLO cross section, a *k-factor* can be obtained. This k-factor is then applied to the LO cross sections of the subsamples to get an estimate of the NLO cross section. This approach is known to be only an approximation, but detailed calculations of NLO cross sections for all jet and  $p_T$  samples are not available. A detailed listing of all samples used, their cross section and number of simulated events can be found in appendix E.

#### 4.1.2 Systematic uncertainties

If one knows the number of expected signal and background events, these numbers can be compared to the number of measured events. Depending on the numbers, the signal may be observed or not. Unfortunately there are various reasons why these numbers may not be precisely known. These uncertainties, systematically influencing the outcome of the experiment, must be taken into account during the significance calculations.

Depending on the type of systematic uncertainties, the effect on the expected number of events may be correlated for all or some samples.

Systematic uncertainties on the following quantities are taken into account in this study.

##### Luminosity

Using the method described in section 3.2.6, a precision for the integrated luminosity of 5% or better is expected. Consequently a luminosity uncertainty of 5% is assumed for this study. The luminosity error is correlated for all samples.

##### Cross sections

Cross sections for various processes may either be measured, e.g. W or Z production, or must be calculated. Uncertainties on measurements are usually easier to access, but may take some time. The precision of theoretical calculations strongly depends on the processes involved. While electroweak interactions are well understood, strong interactions are more difficult to calculate with high accuracy due to large higher order corrections. For all processes the cross sections depend on the parton density functions, which are also known only to a certain precision.

Before detailed cross section studies at CMS are available, an uncertainty of 10% is used on all samples. Internal studies [52] showed a uncertainty of this order induced by

uncertainties on the parton density functions. These errors are assumed to be correlated for samples of one type, i.e. all  $t\bar{t}$  jet bins, but uncorrelated for different processes.

### Jet energy scale

The jet energy calibration is affected by some uncertainty, thus it is not expected to be exact. For  $1 \text{ fb}^{-1}$  an uncertainty of 5% is expected [53] at  $1 \text{ fb}^{-1}$ .

To estimate the effect of the jet energy scale uncertainty, each analysis is run three times. Once with the original jets, once with the jet energy shifted 5% up and once shifted 5% down. The deviation in the number of events can be different for shifting up and down, but the used statistical methods can only work on symmetric errors, hence both deviations are averaged:

$$\Delta N_{JES} = 1/2 \cdot (|\Delta N^{+5\%}| + |\Delta N^{-5\%}|) \quad (4.1)$$

This uncertainty is correlated for all samples.

### Limited number of simulated events

Monte Carlo simulations are prone to statistical fluctuations as they rely on random number generation. For a given process with cross section  $\sigma$ , the number of expected events for an integrated luminosity  $\mathcal{L}$  is  $N_{exp} = \sigma \cdot \mathcal{L}$ . Usually the simulated number of events does not equal this number, hence each simulated event must be weighted with a weight  $w = N_{exp}/N_{sim} = \sigma \mathcal{L}/N_{sim}$ . After applying cuts, the number of events expected to pass these cuts is then  $N_{exp}^{cut} = w \cdot N_{sim}^{cut}$ . Because of the random nature of Monte-Carlo simulations, the number of simulated events passing the cuts  $N_{sim}^{cuts}$  is known only with an uncertainty  $\sigma_{sim} = \sqrt{N_{sim}^{cuts}}$ . This uncertainty is propagated to the expected number of events passing the cuts:  $\sigma_{exp} = w \cdot \sqrt{N_{sim}^{cuts}}$ .

These uncertainties are uncorrelated for all samples.

For some samples the simulated number of events is so low, that the weight  $w$  is much larger than 1, resulting in a very large error. This is in particular a problem, if the number of events passing the cuts drops to zero already for early cuts. Then the efficiency of later cuts can not be determined any more, and an 68% upper limit of  $N_{exp}^{limit} = 1.15 \cdot \sigma \cdot \mathcal{L}/N_{sim}$  must be applied. For W-, Z- and  $t\bar{t}$  samples, the subsamples share a common weight for each group, which allows to handle them at once and only apply the upper limit if no subsample of one sample shows events passing the cuts. The W+0jets sample possesses a weight different than the other W+jets sample, hence it must be treated separately. QCD, boson-pair and Drell-Yan samples possess different weights for each subsample, thus all these samples must be looked at separately.

#### 4.1.3 Statistical interpretation

In order to determine the expected significance of an observation, a modified frequentist approach [54, 55] is applied. If the expected number of signal events  $s$  and the number of background events  $b$  are known without any systematic uncertainties, one can calculate, for a measured number of events  $d$ , the log-likelihood-ratio  $\ln(Q)$ .

Here  $Q$  is the probability of the signal+background hypothesis to yield the measured number of events, divided by the probability of the background-only hypothesis to do this, assuming Poisson distributions for both hypotheses:

$$Q = \frac{(s+b)^d \cdot e^{-(s+b)}}{b^d \cdot e^{-b}} \quad (4.2)$$

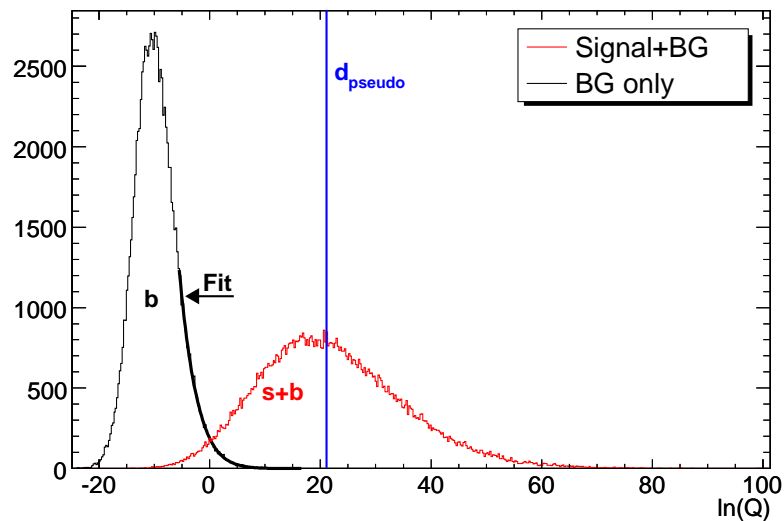


**Figure 4.1:**  $\ln(Q)$  distribution of the background-only hypothesis ( $b$ ) and the signal+background hypothesis ( $s + b$ ), respectively. The separation of both distributions determines the discrimination power between the two hypotheses. An  $\ln(Q)$  for data ( $d$ ) close to the background only curve indicates agreement with the background-only hypothesis. In contrast a large  $\ln(Q)$  for data ( $d$ ) close to the  $s + b$  curve would point to some new physics not consistent with the background only hypothesis.

The higher the value of  $\ln(Q)$ , the more *signal-like* the measured data are.

In case of systematic uncertainties on the expected numbers of events, this approach has to be extended: Pseudo-experiments are performed, in which the expected number of background events  $b$  and signal+background events  $s + b$  are varied according to their statistical and systematic uncertainties, while taking correlations into account. A series of pseudo-experiments is performed assuming  $d$  to be background like, i.e.  $d = \text{Poisson}(b)$  resulting in the expected background-only  $\ln(Q)$  distribution (see  $b$ -curve in Fig. 4.1). In addition pseudo-experiments are generated in which  $d$  is diced according to the expected number of signal+background events, i.e.  $d = \text{Poisson}(s + b)$  (see  $s + b$ -curve in Fig. 4.1).

Finally, these two distributions have to be compared to the  $\ln(Q)$  value of the measured events  $d_{meas}$ . The probability to find a background only pseudo-experiment with a  $\ln(Q)$  larger than the the  $\ln(Q)$  of the measured data is commonly denoted as  $1 - CL_B$ . It corresponds to the fraction of the  $b$ -curve in Fig. 4.1 at the right side of the  $d$ -line. Data are considered incompatible with the background-only hypothesis, if this is sufficiently small. The calculated probability  $CL_B$  can be translated via a one-sided Gaussian into standard deviations. A probability of smaller than  $2.8 \cdot 10^{-7}$ , which corresponds to a Gaussian  $5\sigma$  single-sided deviation, is commonly declared as a discovery.

Since this is a MC only study without any measured data, the expected discovery potential for SUSY can be determined assuming that the data correspond to the median  $\ln(Q)$  of the signal plus background curve (see  $d_{Pseudo}$ -line in Fig. 4.1).

In order to test the sensitivity for a  $5\sigma$  deviation from the background only hypothesis, this approach would need at least  $10^9$  pseudo-experiments to have sufficient statistics in the region of interest. This can easily take days of computing time. Therefore a Gaussian distribution is fitted to the tail of the background-only distribution and extrapolated to regions with very low probability close to the signal plus background distribution (see thick line in Fig. 4.1). Especially for low number of events, the curves usually are non-gaussian, but then the significance is usually small enough to be calculated without a fit.



This extrapolation proved to slightly overestimate the significance, thus values significantly larger than  $5\sigma$  have to be interpreted with care.

Repeatedly applying this method to the same numbers revealed deviations on the significance of the order of 5% for a significance of about  $5\sigma$ , increasing up to around 10% at  $10\sigma$ . This gives an indication of the statistical accuracy of the results shown later.

#### 4.1.4 Preselection

In order not to be overwhelmed by uninteresting events, certain preselection cuts must be applied. They reduce the number of events used later for optimization to a manageable amount. These cuts consist first of the high level trigger: Events which do not pass the trigger would never enter the analysed data sets. The trigger thresholds are described in section 3.2.5. As the the trigger thresholds are not finally decided and the  $p_T$  measurement of the trigger not very precise, the cuts made by the trigger must be refined later on.

#### Muon identification

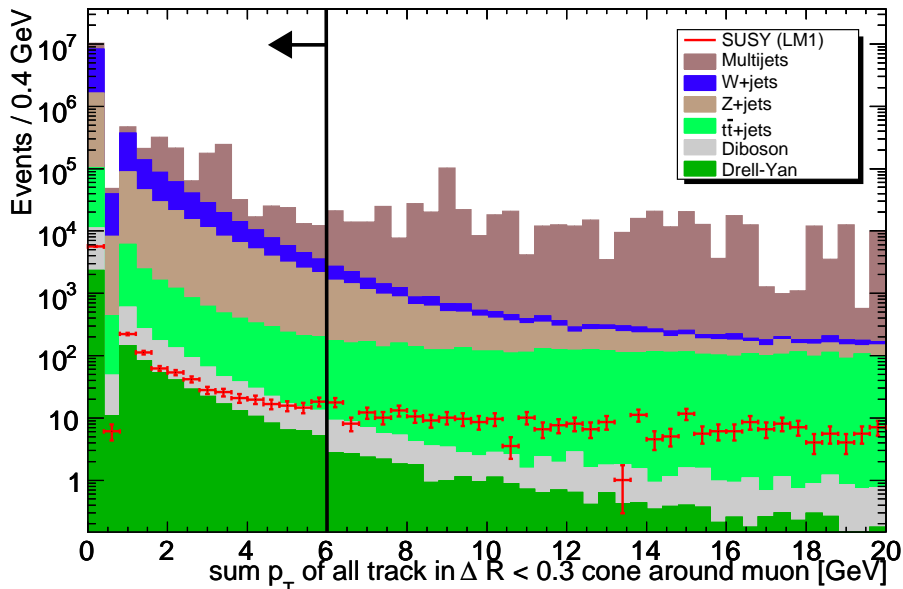


**Figure 4.2:** Isolation of the leading muon, showing the high number of unisolated muons in QCD-multijet,  $t\bar{t}$  and supersymmetric events.

To exclude poorly reconstructed muons, at least 12 hits in the tracker and the muon system together are required. Additionally the track must be fitted with a certain quality, we require  $\chi^2/N_{DOF} \leq 3$ .

Muons are not only produced promptly in interesting decays, but also during or after the hadronization generating a jet in heavy flavor decays. These muons are usually found in jets, hence they are not isolated. To exclude these muons, the transverse momentum sum of all tracks within  $\Delta R < 0.3$  around the muon track must be lower than 6 GeV (Fig. 4.2).

Similar to the trigger acceptance and threshold, only muons with  $\eta < 2.1$  and  $p_T \geq 20$  GeV are considered (Fig. 4.3). At least one muon per event passing all preselection cuts is required.



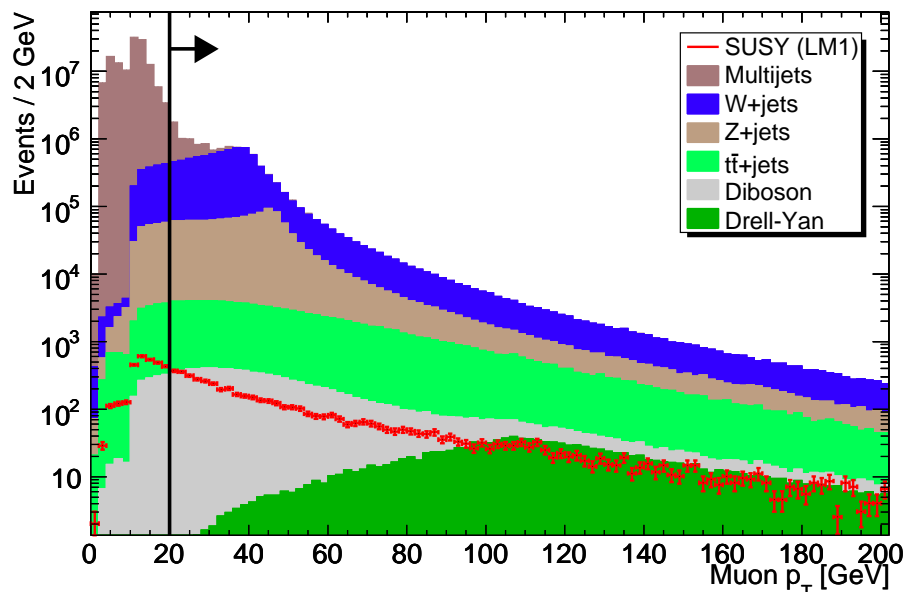


**Figure 4.3:** Transverse momentum of the leading muon, showing the turn-on behavior in  $p_T$  of the triggers and the QCD multijet rejection.

The tables 4.3 and 4.4 show the efficiencies of all cuts. The rejection by the HLT and the muon cuts are roughly the same for signal samples and most of the backgrounds with the exception of Drell-Yan and QCD-multijet. The Drell-Yan samples are restricted to muon production, hence a very high trigger efficiency of about 95% is observed. As expected, the QCD background contains nearly no muons. Consequently it is reduced by about six orders of magnitude by the HLT alone. Most of the muons found by the HLT are either fakes or of such low energy that they do not pass the muon  $p_T$  cut, which can be seen in Fig. 4.3. Hence the muon acceptance cuts further reduce the QCD background by about two orders of magnitude. Samples with a high contribution of heavy flavor decays usually contain a fraction of non-isolated leptons. This is the case for  $t\bar{t}$ , QCD-multijet and not least supersymmetry, which can be seen in Fig. 4.2 and in the efficiency of the muon identification cuts.

### Jets and MET

As shown in Table D.1 of the appendix, the LSP mass is usually of the order of 100 GeV. In R-parity conserving supersymmetry, two of these LSPs will leave the detector unseen. Consequently, we require at least 100 GeV missing transverse energy at the preselection level (see Fig. 4.5). To ensure properly reconstructed jets and a reasonably precise jet energy scale, only jets with  $|\eta| \leq 2.5$  are considered. A minimum of 10% of the jet energy must be reconstructed in the HCAL to exclude electrons and photons from the collection of jets.

Production of squarks and/or gluinos will usually lead to cascade decays (see section 2.2.7). Both decaying gluinos and squarks are expected to generate jet of a about 100 GeV (see Table D.1). Consequently the preselection requires at least three jets with  $E_T \geq 80$  GeV for the cut based analysis. For the BDT analysis a softer preselection of 50 GeV is applied to provide a larger phase space to work with.

Samples containing only one boson (W+jets, Z+jets and Drell-Yan) are mostly rejected

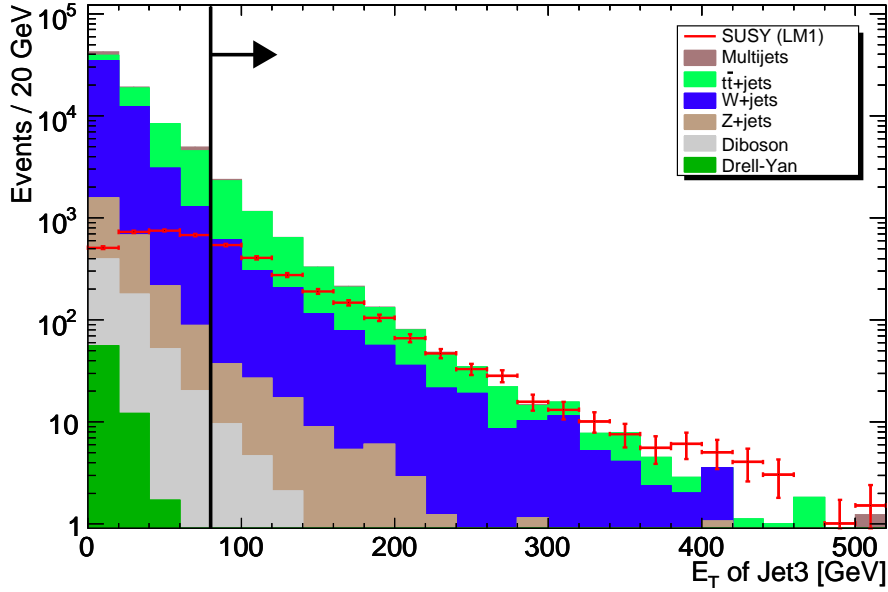


Figure 4.4:  $E_T$  of the third jet at the preselection level shown after application of all other preselection cuts.

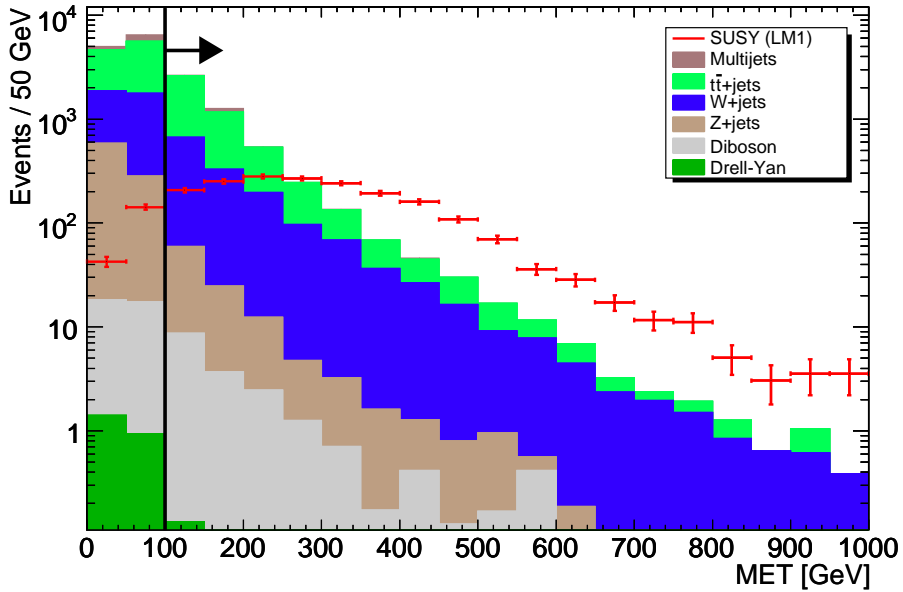


Figure 4.5:  $\cancel{E}_T$  at the preselection level shown after application of all other preselection cuts.

by the jet preselection cuts (see tables 4.3 and 4.4), as the boson must have decayed leptonically to fulfill the requirements of the muon preselection. The probability of getting enough highly energetic jets from ISR/FSR increases with the number and energy of the additional jets, which is confirmed by detailed examination of the cut efficiencies for each subsample. This is also the case for  $t\bar{t}$ , however a hadronically decaying top quark may generate two 80 GeV jets, as long as it is slightly boosted and the energy is evenly distributed among both jets. In vector boson pair production, one of the bosons may decay hadronically, resulting in a slightly higher probability of passing the jet preselection. A detailed examination of the QCD-multijet subsamples confirms that only these subsamples

pass the cuts, in which the  $\hat{p}_T$  of one of the partons at least roughly doubles the 80 GeV of the jet preselection cut.

The *MET preselection* row of the cut efficiency Table 4.3 and a separated examination of the boson pair samples proves that W bosons produce more  $\cancel{E}_T$  than Z bosons in decays with charged leptons. For QCD-multijet samples passing the jet preselection, the probability to fake a  $\cancel{E}_T$  greater than 100 GeV is high enough to allow for about 10% of the events to pass the  $\cancel{E}_T$  cut. However the simulated statistics are at this point already too low to allow investigation of the correlation between this probability and the  $\hat{p}_T$ .

Distributions of the variables used in the preselection, which are not shown here, can be found in the figures in appendix A.

The preselection cuts reduce the total background by about ten orders of magnitude, while reducing the signal by only about one order of magnitude. This results in a signal to background ratio of about 40% for LM1. As the uncertainty of the background is about 20%, the signal to background ratio is still too low to allow for a significant observation. To increase the significance, existing or new cuts must be optimized. This is done in the next two sections with two different approaches, which are compared afterwards.

## 4.2 Conventional Analysis: Rectangular cuts

In this section additional cuts are introduced and optimized in a rather straight forward way. In addition to the muon variables, the  $E_T$  of the three leading jets and the  $\cancel{E}_T$ , angular correlations between the leading muon, the three leading jets and the  $\cancel{E}_T$  are used to improve the selection.

In QCD multijet events and other events without highly energetic invisible particles, high  $\cancel{E}_T$  is likely to be caused by mis-reconstructed jets or muons. Consequently we restrict the angle in the transverse plane between  $\cancel{E}_T$  and the leading jets, likewise the angle between the leading muon and the  $\cancel{E}_T$ :  $|\Delta\phi|(\cancel{E}_T, \text{Muon}_1)$  and  $|\Delta\phi|(\cancel{E}_T, \text{Jet}_{1,2,3})$ .

### 4.2.1 Optimization strategy

The following optimization is performed on LM1, the resulting cuts are then applied to all LM points. Optimizing the cuts for each LM point separately is the task of the BDT based analysis, as it is rather labor intensive.

As a quick, but reasonable estimate of the expected significance,  $N_s/\sigma_b$  is used.  $N_s$  is the number of expected signal events,  $\sigma_b$  the uncertainty on the number of background events. This uncertainty is the squared sum of all systematic errors (see section 4.1.2) and the statistical Poisson uncertainty  $\sigma_{stat} = \sqrt{N_B}$  of the background. Due to technical limitations, the correlation of the cross section errors can not be taken into account, hence a global error of 8% on the number of background events is used as a substitution for an exact calculation.

Using this estimator, first  $|\Delta\phi|(\cancel{E}_T, \text{Muon}_1)$  (Fig. 4.6(a)) and then  $|\Delta\phi|(\cancel{E}_T, \text{Jet}_{1,2,3})$  (Fig. 4.6(b) to 4.7(b)) is optimized to deliver a high significance. Afterwards each of these cuts is again optimized, while fixing the three other angular cuts. Each time a large change occurred, the process is started over.

As expected, this reduces the QCD-multijet background by at least two orders of magnitude, as shown in Table 4.3. The rejection may be even higher, but the statistics are too low to say more. For samples without invisible particles, like Z+jets fulfilling the muon cuts, the rejection is slightly higher than for the other samples. High mass Drell-Yan is an exception, as at least one high energetic muon tends to fly along the beam and is hence lost to the reconstruction, which causes a real missing energy.

In the same way, the cuts on  $E_T$  of the first and second jet and  $\cancel{E}_T$  are then optimized (see Fig. 4.2.1 and 4.2.1). Hardening the cut on the third jet proved to yield no significance gain.

As a last step, each of the above cuts is reevaluated while fixing all other cuts.

Following this procedure, the following cut values are obtained:

- $|\Delta\phi(\mu, \cancel{E}_T)| \geq 0.8$
- $|\Delta\phi(\cancel{E}_T, \text{Jet}_{1,2,3})| \geq 0.6$
- $p_T^{\text{Jet1}} \geq 200 \text{ GeV}$
- $p_T^{\text{Jet2}} \geq 150 \text{ GeV}$
- $p_T^{\text{Jet3}} \geq 80 \text{ GeV}$
- $\cancel{E}_T \geq 250 \text{ GeV}$

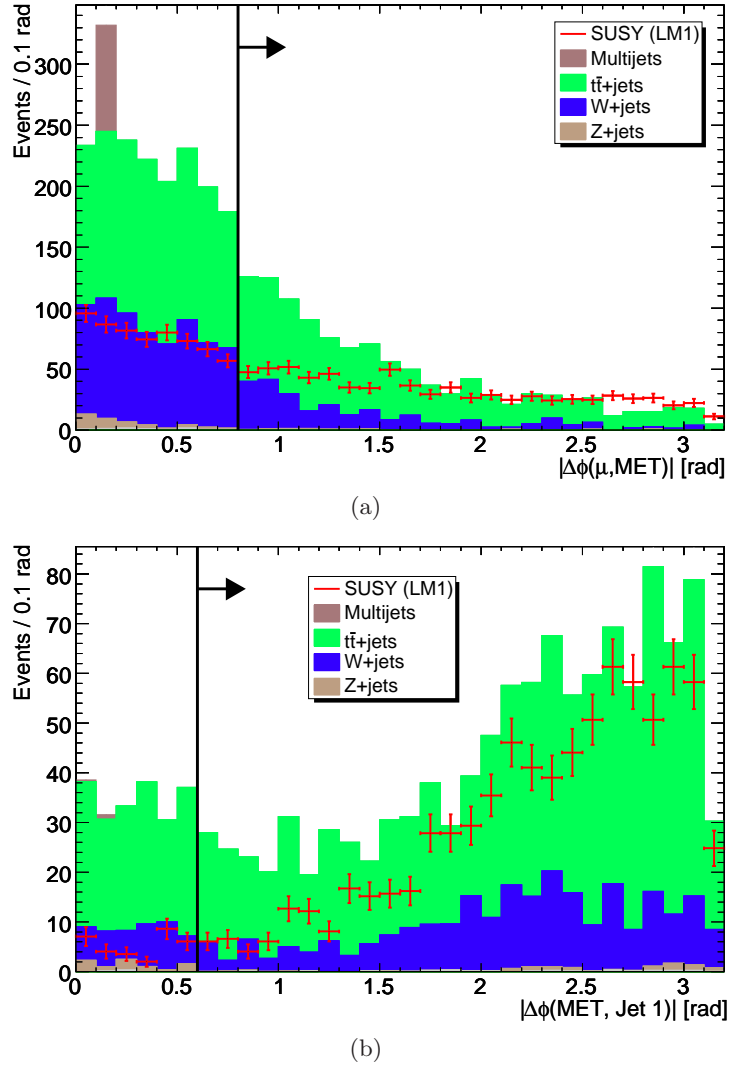


**Figure 4.6:** Angular correlations between the leading jet and leading muon respectively the missing transverse energy. Each distribution is shown after all preselection cuts and after the three other angular cuts.

The significance proved to be usually insensitive to small changes of the cut values. However low statistics of some background samples sometimes lead to abrupt changes of the significance during small changes of the cuts. To take this into account, the cut values are later rounded to amounts roughly matching the detector resolution and accounting for the statistics left after previous cuts.

All these cuts work well against the dominant remaining backgrounds,  $W$ +jets and  $t\bar{t}$ , as for both samples the particles must be severely boosted to yield jets and  $\cancel{E}_T$  of such energies. They reduce the background by more than two orders of magnitude, while the signal is reduced by less than one order of magnitude. This leads to a signal to background ratio of about 10 for LM1 after applying the upper limits to the background.

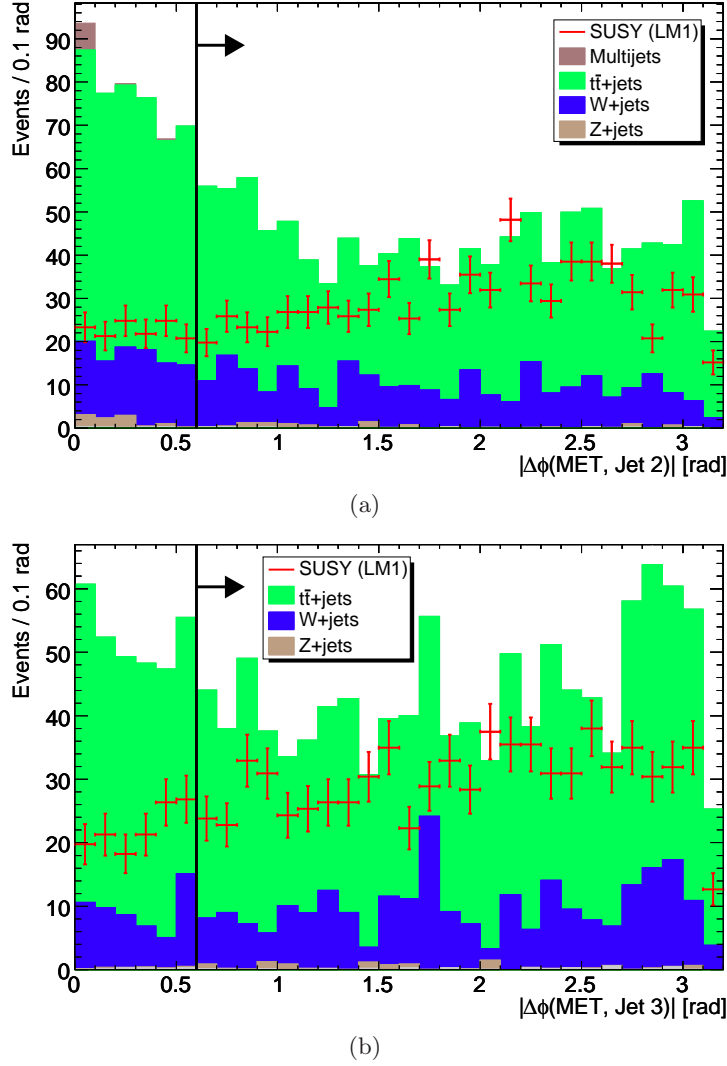


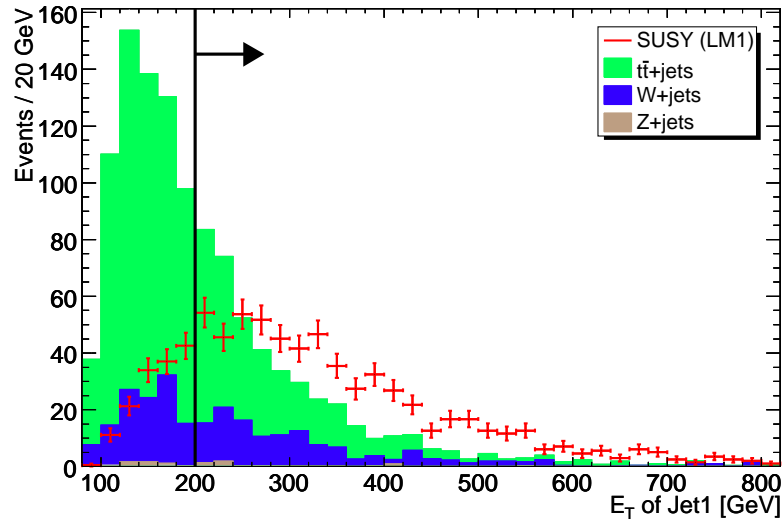
**Figure 4.7:** Angular correlations between the missing transverse energy and the second and third leading jet, respectively. Each distribution is shown after all preselection cuts and after the three other angular cuts.

#### 4.2.2 Results

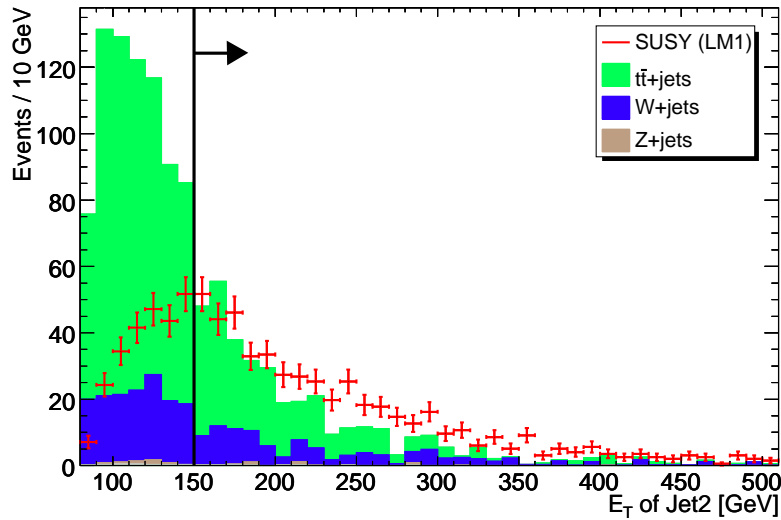
Table 4.1 shows the number of events expected to pass the cuts for  $1 \text{ fb}^{-1}$ . The dominant backgrounds after the optimized selection are W+jets and  $t\bar{t}$ . As one can see by comparing the *no limit* column with the *upper limit* column, the QCD multijet background contributes mainly due to the upper limits caused by insufficient Monte Carlo statistics.

Upper limits are not applied for the W+0jets sample and all QCD multijet samples with  $\hat{p}_T < 300 \text{ GeV}$ . As no W+0jets events pass the jet preselection cuts (see Table 4.3) and no events in the W+1jet samples pass all cuts, the W+0jets contribution can safely be assumed to be negligible. Already after the angular correlation cuts, no QCD multijet event is left, as shown in Table 4.3. The following three hard cuts on jets and  $\cancel{E}_T$  are expected to further suppress this background by several orders of magnitude. Hence the QCD multijet background contribution is expected to be negligibly.

A conservative upper limit is applied on all QCD multijet samples with hard parton  $\hat{p}_T > 300 \text{ GeV}$ , because in these events the  $\hat{p}_T$  of the hard interaction is of the order of



(a) Leading jet



(b) Second leading jet

**Figure 4.8:** Transverse energy of the first and second jet shown after all other cuts, except for  $\cancel{E}_T$ .

magnitude of the  $\sum p_t$  of all selected objects. Ultimately the QCD multijet background must be estimated from data, i.e. by the *cut inversion* technique, which has been used in various TEVATRON analyses, e.g. [56].

Table 4.1 also shows the uncertainty caused by limited Monte-Carlo statistics  $\sigma_{MC}$  and the other systematic uncertainties combined in  $\sigma_{sys}$ .

The last column shows the expected significance, calculated as described in section 4.1.3, for each LM point, indicating the discovery reach for  $1 \text{ fb}^{-1}$ .

LM1, LM4 and LM8 are fairly easy to discover, reaching a  $5 \sigma$  discovery already at  $100 \text{ pb}^{-1}$ , as shown in Table 4.2. As shown in this table, it appears to be possible to discover LM1 even at  $40 \text{ pb}^{-1}$ , because of its high cross section and because it is the point, on which the analysis has been optimized. However in the first  $40 \text{ pb}^{-1}$  of data the systematic uncertainties are not expected to be controlled as well as assumed in this study. Hence a discovery before  $100 \text{ pb}^{-1}$  is highly unlikely.

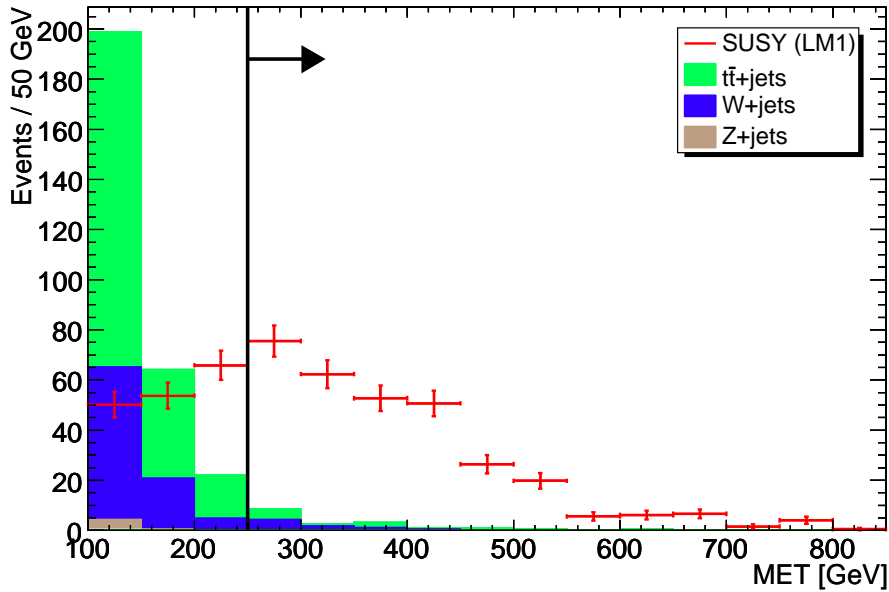


**Figure 4.9:** Final cut: Missing transverse energy  $\cancel{E}_T$ . Distribution is shown after all other cuts.

While LM6 is reachable at  $1 \text{ fb}^{-1}$ , all other LM points need a higher integrated luminosity, better controlled systematic uncertainties and/or other separators.

Looking at the number of events versus the cross section in Fig. 4.10(a), no strong correlation is found. Hence the different properties of the various LM points affect the efficiencies of the cuts. Figure 4.10(b) shows the cut efficiency depending on the mass of the LSP. As the mass of the LSP directly affects  $\cancel{E}_T$  and thus the efficiency of one of the most important cuts, there is an obvious correlation. However there are some outliers: For LM10, the squarks are heavier than the gluino, forcing it to decay via virtual squarks. This leads to soft jets at the beginning of the decay chain, reducing the efficiency of the jet preselection cuts, as shown in Table 4.4. This is partly compensated by the hard jets and rich muon content of the top-stop based decays.

For LM8 the squark and gluino masses are almost degenerated, allowing an additional  $\tilde{q} \rightarrow q\tilde{g}$  decay, which yields an additional soft jet. All gluino or squark based production will end up in stops, hence a large top content leads to even more soft jets and many muons. This increases the efficiency of the muon cuts and the jet preselection cuts.

The chargino/neutralino and slepton mass hierarchy of LM6 leads to a large number of muons. Generally heavy squarks generate hard jets, increasing the efficiency of the two hard jet cuts.

For LM2, the stau is much lighter than the smuon, decreasing the number of muons per event. Hence the efficiencies of the muon cuts are relatively small, however this is partly compensated by the hard jets due to heavy squarks.

### Comparison to previous studies

The most notable study about the mSUGRA discovery potential of CMS have been done for the *Physics TDR, Volume II* [18, 24]. It is based on rectangular cuts, which have been optimized using a genetic algorithm. The optimization has been aimed to maximize the significance at  $10 \text{ fb}^{-1}$ . At this integrated luminosity, about 311 LM1 signal events and 2.5 background events are expected to pass the cuts. Some systematic uncertainties are ex-



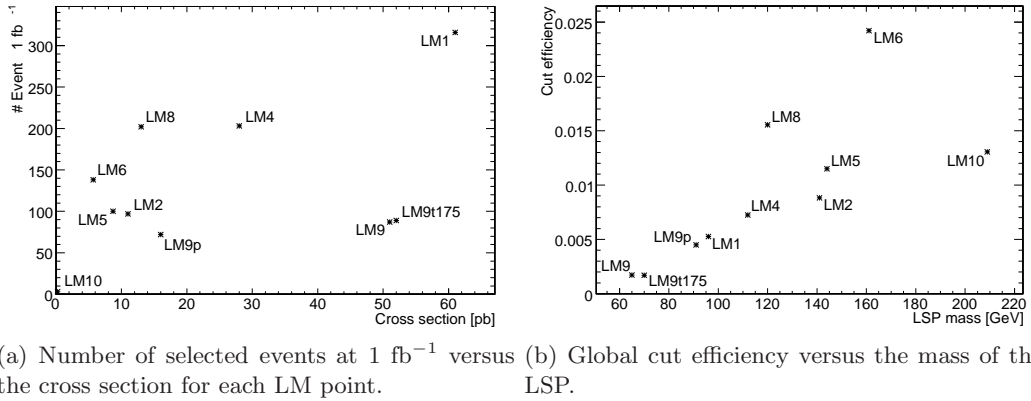


Figure 4.10:

pected to be better controlled at  $10 \text{ fb}^{-1}$  with respect to  $1 \text{ fb}^{-1}$ . Especially the uncertainty on the jet energy scale has been assumed to be only 3%, which results in a uncertainty on the number of events of 10%. A significance estimator based on a convolution of a poisson distribution and Gaussian distribution has been used. The stochastic fluctuation of the number of events is covered by the poisson distribution, while the Gaussian distribution takes the systematic uncertainties into account. The following significances have been reached:

- LM1: 34
- LM4: 29
- LM5: 23
- LM6: 32

The high significances can be reached because of the low expected background. However the main backgrounds ( $t\bar{t}$ ,  $W$ +jets,  $Z$ +jets) have been simulated using PYTHIA. With respect to ALPGEN, which has been used in the present study, PYTHIA underestimates the number and energy of ISR/FSR jets. Also only LO cross sections have been used.

If one applies the cuts used by the PTDR analysis on the samples used in the present study, the background increases by more than one order of magnitude. This reduces the significance to the about the order of magnitude reached in the present study, however at ten times the integrated luminosity.

| Sample         | # Events @ $1 \text{ fb}^{-1}$ |             | $\sigma_{MC}$ | $\sigma_{sys}$ | Significance<br>@ $1 \text{ fb}^{-1}$ |
|----------------|--------------------------------|-------------|---------------|----------------|---------------------------------------|
|                |                                | upper limit | [# Events]    |                |                                       |
| W+jets         | 8.3                            | 8.6         | 1.7           | 2.3            | -                                     |
| Z+jets         | 0.095                          | 1.2         | 1.0           | 0.28           | -                                     |
| $t\bar{t}$     | 9.2                            | 9.2         | 1.9           | 4.7            | -                                     |
| Diboson        | 0.25                           | 0.44        | 0.19          | 0.088          | -                                     |
| Drell-Yan      | 0.013                          | 0.058       | 0.043         | 0.013          | -                                     |
| QCD            | 0.0                            | 9.8         | 6.0           | 2.2            | -                                     |
| Background sum | 18                             | 29          | 6.6           | 9.3            | -                                     |
| LM1            | 316                            | -           | 13            | 57             | 9.9                                   |
| LM2            | 97                             | -           | 3.1           | 13             | 3.7                                   |
| LM4            | 203                            | -           | 7.5           | 34             | 6.7                                   |
| LM5            | 100                            | -           | 3.0           | 14             | 3.9                                   |
| LM6            | 138                            | -           | 2.8           | 15             | 5.1                                   |
| LM8            | 202                            | -           | 5.1           | 34             | 6.8                                   |
| LM9            | 89                             | -           | 6.5           | 23             | 3.6                                   |
| LM10           | 3.0                            | -           | 0.08          | 0.6            | 0.18                                  |
| LM9p           | 72                             | -           | 3.3           | 13             | 2.9                                   |
| LM9t175        | 87                             | -           | 6.4           | 23             | 3.5                                   |

**Table 4.1:** Numbers of events for backgrounds and signals after all cuts with uncertainties scaled to an integrated luminosity of  $1 \text{ fb}^{-1}$ . The column labeled upper limit contains numbers of events after implementing an upper limit in samples with zero selected events, as described in the text.  $\sigma_{MC}$  is the uncertainty due to the limited number of simulated events;  $\sigma_{sys}$  the combined systematic uncertainty.

| LM-Point | Integrated luminosity |                      |                       |                     |
|----------|-----------------------|----------------------|-----------------------|---------------------|
|          | $10 \text{ pb}^{-1}$  | $40 \text{ pb}^{-1}$ | $100 \text{ pb}^{-1}$ | $1 \text{ fb}^{-1}$ |
| LM1      | 2.9                   | 5.6                  | 7.3                   | 9.9                 |
| LM2      | 1.1                   | 2.1                  | 2.7                   | 3.7                 |
| LM4      | 2.1                   | 4.1                  | 5.2                   | 6.7                 |
| LM5      | 1.2                   | 2.2                  | 2.8                   | 3.9                 |
| LM6      | 1.7                   | 2.7                  | 4.1                   | 5.1                 |
| LM8      | 2.1                   | 4.1                  | 5.0                   | 6.8                 |
| LM9      | 1.1                   | 2.0                  | 2.6                   | 3.6                 |
| LM10     | 0.04                  | 0.09                 | 0.13                  | 0.18                |
| LM9p     | 0.9                   | 1.7                  | 2.2                   | 2.9                 |
| LM9t175  | 1.0                   | 2.0                  | 2.6                   | 3.5                 |

**Table 4.2:** Modified Frequentist significances expected for the different SUSY benchmark points and different amounts of integrated luminosity.

| Cut                                | W+0jets         | W+jets          | Z+jets          | $t\bar{t}$      | Diboson          | Drell-Yan    | QCD              | All BG            |
|------------------------------------|-----------------|-----------------|-----------------|-----------------|------------------|--------------|------------------|-------------------|
| No cuts                            | 5.07e+07        | 1.48e+07        | 6.58e+06        | 8.28e+05        | 1.08e+05         | 1750         | 8.03e+13         | 8.03e+13          |
| Trigger<br>Efficiency              | 6.67e+06<br>13% | 2.22e+06<br>15% | 1.44e+06<br>22% | 1.24e+05<br>15% | 1.07e+04<br>9.9% | 1652<br>94%  | 2.25e+08<br>0.0% | 2.35e+08<br>0.0%  |
| Muon acceptance<br>Efficiency      | 5.39e+06<br>81% | 1.85e+06<br>84% | 1.19e+06<br>83% | 1.04e+05<br>84% | 9199<br>86%      | 1635<br>99%  | 4.17e+06<br>1.9% | 1.27e+07<br>5.4%  |
| Muon identification<br>Efficiency  | 5.33e+06<br>99% | 1.82e+06<br>98% | 1.18e+06<br>99% | 9.86e+04<br>95% | 9037<br>98%      | 1621<br>99%  | 3.17e+06<br>76%  | 1.16e+07<br>91%   |
| Jet preselection<br>Efficiency     | 0<br>0%         | 4130<br>0.23%   | 927<br>0.078%   | 1.01e+04<br>10% | 51<br>0.57%      | 2.7<br>0.17% | 1278<br>0.04%    | 1.65e+04<br>0.14% |
| MET preselection<br>Efficiency     | 0<br>0%         | 1362<br>33%     | 92<br>9.9%      | 3431<br>34%     | 18<br>35%        | 0.39<br>14%  | 113<br>8.8%      | 5016<br>30%       |
| Angular correlations<br>Efficiency | 0<br>0%         | 247<br>18%      | 8.4<br>9.2%     | 862<br>25%      | 3.6<br>20%       | 0.14<br>37%  | 0<br>0%          | 1121<br>22%       |
| Leading jet<br>Efficiency          | 0<br>0%         | 131<br>53%      | 5.0<br>60%      | 310<br>36%      | 1.7<br>49%       | 0.12<br>85%  | 0<br>0%          | 447<br>40%        |
| Second leading jet<br>Efficiency   | 0<br>0%         | 94<br>72%       | 4.3<br>85%      | 204<br>66%      | 0.91<br>52%      | 0.068<br>56% | 0<br>0%          | 303<br>68%        |
| MET<br>Efficiency                  | 0<br>0%         | 8.3<br>8.8%     | 0.095<br>2.2%   | 9.2<br>4.5%     | 0.25<br>27%      | 0.013<br>18% | 0<br>0%          | 18<br>5.9%        |

**Table 4.3:** Expected number of events for the backgrounds at  $1 \text{ fb}^{-1}$  after each cut. Efficiencies are relative to the number of events passing the previous cut.

| Cut                  | LM1      | LM2      | LM4      | LM5  | LM6  | LM8      | LM9      | LM10 | LM9p     | LM9t175  |
|----------------------|----------|----------|----------|------|------|----------|----------|------|----------|----------|
| No cuts              | 6.11e+04 | 1.05e+04 | 2.77e+04 | 8682 | 5701 | 1.34e+04 | 5.21e+04 | 234  | 1.62e+04 | 5.14e+04 |
| Trigger              | 8880     | 1331     | 3333     | 1069 | 1245 | 3037     | 7094     | 45   | 2747     | 6645     |
| Efficiency           | 15%      | 13%      | 12%      | 12%  | 22%  | 23%      | 14%      | 19%  | 17%      | 13%      |
| Muon acceptance      | 6083     | 977      | 2885     | 919  | 1084 | 2635     | 5465     | 40   | 2264     | 5313     |
| Efficiency           | 69%      | 73%      | 87%      | 86%  | 87%  | 87%      | 77%      | 87%  | 82%      | 80%      |
| Muon identification  | 5422     | 844      | 2613     | 807  | 1002 | 2265     | 4548     | 35   | 1951     | 4627     |
| Efficiency           | 89%      | 86%      | 91%      | 88%  | 92%  | 86%      | 83%      | 89%  | 86%      | 87%      |
| Jet preselection     | 2095     | 442      | 1389     | 491  | 492  | 1584     | 2340     | 13   | 1066     | 2399     |
| Efficiency           | 39%      | 52%      | 53%      | 61%  | 49%  | 70%      | 51%      | 37%  | 55%      | 52%      |
| MET preselection     | 1910     | 418      | 1241     | 456  | 469  | 1389     | 1692     | 12   | 848      | 1786     |
| Efficiency           | 91%      | 94%      | 89%      | 93%  | 95%  | 88%      | 72%      | 91%  | 80%      | 74%      |
| Angular correlations | 776      | 180      | 504      | 195  | 211  | 583      | 607      | 5.0  | 308      | 623      |
| Efficiency           | 41%      | 43%      | 41%      | 43%  | 45%  | 42%      | 36%      | 42%  | 36%      | 35%      |
| Leading jet          | 624      | 157      | 421      | 174  | 198  | 458      | 400      | 4.6  | 235      | 422      |
| Efficiency           | 80%      | 88%      | 84%      | 89%  | 94%  | 79%      | 66%      | 91%  | 76%      | 68%      |
| Second leading jet   | 485      | 129      | 326      | 144  | 172  | 363      | 314      | 4.2  | 189      | 329      |
| Efficiency           | 78%      | 82%      | 77%      | 83%  | 87%  | 79%      | 79%      | 93%  | 80%      | 78%      |
| MET                  | 316      | 97       | 203      | 100  | 138  | 202      | 89       | 3.0  | 72       | 87       |
| Efficiency           | 65%      | 75%      | 62%      | 70%  | 80%  | 56%      | 28%      | 71%  | 38%      | 26%      |

**Table 4.4:** Expected number of events for the signals at  $1 \text{ fb}^{-1}$  after each cut. Efficiencies are relative to the number of events passing the previous cut.

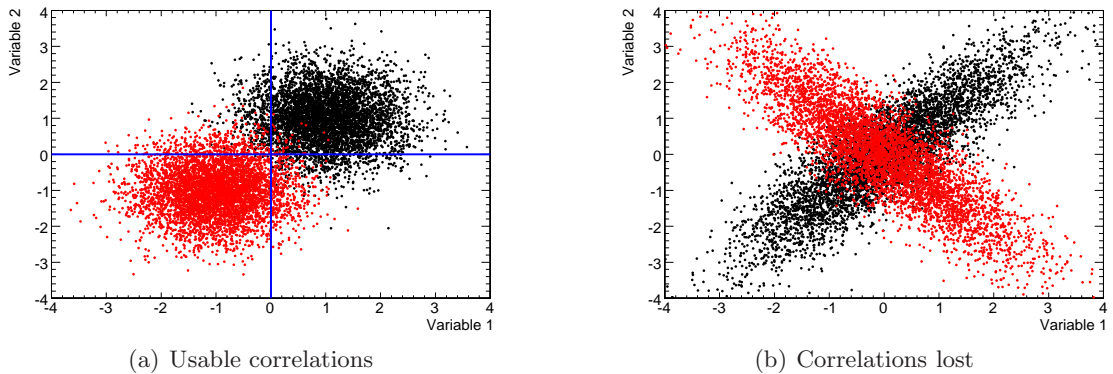


**Figure 4.11:** Distribution of a toy signal (red) and background (black) with and without usable correlations. Trivial cuts are shown in the usable case.

### 4.3 Boosted decision trees

Analyses based on one dimensional cuts, like the one presented in the previous section, are straightforward, robust, and easily enjoy acceptance in the community. However, they have their limitations. In a situation like in Fig. 4.11(a) the optimal cuts are quite easy to determine. In Fig. 4.11(b) the variables are correlated differently for signal and background. Projecting both background and signal on the variable axes hides these correlations, hence they can not be exploited using the chosen variables with one dimensional cuts. In this artificial example it is rather simple to define two new variables accounting for the correlations, effectively rotating Fig. 4.11(b) by  $45^\circ$ . Confronted with real world problems, this will quickly become excessively complicated, as there is usually a rather high number of possible variables, resulting in many combinations to be tested for correlations. The situation is even worse if there are correlations between three or more variables. In addition all correlations would have to be reinvestigated for different model parameters.

Fig. 4.12 shows an exemplary cut based analysis as a decision tree. One can see an event being classified as signal, if and only if it passes all cuts. Mathematically speaking, in the space defined by all variables, exactly one region is selected, whose borders are perpendicular to the variable axes. Ideally this region is located and sized such that the

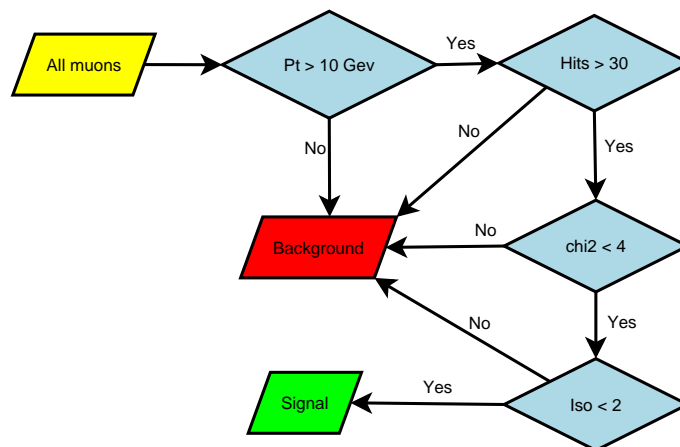


**Figure 4.12:** Conventional analysis based one dimensional cuts shown as a simple decision tree: Events failing one cut are considered background.

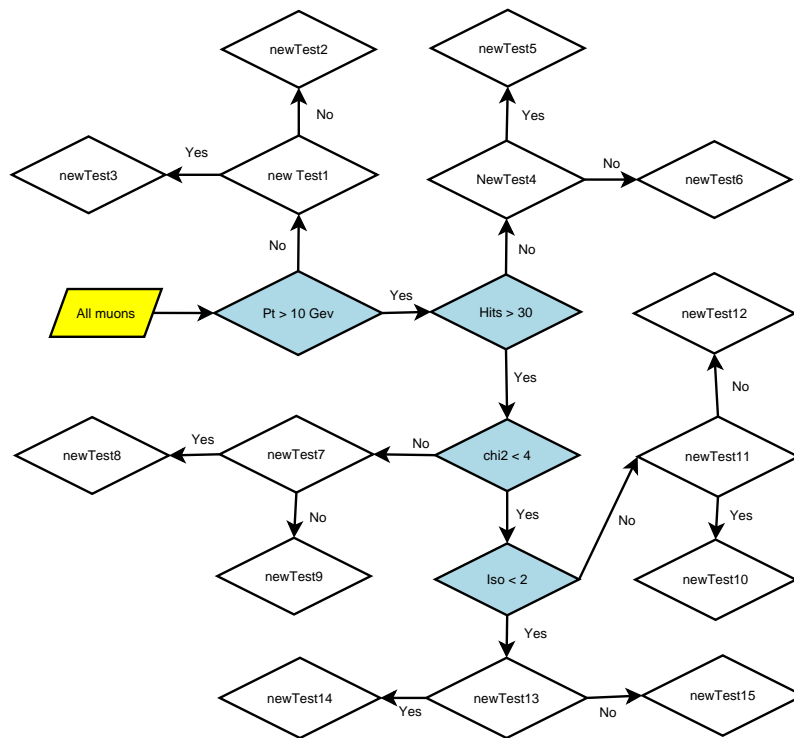


**Figure 4.13:** Extend decision tree: Leaves may considered as signal or background.

separation of signal and background is maximized. However, depending on the physics involved, the best region may be irregularly shaped or even separated in numerous unconnected regions. One way to get near this best region is to extend the simple decision tree of Fig. 4.12 to a more complex one like shown in Fig. 4.13. The leaves of this tree can then be classified as either signal or background, thus selecting more than one region. These regions are still rectangular, but can approximate any shape, if they are small and numerous enough.

To gain information about the *signal likeness* of an event and reduce the vulnerability to statistical fluctuations, not only one but several decision trees are used, whose outputs are weighted according to their overall performance. This is called *boosting*, hence the name *Boosted decision trees*.

In this analysis the ROOT [57] based multivariate analysis framework TMVA [58] in version 3.8.14 is used.

### 4.3.1 Training

The number of possible trees with all combinations of cut variables and values is basically unlimited, so it is obviously impossible to investigate all trees to find the best separating one. Thus the so called *growing* of the tree is done in a rather straightforward way: Using all events, the variable and the corresponding cut value resulting in the best separation is determined. The events are then split into two subgroups, one containing all events which pass this cut and the second group containing all events which do not pass. For each of these two subgroups the procedure is repeated, resulting in now four subgroups. This splitting is then repeated recursively. The splitting of a subgroup is stopped, if the number of events in one of the two new subgroups would drop under a certain number  $N_0$ .

This is done for two reasons:

- Avoid overtraining: If the splitting is performed until the events in each leaf are either signal or background, the separation is perfect on the training sample, but on any other sample it is most likely deteriorated.
- Manageable tree size: A sample of  $N_{training}$  events will lead to a tree with about  $N_{training}$  splitting nodes.

In TMVA  $N_0$  is set to

$$\max(20, 10 \cdot N_{training}/N_{variables}^2) \quad (4.3)$$

which leads to a maximum size of  $N_{variables}^2/10$  splitting nodes and a sufficient chance for every variable to be used for splitting.

The best separating variable and its value is determined by trying each variable at  $N_{Cuts} = 20$  values, equidistant between the minimum and maximum of this variable in all events in this node, and calculating the weighted average (weighted with the number of events in the nodes) of a *separation index* for both daughter nodes. Increasing  $N_{Cuts}$  increases the computing time during training, however it may increase the quality of a cut. The influence of  $N_{Cuts}$  is not evaluated in this study, as new algorithms using a continuous scan are under development. However these new algorithms have not been released yet, hence the TMVA default of  $N_{Cuts} = 20$  is used in this study.

The *Gini index*  $p \cdot (1 - p)$  with *purity*  $p = N_S/(N_S + N_B)$  is used to determine the best separation, which is at its maximum for perfectly mixed samples ( $p = 0.5$ ) and drops to zero for samples which consist of signal or background only. Then the variable-value pair with the smallest separation index is used.

### 4.3.2 Boosting

A single decision tree grown as described above is a rather weak classifier, as it is quite likely affected by statistical fluctuations of the sample. Furthermore it yields a binary yes-no decision whether it considers an event to be signal or background, and gives no information how signal- or background-like the event might be.

One way to overcome these drawbacks is *boosting*, which can be applied to most MVA classifiers. A common boosting algorithm is *AdaBoost* [59] (adaptive boosting), where the weights of events misclassified by one decision tree are multiplied by a boost weight  $\alpha$ , before an additional tree is grown using the modified sample. The boost weight is determined from the fraction

$$\epsilon_{err} = \frac{N_{misclassified}}{N_{total}} \quad (4.4)$$

of events misclassified by the previous tree:

$$\alpha = \frac{1 - \epsilon_{err}}{\epsilon_{err}} \quad (4.5)$$

Thus events misclassified by an otherwise well performing tree have the highest impact during the growing of the next tree. The final response of this *forest* of decision trees is then calculated via

$$response = \sum \ln(\alpha_i) h_i \quad (4.6)$$

with the individual responses  $h_i$  of each tree, which is  $-1$  for background and  $1$  for signal. The combined response will then be somewhere between  $-1$  and  $1$ , showing the signal-likeness the forest assigns to this event.

### 4.3.3 Pruning

A tree will quite likely contain splitting nodes, especially near its leaves, which are statistically insignificant. These nodes will increase the size of the tree without a significant performance gain and may lead to overtraining, as their cut values are just caused by statistical fluctuations. So they can be removed, if their gain in performance is beneath a certain threshold, depending on the number of events left. It is recommendable to first grow a tree to its maximum size and then cut it recursively back, starting at the leaves, because a cut may seem insignificant on its own, but lead to improved performance in subsequent cuts. This will e.g. be the case in a situation like in Fig. 4.11(b).

Experience so far for the present application shows no performance increase on independent test samples, hence the trees will not be pruned at all.

### 4.3.4 Workflow

The preselection cuts of section 4.1.4 are relaxed in the jet selection: Tree jets with  $E_T \geq 50$  GeV are required. This should give the BDTs more events to optimize.

The following attributes are used to train the BDTs:

#### Muons

- Transverse momentum  $p_T$
- Pseudorapidity  $|\eta|$
- Isolation:  $\sum p_T^{tracks}$ ,  $\sum E_T^{calo}$ ,  $N_{Tracks}$  ( $\Delta R \leq 0.3$  cone)
- Calorimeter compatibility: Likelihood based testing, whether the energy deposit in the calorimeter along the muon trajectory looks like a minimal ionizing particle.

#### Jets

- Transverse energy  $E_T$
- Pseudorapidity  $|\eta|$

#### Missing transverse energy $\cancel{E}_T$

#### Energy differences

Absolute value of the transverse energy difference of each pairwise combination of the three leading jets.

#### Angular correlations

$|\Delta\phi|$  in transverse plane between

- Muon and  $\cancel{E}_T$
- Muon and each of the three leading jets
- $\cancel{E}_T$  and each of the three leading jets
- Each pairwise combination of the three leading jets

#### Invariant mass

Invariant mass of the sum of the four-momenta of

- Muon and each of the three leading jets
- Each pairwise combination of the three leading jets
- The three leading jets



- All jets fulfilling the preselection

#### Transverse invariant mass

Transverse component of the invariant mass ( $m_T^2 = E_T^2 - p_T^2$ ) of

- The two leading jets
- The three leading jets
- All jets fulfilling the preselection

#### (Transverse) Energy sum

Scalar sum of the energy and of the transverse energy of

- The two leading jets
- The three leading jets
- All jets fulfilling the preselection
- Total transverse energy

If no pruning is performed, the BDTs are most likely overtrained on the set of events used for training, resulting in a unphysical high separation power. Thus the events used for training and validation must be statistically independent. Consequently we separate the simulated events in two sets: One used for training, one for validation.

On the first third of the MC samples one set of BDTs is trained for each of the ten LM points, resulting in ten sets of BDTs. The last two thirds of the MC samples are then used to determine the minimal response, which yields the best significance, and to calculate the significance. The optimal cut on the BDT response is determined by optimizing  $N_S/\sigma_B$  including systematics like described in section 4.2.1. In analogy to the cut-based analysis the expected significance is determined using the modified frequentist approach including systematic uncertainties as explained in section 4.1.3.

### 4.3.5 Results

For reasons of comparability, the background samples considered negligible in the cut based analysis are also not used here. As shown in detail in tables C.1(a) to C.10(a), the dominant background is  $t\bar{t}$ , while W+jets is less important. All other backgrounds are either negligible or contribute only due to upper limits.

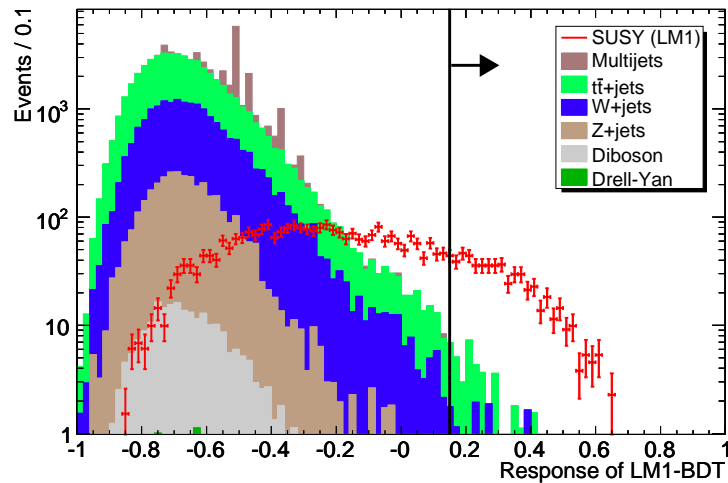
Fig. 4.14 shows the response for LM1 and LM10 of two BDTs trained accordingly. LM1 and most of the other LM points, see appendix B, are easy to separate from the background, while LM9 is a bit harder to separate. LM10 shows a signal shape clearly different from the background, but its very low cross section spoils the discovery potential. The visible separation for responses greater than 0.6 in Fig. 4.14(b) is caused by insufficient Monte Carlo statistics.

Looking at Table 4.5, a discovery of supersymmetry for LM1 to LM6, with the exception of LM2, appears to be possible with an integrated luminosity of  $1 \text{ fb}^{-1}$  or less. LM points with heavier sparticles like LM9 and LM10 are hard to detect, either because of difficult signatures or a very low cross section.

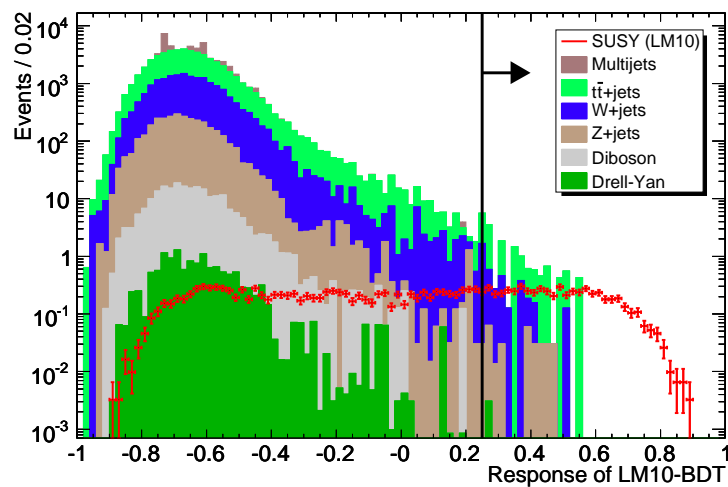
Table 4.6 shows the expected significance at  $1 \text{ fb}^{-1}$  for each LM point, when also applied to all other LM points. Highlighted are the significances, where a BDT trained on a certain LM point is applied to the same LM point. Comparing the highlighted numbers to all other numbers in one line, one can see that for most LM points at least one BDT trained on another LM point performs slightly better. Besides fluctuations of the significance estimation (see section 4.1.3), this is most likely caused by disregarding of the

systematic uncertainties during the BDT training. For a detailed discussion of this effect see section 4.4.

The fact that a single BDT performs well for many LM points illustrates that the BDTs in general are suitable for covering a wide range in the SUSY parameter space. Detailed tables of the expected numbers of events and expected significances for all BDTs can be found in appendix C.



(a) Trained and applied on LM1



(b) Trained and applied on LM10

**Figure 4.14:** Response of a BDT trained and applied on the same LM point. LM1 and LM10 are shown here. Histograms are scaled to  $1 \text{ fb}^{-1}$ .

| LM-Point | Integrated luminosity |                     |                      |                    |
|----------|-----------------------|---------------------|----------------------|--------------------|
|          | 10 pb <sup>-1</sup>   | 40 pb <sup>-1</sup> | 100 pb <sup>-1</sup> | 1 fb <sup>-1</sup> |
| LM1      | 4.3                   | 7.0                 | 8.8                  | 11                 |
| LM2      | 1.4                   | 2.4                 | 3.0                  | 4.0                |
| LM4      | 2.5                   | 4.5                 | 5.3                  | 6.5                |
| LM5      | 1.6                   | 2.8                 | 4.1                  | 4.7                |
| LM6      | 1.9                   | 3.2                 | 4.8                  | 6.2                |
| LM8      | 3.1                   | 5.7                 | 7.5                  | 10                 |
| LM9      | 2.0                   | 3.0                 | 3.9                  | 3.9                |
| LM10     | 0.07                  | 0.17                | 0.21                 | 0.28               |
| LM9p     | 1.3                   | 2.2                 | 2.7                  | 3.4                |
| LM9t175  | 1.5                   | 2.4                 | 3.0                  | 3.5                |

**Table 4.5:** Modified Frequentist significances expected for the different SUSY benchmark points and different amounts of integrated luminosity. Each line shows the results for of a BDT trained an a certain point, applied to the same point.

| applied to | trained on |            |            |            |            |           |            |             |            |            |
|------------|------------|------------|------------|------------|------------|-----------|------------|-------------|------------|------------|
|            | LM1        | LM2        | LM4        | LM5        | LM6        | LM8       | LM9        | LM10        | LM9p       | LM9t175    |
| LM1        | <b>11</b>  | 9.8        | 9.1        | 11         | 12         | 8.4       | 3.2        | 6.0         | 3.1        | 3.1        |
| LM2        | 3.6        | <b>4.0</b> | 3.5        | 4.4        | 5.0        | 3.3       | 1.5        | 2.8         | 1.5        | 1.2        |
| LM4        | 6.6        | 6.8        | <b>6.5</b> | 8.7        | 9.2        | 7.5       | 3.2        | 4.9         | 3.3        | 2.4        |
| LM5        | 3.3        | 3.7        | 3.8        | <b>4.7</b> | 5.2        | 4.1       | 1.8        | 3.4         | 2.1        | 1.4        |
| LM6        | 3.7        | 4.2        | 3.9        | 5.2        | <b>6.2</b> | 3.9       | 1.4        | 3.3         | 1.6        | 1.2        |
| LM8        | 6.9        | 7.4        | 7.3        | 8.9        | 9.5        | <b>10</b> | 4.8        | 7.9         | 5.5        | 4.4        |
| LM9        | 3.7        | 3.2        | 3.9        | 4.2        | 4.1        | 5.0       | <b>3.9</b> | 3.9         | 3.7        | 3.6        |
| LM10       | 0.09       | 0.13       | 0.11       | 0.17       | 0.18       | 0.17      | 0.06       | <b>0.28</b> | 0.13       | 0.06       |
| LM9p       | 2.7        | 2.7        | 3.0        | 3.9        | 3.8        | 4.5       | 3.0        | 4.3         | <b>3.4</b> | 2.8        |
| LM9t175    | 3.8        | 3.1        | 3.7        | 4.5        | 4.3        | 5.4       | 3.9        | 4.4         | 3.8        | <b>3.5</b> |

**Table 4.6:** Comparison of the significances at 1 fb<sup>-1</sup> of each BDT applied to all LM points. Training and application on the same point is printed in bold.

## 4.4 Comparison of analysis techniques

Comparing Tables 4.2 and 4.5 reveals a modest gain in significance for most LM points, only for LM8 a large gain is observed. This is most likely caused by the unique signature of LM8 because of the gluino-squark degeneration, which is taken into account by the BDT training. Most likely a manual optimization of cuts for such signatures will yield a comparable significance. Hence one may conclude the BDTs are not worth the effort.

But looking at sections 4.2.1 and 4.3.1, there is an important difference to be seen between the cut based approach and the BDTs: While the systematic uncertainties are taken into account at each optimization step in the cut based analysis, the BDT training cannot account for any systematic uncertainty at all and just tries to maximize the separation. Only in the last step, when choosing the cut value on the BDT response, systematic errors are again considered. Additionally most of the variables used by the BDTs, see section 4.3.4, are highly affected by uncertainties on the jet energy scale.

It is consequently to be concluded that BDTs may not be the right approach for physics dominated by systematic uncertainties. To proof the performance of BDTs in a more friendly environment, a second study ignoring systematic uncertainties has been performed.

### 4.4.1 Study without systematic uncertainties

The rather complex significance estimation of section 4.1.3 is not necessary for a study without systematic errors. Hence a poisson p-value, translated to Gaussian standard deviations, is used: It shows the probability of a poisson distributed background  $N_B$  to fluctuate to the signal  $N_S$  or more:

$$p_{Poisson} = \int_{N_S}^{\infty} \frac{N_B^x e^{-N_B}}{x!} dx \quad (4.7)$$

Both the cuts on the BDT response as well as the conventional cuts are optimized to maximize this estimator. This leads to only one additional BDT cut after the preselection for the cut based analysis:  $\cancel{E}_T \geq 300$  GeV. Using the same BDTs as before, only the cut on the response is reoptimized to maximize the poisson significance.

The expected number of events for both cut based and all BDTs are shown in Table 4.7. Also shown in this table are the expected significances for both cut based analysis as well as for BDTs.

Now the BDTs provide a clear gain for each LM point. Again applying each BDT to all LM points (see Table 4.8) shows only for LM2 that another BDT yields a higher significance, however this is most likely caused by statistical fluctuations.

| Analysis      | Sample     | Events @ 1 fb <sup>-1</sup> | Significance @       |                    |
|---------------|------------|-----------------------------|----------------------|--------------------|
|               |            |                             | 100 pb <sup>-1</sup> | 1 fb <sup>-1</sup> |
| Cut based     | Background | 336                         | –                    | –                  |
|               | LM1        | 902                         | 12                   | >38                |
|               | LM2        | 250                         | 3.9                  | 12                 |
|               | LM4        | 523                         | 7.5                  | 24                 |
|               | LM5        | 255                         | 4.0                  | 13                 |
|               | LM6        | 313                         | 4.8                  | 15                 |
|               | LM8        | 532                         | 7.7                  | 24                 |
|               | LM9        | 263                         | 4.1                  | 13                 |
|               | LM10       | 6.3                         | 0.13                 | 0.34               |
|               | LM9p       | 196                         | 3.1                  | 9.8                |
| LM9t175       | 291        | 4.5                         | 14                   |                    |
| BDT - LM1     | Background | 382                         | –                    | –                  |
|               | LM1        | 1368                        | 16                   | >38                |
| BDT - LM2     | Background | 44                          | –                    | –                  |
|               | LM2        | 152                         | 6.3                  | 17                 |
| BDT - LM4     | Background | 167                         | –                    | –                  |
|               | LM4        | 602                         | 11                   | 34                 |
| BDT - LM5     | Background | 65                          | –                    | –                  |
|               | LM5        | 202                         | 6.7                  | 19                 |
| BDT - LM6     | Background | 81                          | –                    | –                  |
|               | LM6        | 265                         | 7.6                  | 22                 |
| BDT - LM8     | Background | 54                          | –                    | –                  |
|               | LM8        | 503                         | 13                   | >38                |
| BDT - LM9     | Background | 1120                        | –                    | –                  |
|               | LM9        | 1197                        | 9.9                  | 31                 |
| BDT - LM10    | Background | 23                          | –                    | –                  |
|               | LM10       | 3.8                         | 0.34                 | 0.79               |
| BDT - LM9p    | Background | 152                         | –                    | –                  |
|               | LM9p       | 345                         | 7.0                  | 22                 |
| BDT - LM9t175 | Background | 987                         | –                    | –                  |
|               | LM9t175    | 1161                        | 10                   | 32                 |

**Table 4.7:** Number of expected events for an integrated luminosity of 1 fb<sup>-1</sup>. Significances are shown for 100 pb<sup>-1</sup> and 1 fb<sup>-1</sup>. Due to numerical limitations, no significances above 38  $\sigma$  can be calculated.

| applied<br>to | trained on  |           |           |           |           |             |           |             |           |           |
|---------------|-------------|-----------|-----------|-----------|-----------|-------------|-----------|-------------|-----------|-----------|
|               | LM1         | LM2       | LM4       | LM5       | LM6       | LM8         | LM9       | LM10        | LM9p      | LM9t175   |
| LM1           | > <b>38</b> | >38       | >38       | >38       | >38       | 36          | 29        | 12          | 26        | 30        |
| LM2           | 14          | <b>17</b> | 15        | 17        | 18        | 15          | 7.7       | 5.8         | 10        | 7.8       |
| LM4           | 30          | 29        | <b>34</b> | 33        | 33        | 32          | 21        | 11          | 24        | 21        |
| LM5           | 13          | 17        | 16        | <b>19</b> | 19        | 17          | 8.1       | 8.3         | 12        | 8.3       |
| LM6           | 14          | 18        | 17        | 21        | <b>22</b> | 17          | 7.5       | 7.7         | 10        | 7.6       |
| LM8           | 31          | 31        | 36        | 36        | 35        | > <b>38</b> | 27        | 19          | 36        | 27        |
| LM9           | 24          | 16        | 23        | 19        | 18        | 25          | <b>31</b> | 7.7         | 28        | 31        |
| LM10          | 0.33        | 0.49      | 0.44      | 0.62      | 0.59      | 0.62        | 0.24      | <b>0.79</b> | 0.49      | 0.24      |
| LM9p          | 15          | 13        | 17        | 16        | 15        | 20          | 17        | 11          | <b>22</b> | 17        |
| LM9t175       | 24          | 16        | 24        | 20        | 18        | 25          | 31        | 7.6         | 29        | <b>32</b> |

**Table 4.8:** Comparison of the significances at  $1 \text{ fb}^{-1}$  of each BDT applied to all LM points without systematic uncertainties. Training and application on the same point is printed in bold. Due to numerical limitations, no significances above  $38 \sigma$  can be calculated.

## 5 Conclusion

A study on the potential of CMS to detect supersymmetry in the  $\mu+\text{jet}+\cancel{E}_T$  channel has been presented in this thesis. mSUGRA with R-parity conservation has been assumed to calculate the characteristics of the new particles at a number of benchmark points in the mSUGRA parameter space.

The most important standard model backgrounds have been taken into account and the effects of the main systematic uncertainties have been evaluated.

It has been shown that the mSUGRA parameter space just beyond the reach of TEVATRON is explorable with more than  $5\sigma$  with an integrated luminosity of  $100 \text{ pb}^{-1}$  or less. Some regions of the parameter space are observable with  $1 \text{ fb}^{-1}$ , while others need more integrated luminosity or better controlled systematic uncertainties.

The use of boosted decision trees increases the reach into the parameter space, however this method presently provides no large significance gain, as the systematic deviations are not taken into account during training.

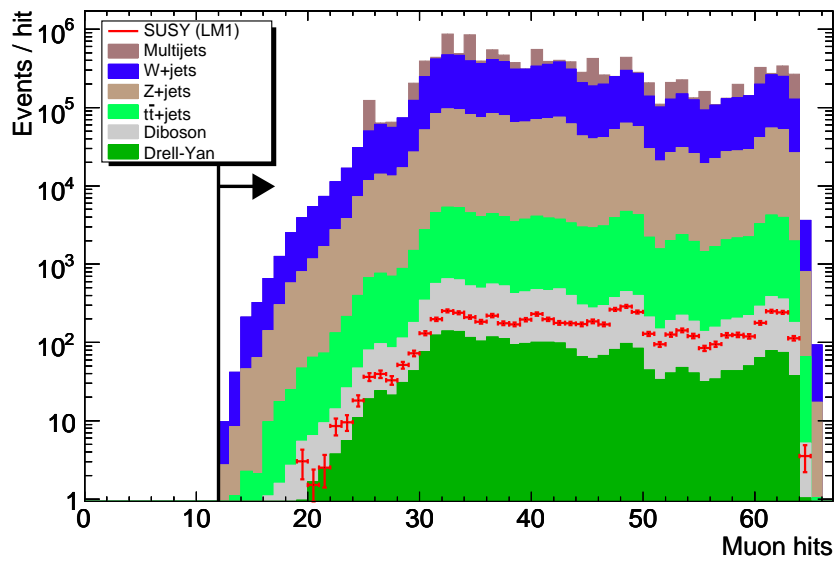
Further studies are necessary to determine the effect of cosmic radiation, detector misalignment and pileup. Ideas to incorporate systematic uncertainties during BDT training must be evaluated.



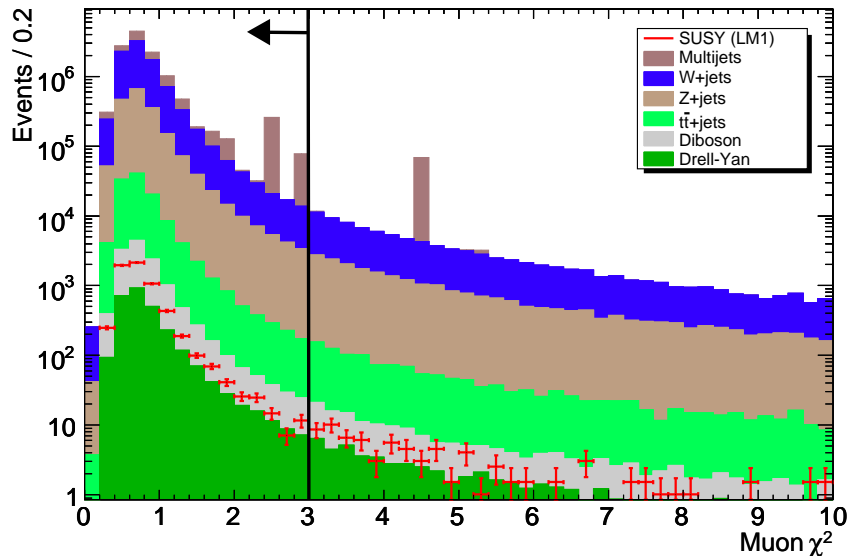


# Appendix A

## Preselection distributions

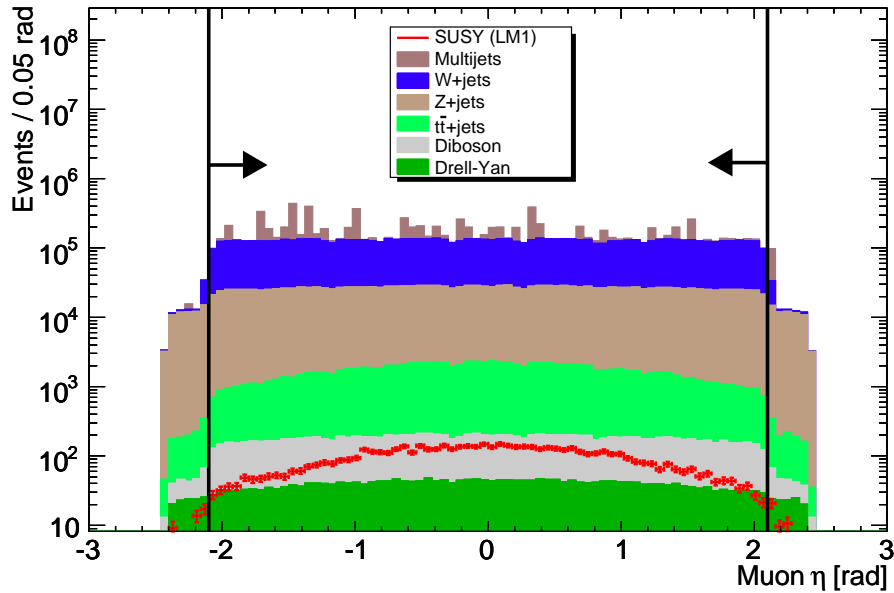


(a) Number of hits

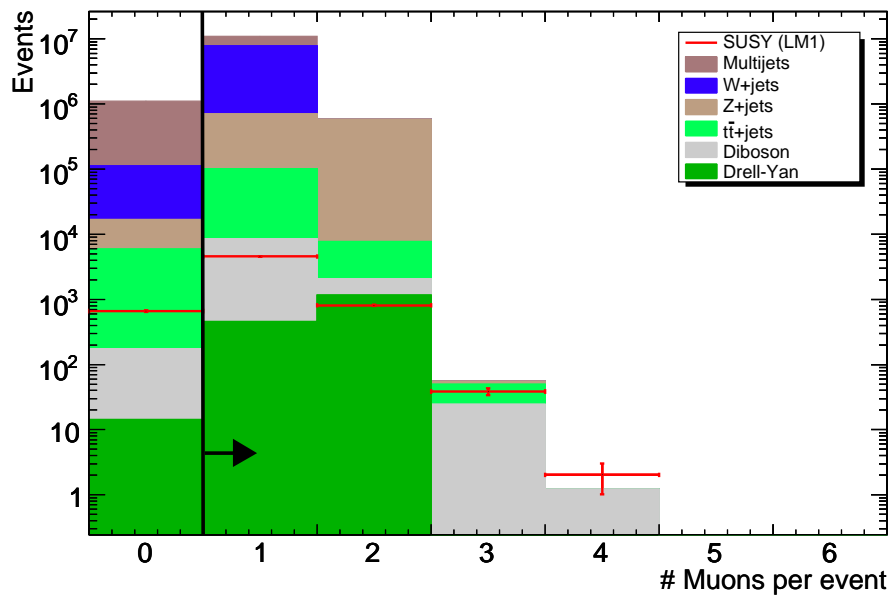


(b) Fit quality  $\chi^2/N_{DOF}$

Figure A.1: Muon fit quality variables used for identification and preselection. Each variable is shown after applying all other muon identification cuts.

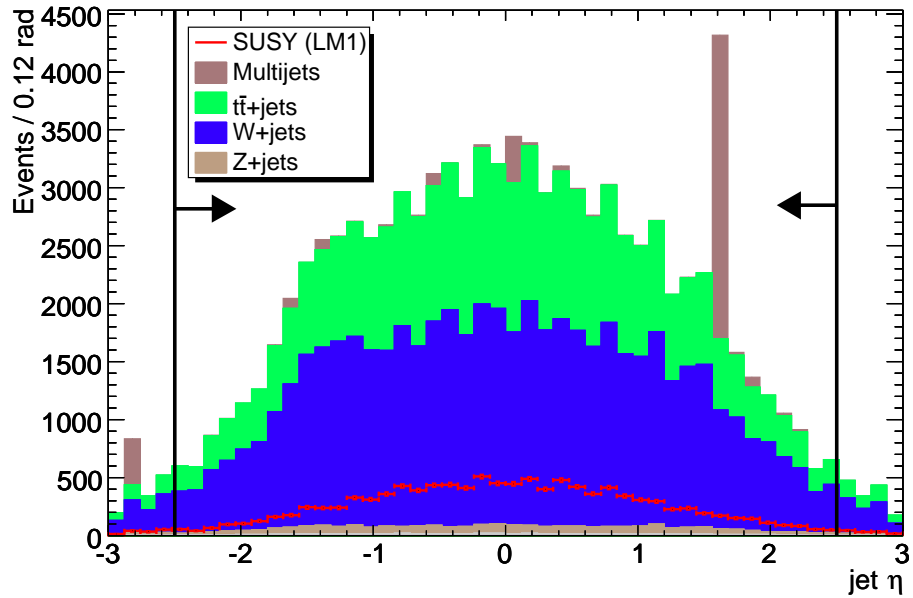


(a) Pseudorapidity

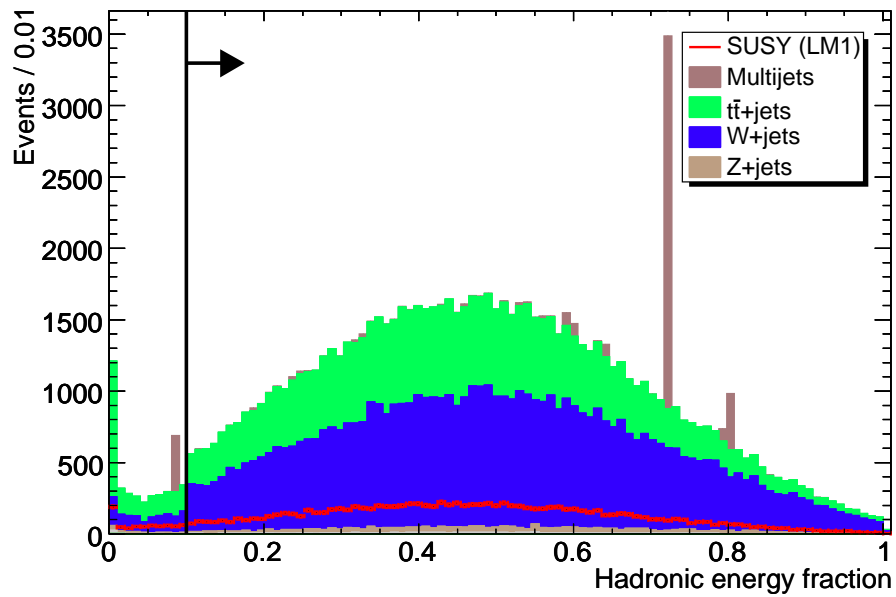


(b) Number of muons

Figure A.2: Muon variables used for identification and preselection: Pseudorapidity and Isolation. Each variable is shown after applying all other muon identification cuts.



(a)



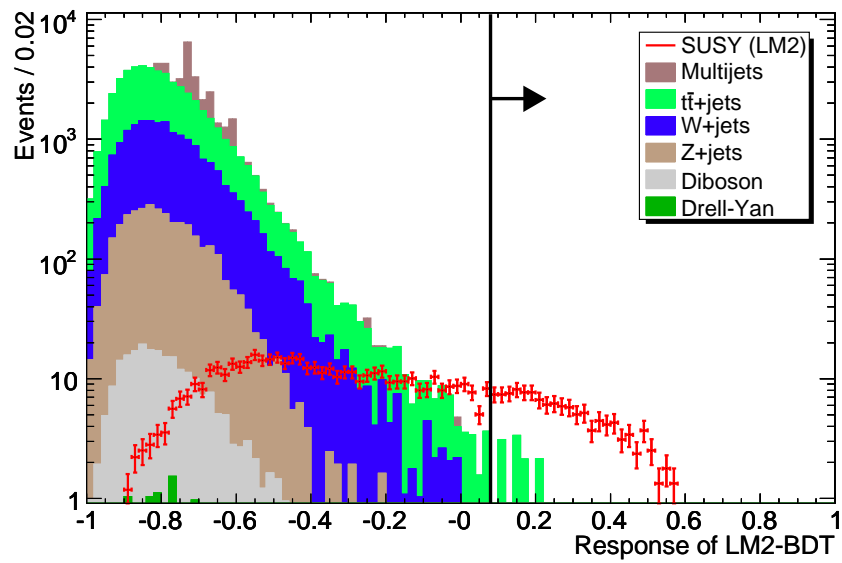
(b)

**Figure A.3:** Pseudorapidity and hadronic energy fraction of jets at the preselection level. Both variables are shown after application of all other preselection cuts.

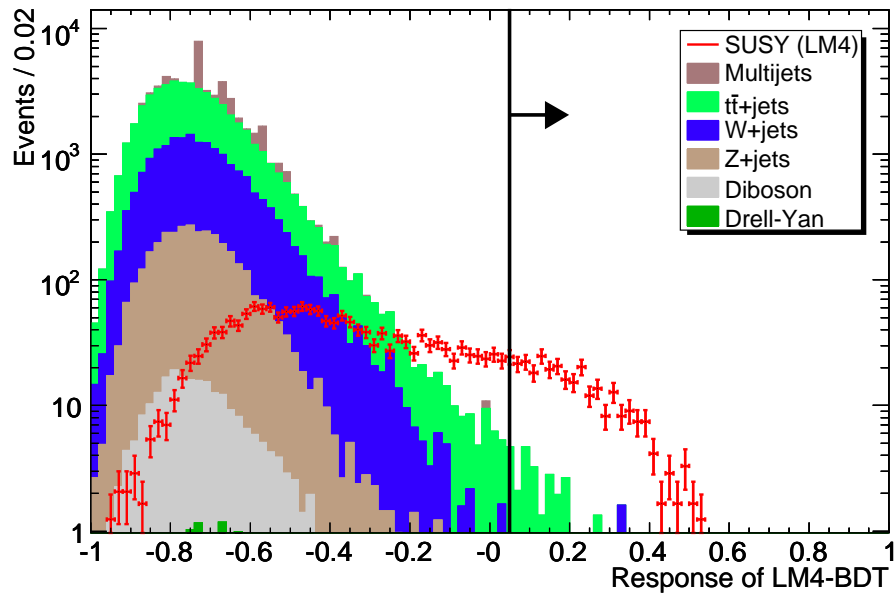


## Appendix B

### BDT Response distributions

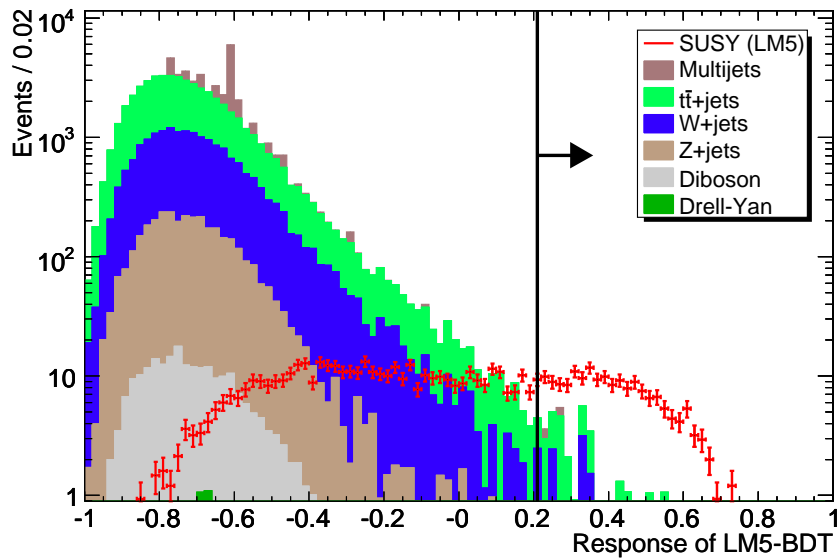


(a) Trained and applied on LM2

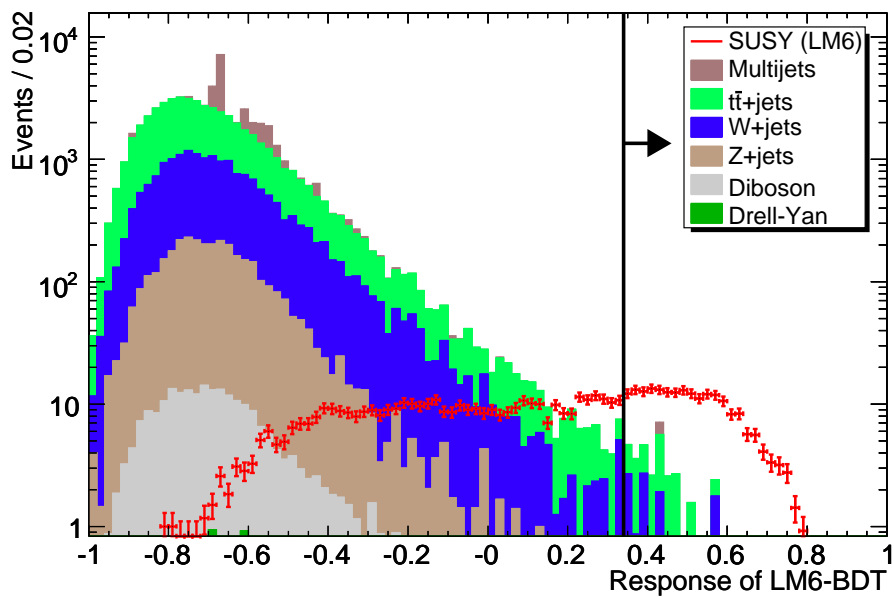


(b) Trained and applied on LM4

**Figure B.1:** Response of a BDT trained and applied on the LM2 and LM4. Histograms scaled to  $1 \text{ fb}^{-1}$ .

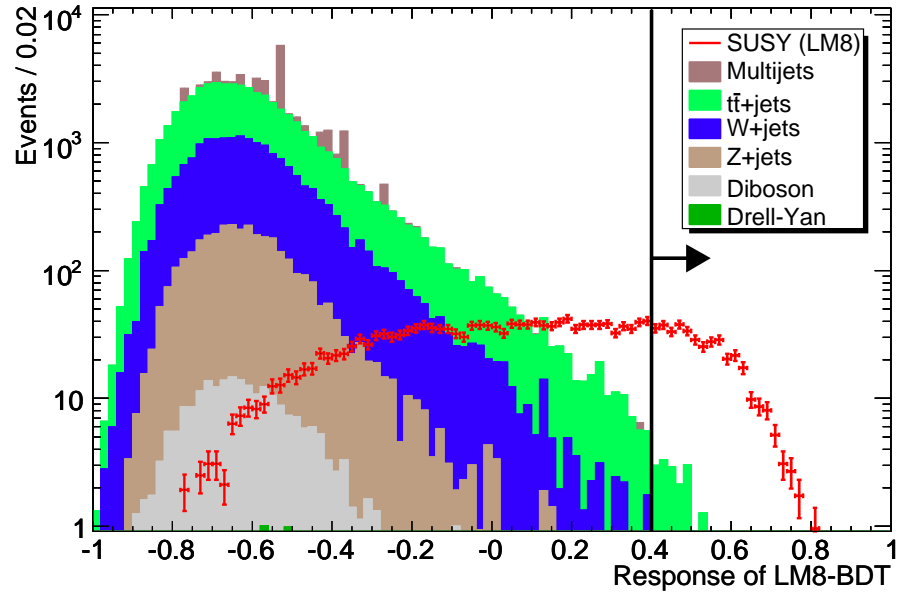


(a) Trained and applied on LM5

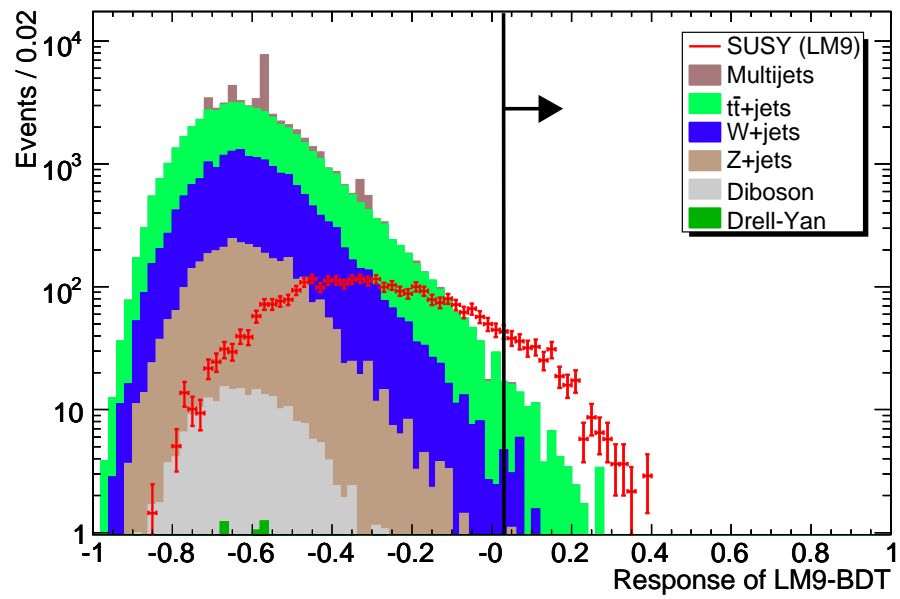


(b) Trained and applied on LM6

**Figure B.2:** Response of a BDT trained and applied on the LM5 and LM6. Histograms scaled to  $1 \text{ fb}^{-1}$ .

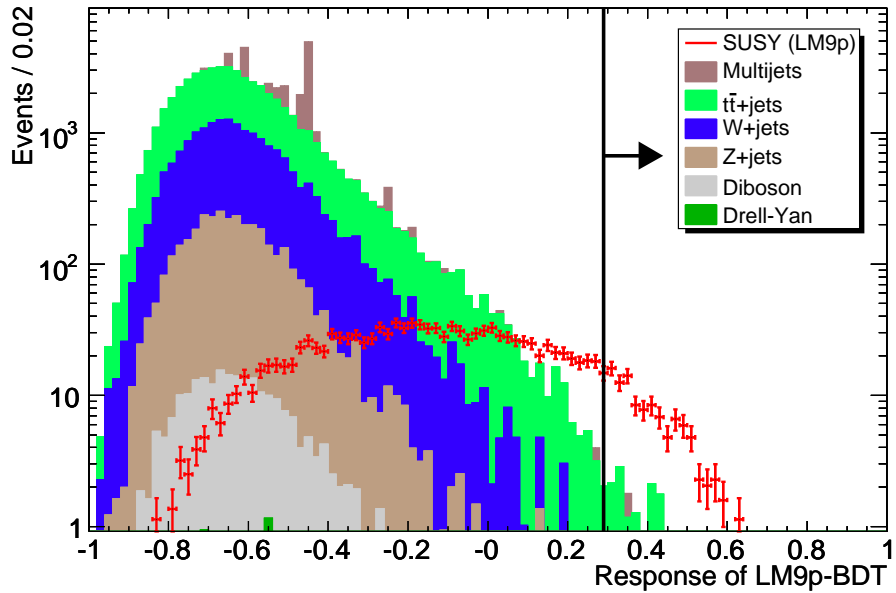


(a) Trained and applied on LM8

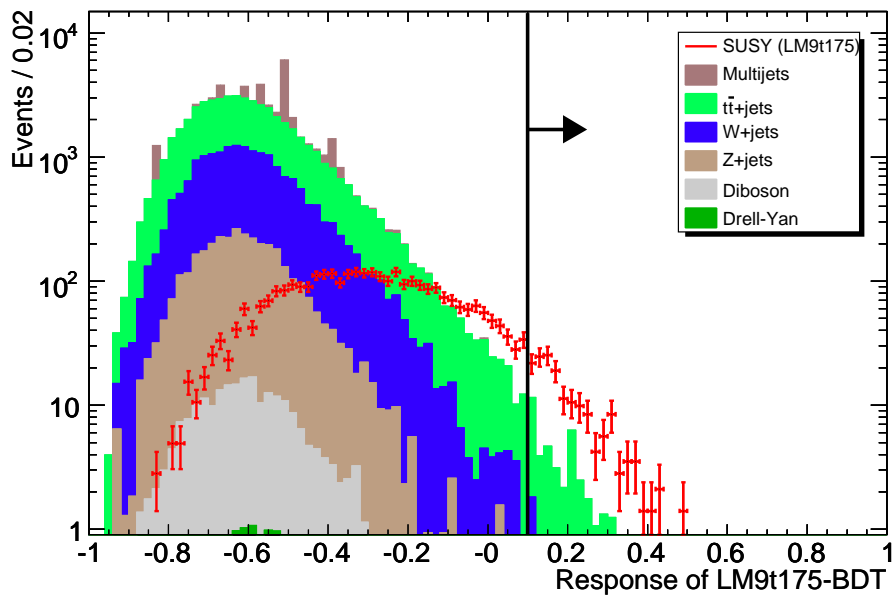


(b) Trained and applied on LM9

**Figure B.3:** Response of a BDT trained and applied on the LM8 and LM9. Histograms scaled to  $1 \text{ fb}^{-1}$ .



(a) Trained and applied on LM9p



(b) Trained and applied on LM9t175

Figure B.4: Response of a BDT trained and applied on the LM9p and LM9t175. Histograms scaled to  $1 \text{ fb}^{-1}$ .



## Appendix C

# Expected events and significances for BDT based analysis

**Table C.1:** *Trained on LM1*

(a) Numbers of selected events for backgrounds and signals; scaled to an integrated luminosity of  $1 \text{ fb}^{-1}$ .

| Sample         | # Events @ $1 \text{ fb}^{-1}$ |             | $\sigma_{MC}$ | $\sigma_{sys}$ | Significance @ $1 \text{ fb}^{-1}$ |
|----------------|--------------------------------|-------------|---------------|----------------|------------------------------------|
|                |                                | upper limit |               |                |                                    |
| W+jets         | 8.4                            | 8.8         | 2.8           | 2.7            | -                                  |
| Z+jets         | 0.11                           | 1.8         | 1.5           | 0.43           | -                                  |
| $t\bar{t}$     | 29                             | 29          | 4.4           | 9.5            | -                                  |
| Diboson        | 0.37                           | 0.66        | 0.29          | 0.25           | -                                  |
| Drell-Yan      | 0.0                            | 0.073       | 0.064         | 0.017          | -                                  |
| QCD            | 0.0                            | 15          | 8.9           | 3.4            | -                                  |
| Background sum | 38                             | 55          | 10            | 16             | -                                  |
| LM1            | 559                            | -           | 21            | 66             | 11                                 |
| LM2            | 156                            | -           | 4.8           | 11             | 3.6                                |
| LM4            | 324                            | -           | 12            | 37             | 6.6                                |
| LM5            | 141                            | -           | 4.3           | 10             | 3.3                                |
| LM6            | 156                            | -           | 3.6           | 9.7            | 3.7                                |
| LM8            | 329                            | -           | 7.9           | 36             | 6.9                                |
| LM9            | 168                            | -           | 11            | 37             | 3.7                                |
| LM10           | 2.6                            | -           | 0.092         | 0.53           | 0.09                               |
| LM9p           | 109                            | -           | 5.0           | 16             | 2.7                                |
| LM9t175        | 167                            | -           | 11            | 34             | 3.8                                |

(b) Modified Frequentist significances expected for the different SUSY benchmark points and different amounts of integrated luminosity.

| LM-Point | $10 \text{ pb}^{-1}$ | $40 \text{ pb}^{-1}$ | $100 \text{ pb}^{-1}$ | $1 \text{ fb}^{-1}$ |
|----------|----------------------|----------------------|-----------------------|---------------------|
| LM1      | 4.3                  | 7.0                  | 8.8                   | 11                  |
| LM2      | 1.5                  | 2.4                  | 3.0                   | 3.6                 |
| LM4      | 2.5                  | 4.5                  | 5.7                   | 6.6                 |
| LM5      | 1.4                  | 2.2                  | 2.7                   | 3.3                 |
| LM6      | 1.5                  | 2.4                  | 2.9                   | 3.7                 |
| LM8      | 2.6                  | 4.6                  | 5.4                   | 6.9                 |
| LM9      | 1.5                  | 2.5                  | 3.1                   | 3.7                 |
| LM10     | 0.03                 | 0.06                 | 0.07                  | 0.09                |
| LM9p     | 1.1                  | 1.8                  | 2.2                   | 2.7                 |
| LM9t175  | 1.5                  | 2.5                  | 3.0                   | 3.8                 |

**Table C.2:** Trained on LM2

(a) Numbers of selected events for backgrounds and signals; scaled to an integrated luminosity of  $1 \text{ fb}^{-1}$ .

| Sample         | # Events @ $1 \text{ fb}^{-1}$ |             | $\sigma_{MC}$ | $\sigma_{sys}$ | Significance @ $1 \text{ fb}^{-1}$ |
|----------------|--------------------------------|-------------|---------------|----------------|------------------------------------|
|                |                                | upper limit |               |                |                                    |
| W+jets         | 1.3                            | 3.8         | 2.0           | 1.0            | -                                  |
| Z+jets         | 0.0                            | 1.7         | 1.5           | 0.4            | -                                  |
| $t\bar{t}$     | 14                             | 14          | 3.0           | 4.7            | -                                  |
| Diboson        | 0.12                           | 0.42        | 0.23          | 0.089          | -                                  |
| Drell-Yan      | 0.0                            | 0.073       | 0.064         | 0.017          | -                                  |
| QCD            | 0.0                            | 15          | 8.9           | 3.4            | -                                  |
| Background sum | 16                             | 35          | 9.8           | 9.2            | -                                  |
| LM1            | 347                            | -           | 16            | 45             | 9.8                                |
| LM2            | 125                            | -           | 4.3           | 12             | 4.0                                |
| LM4            | 240                            | -           | 10.0          | 32             | 6.8                                |
| LM5            | 120                            | -           | 4.0           | 13             | 3.7                                |
| LM6            | 138                            | -           | 3.4           | 10             | 4.2                                |
| LM8            | 256                            | -           | 7.0           | 34             | 7.4                                |
| LM9            | 96                             | -           | 8.3           | 25             | 3.2                                |
| LM10           | 2.6                            | -           | 0.092         | 0.54           | 0.13                               |
| LM9p           | 76                             | -           | 4.2           | 11             | 2.7                                |
| LM9t175        | 97                             | -           | 8.3           | 28             | 3.1                                |

(b) Modified Frequentist significances expected for the different SUSY benchmark points and different amounts of integrated luminosity.

| LM-Point | $10 \text{ pb}^{-1}$ | $40 \text{ pb}^{-1}$ | $100 \text{ pb}^{-1}$ | $1 \text{ fb}^{-1}$ |
|----------|----------------------|----------------------|-----------------------|---------------------|
| LM1      | 3.0                  | 5.5                  | 6.9                   | 9.8                 |
| LM2      | 1.4                  | 2.4                  | 3.0                   | 4.0                 |
| LM4      | 2.3                  | 4.4                  | 5.1                   | 6.8                 |
| LM5      | 1.4                  | 2.3                  | 2.9                   | 3.7                 |
| LM6      | 1.6                  | 2.6                  | 3.3                   | 4.2                 |
| LM8      | 2.4                  | 4.6                  | 5.5                   | 7.4                 |
| LM9      | 1.1                  | 1.9                  | 2.5                   | 3.2                 |
| LM10     | 0.03                 | 0.07                 | 0.1                   | 0.13                |
| LM9p     | 0.9                  | 1.6                  | 2.1                   | 2.7                 |
| LM9t175  | 1.1                  | 2.0                  | 2.5                   | 3.1                 |

**Table C.3:** *Trained on LM4*

(a) Numbers of selected events for backgrounds and signals; scaled to an integrated luminosity of  $1 \text{ fb}^{-1}$ .

| Sample         | # Events @ $1 \text{ fb}^{-1}$ |             | $\sigma_{MC}$ | $\sigma_{sys}$ | Significance @ $1 \text{ fb}^{-1}$ |
|----------------|--------------------------------|-------------|---------------|----------------|------------------------------------|
|                |                                | upper limit |               |                |                                    |
| W+jets         | 2.9                            | 3.3         | 1.7           | 0.83           | -                                  |
| Z+jets         | 0.031                          | 1.7         | 1.5           | 0.42           | -                                  |
| $t\bar{t}$     | 24                             | 24          | 3.9           | 7.7            | -                                  |
| Diboson        | 0.0                            | 0.43        | 0.23          | 0.13           | -                                  |
| Drell-Yan      | 0.001                          | 0.073       | 0.064         | 0.019          | -                                  |
| QCD            | 0.0                            | 15          | 8.9           | 3.6            | -                                  |
| Background sum | 27                             | 44          | 10            | 12             | -                                  |
| LM1            | 404                            | -           | 18            | 54             | 9.1                                |
| LM2            | 134                            | -           | 4.4           | 13             | 3.5                                |
| LM4            | 291                            | -           | 11            | 41             | 6.5                                |
| LM5            | 141                            | -           | 4.3           | 12             | 3.8                                |
| LM6            | 148                            | -           | 3.5           | 12             | 3.9                                |
| LM8            | 326                            | -           | 7.9           | 40             | 7.3                                |
| LM9            | 155                            | -           | 11            | 32             | 3.9                                |
| LM10           | 2.9                            | -           | 0.097         | 0.56           | 0.11                               |
| LM9p           | 108                            | -           | 4.9           | 16             | 3.0                                |
| LM9t175        | 144                            | -           | 10            | 29             | 3.7                                |

(b) Modified Frequentist significances expected for the different SUSY benchmark points and different amounts of integrated luminosity.

| LM-Point | $10 \text{ pb}^{-1}$ | $40 \text{ pb}^{-1}$ | $100 \text{ pb}^{-1}$ | $1 \text{ fb}^{-1}$ |
|----------|----------------------|----------------------|-----------------------|---------------------|
| LM1      | 3.1                  | 5.7                  | 7.5                   | 9.1                 |
| LM2      | 1.4                  | 2.3                  | 2.9                   | 3.5                 |
| LM4      | 2.5                  | 4.5                  | 5.3                   | 6.5                 |
| LM5      | 1.5                  | 2.4                  | 3.0                   | 3.8                 |
| LM6      | 1.5                  | 2.5                  | 3.1                   | 3.9                 |
| LM8      | 2.7                  | 4.8                  | 6.0                   | 7.3                 |
| LM9      | 1.6                  | 2.6                  | 3.2                   | 3.9                 |
| LM10     | 0.03                 | 0.07                 | 0.1                   | 0.11                |
| LM9p     | 1.1                  | 2.0                  | 2.4                   | 3.0                 |
| LM9t175  | 1.5                  | 2.4                  | 3.0                   | 3.7                 |

**Table C.4:** Trained on LM5

 (a) Numbers of selected events for backgrounds and signals; scaled to an integrated luminosity of  $1 \text{ fb}^{-1}$ .

| Sample         | # Events @ $1 \text{ fb}^{-1}$ |             | $\sigma_{MC}$ | $\sigma_{sys}$ | Significance @ $1 \text{ fb}^{-1}$ |
|----------------|--------------------------------|-------------|---------------|----------------|------------------------------------|
|                |                                | upper limit |               |                |                                    |
| W+jets         | 11                             | 11          | 3.9           | 2.7            | -                                  |
| Z+jets         | 0.084                          | 1.7         | 1.5           | 0.4            | -                                  |
| $t\bar{t}$     | 26                             | 26          | 4.1           | 6.7            | -                                  |
| Diboson        | 0.0                            | 0.43        | 0.23          | 0.27           | -                                  |
| Drell-Yan      | 0.001                          | 0.073       | 0.064         | 0.017          | -                                  |
| QCD            | 1.4                            | 14          | 8.9           | 3.5            | -                                  |
| Background sum | 39                             | 54          | 11            | 13             | -                                  |
| LM1            | 486                            | -           | 19            | 78             | 11                                 |
| LM2            | 164                            | -           | 4.9           | 19             | 4.4                                |
| LM4            | 355                            | -           | 12            | 51             | 8.7                                |
| LM5            | 179                            | -           | 4.9           | 17             | 4.7                                |
| LM6            | 200                            | -           | 4.1           | 18             | 5.2                                |
| LM8            | 401                            | -           | 8.8           | 58             | 8.9                                |
| LM9            | 155                            | -           | 11            | 36             | 4.2                                |
| LM10           | 4.4                            | -           | 0.12          | 0.71           | 0.17                               |
| LM9p           | 142                            | -           | 5.7           | 23             | 3.9                                |
| LM9t175        | 170                            | -           | 11            | 40             | 4.5                                |

(b) Modified Frequentist significances expected for the different SUSY benchmark points and different amounts of integrated luminosity.

| LM-Point | $10 \text{ pb}^{-1}$ | $40 \text{ pb}^{-1}$ | $100 \text{ pb}^{-1}$ | $1 \text{ fb}^{-1}$ |
|----------|----------------------|----------------------|-----------------------|---------------------|
| LM1      | 4.1                  | 6.4                  | 8.3                   | 11                  |
| LM2      | 1.5                  | 2.6                  | 3.3                   | 4.4                 |
| LM4      | 2.8                  | 5.2                  | 6.6                   | 8.7                 |
| LM5      | 1.6                  | 2.8                  | 4.1                   | 4.7                 |
| LM6      | 1.8                  | 3.0                  | 4.4                   | 5.2                 |
| LM8      | 3.0                  | 5.5                  | 7.2                   | 8.9                 |
| LM9      | 1.5                  | 2.5                  | 3.1                   | 4.2                 |
| LM10     | 0.04                 | 0.1                  | 0.13                  | 0.17                |
| LM9p     | 1.4                  | 2.3                  | 2.9                   | 3.9                 |
| LM9t175  | 1.5                  | 2.6                  | 3.9                   | 4.5                 |

**Table C.5:** *Trained on LM6*

(a) Numbers of selected events for backgrounds and signals; scaled to an integrated luminosity of  $1 \text{ fb}^{-1}$ .

| Sample         | # Events @ $1 \text{ fb}^{-1}$ |             | $\sigma_{MC}$ | $\sigma_{sys}$ | Significance @ $1 \text{ fb}^{-1}$ |
|----------------|--------------------------------|-------------|---------------|----------------|------------------------------------|
|                |                                | upper limit |               |                |                                    |
| W+jets         | 11                             | 12          | 3.6           | 3.5            | -                                  |
| Z+jets         | 0.061                          | 1.8         | 1.5           | 0.4            | -                                  |
| $t\bar{t}$     | 21                             | 21          | 3.7           | 3.4            | -                                  |
| Diboson        | 0.12                           | 0.42        | 0.23          | 0.19           | -                                  |
| Drell-Yan      | 0.0                            | 0.073       | 0.064         | 0.017          | -                                  |
| QCD            | 1.4                            | 14          | 8.9           | 3.3            | -                                  |
| Background sum | 35                             | 50          | 10            | 9.9            | -                                  |
| LM1            | 464                            | -           | 19            | 74             | 12                                 |
| LM2            | 158                            | -           | 4.8           | 19             | 5.0                                |
| LM4            | 324                            | -           | 12            | 51             | 9.2                                |
| LM5            | 170                            | -           | 4.8           | 19             | 5.2                                |
| LM6            | 205                            | -           | 4.1           | 21             | 6.2                                |
| LM8            | 339                            | -           | 8.1           | 52             | 9.5                                |
| LM9            | 126                            | -           | 9.5           | 30             | 4.1                                |
| LM10           | 4.1                            | -           | 0.12          | 0.7            | 0.18                               |
| LM9p           | 114                            | -           | 5.1           | 18             | 3.8                                |
| LM9t175        | 136                            | -           | 9.8           | 24             | 4.3                                |

(b) Modified Frequentist significances expected for the different SUSY benchmark points and different amounts of integrated luminosity.

| LM-Point | $10 \text{ pb}^{-1}$ | $40 \text{ pb}^{-1}$ | $100 \text{ pb}^{-1}$ | $1 \text{ fb}^{-1}$ |
|----------|----------------------|----------------------|-----------------------|---------------------|
| LM1      | 4.0                  | 6.6                  | 9.1                   | 12                  |
| LM2      | 1.5                  | 2.7                  | 4.0                   | 5.0                 |
| LM4      | 2.6                  | 5.1                  | 6.5                   | 9.2                 |
| LM5      | 1.6                  | 2.8                  | 4.2                   | 5.2                 |
| LM6      | 1.9                  | 3.2                  | 4.8                   | 6.2                 |
| LM8      | 2.8                  | 5.4                  | 6.7                   | 9.5                 |
| LM9      | 1.3                  | 2.2                  | 2.9                   | 4.1                 |
| LM10     | 0.06                 | 0.1                  | 0.13                  | 0.18                |
| LM9p     | 1.2                  | 2.1                  | 2.8                   | 3.8                 |
| LM9t175  | 1.4                  | 2.4                  | 3.1                   | 4.3                 |

**Table C.6:** *Trained on LM8*

(a) Numbers of selected events for backgrounds and signals; scaled to an integrated luminosity of  $1 \text{ fb}^{-1}$ .

| Sample         | # Events @ $1 \text{ fb}^{-1}$ |             | $\sigma_{MC}$ | $\sigma_{sys}$ | Significance @ $1 \text{ fb}^{-1}$ |
|----------------|--------------------------------|-------------|---------------|----------------|------------------------------------|
|                |                                | upper limit |               |                |                                    |
| W+jets         | 1.8                            | 4.3         | 2.1           | 1.4            | -                                  |
| Z+jets         | 0.0                            | 1.7         | 1.5           | 0.4            | -                                  |
| $t\bar{t}$     | 17                             | 17          | 3.2           | 6.9            | -                                  |
| Diboson        | 0.0                            | 0.43        | 0.23          | 0.093          | -                                  |
| Drell-Yan      | 0.0                            | 0.073       | 0.064         | 0.017          | -                                  |
| QCD            | 0.0                            | 15          | 8.9           | 3.4            | -                                  |
| Background sum | 19                             | 38          | 9.8           | 12             | -                                  |
| LM1            | 320                            | -           | 16            | 59             | 8.4                                |
| LM2            | 117                            | -           | 4.2           | 13             | 3.3                                |
| LM4            | 272                            | -           | 11            | 37             | 7.5                                |
| LM5            | 134                            | -           | 4.2           | 13             | 4.1                                |
| LM6            | 127                            | -           | 3.3           | 10.0           | 3.9                                |
| LM8            | 388                            | -           | 8.6           | 51             | 10                                 |
| LM9            | 178                            | -           | 11            | 37             | 5.0                                |
| LM10           | 3.6                            | -           | 0.11          | 0.63           | 0.17                               |
| LM9p           | 150                            | -           | 5.8           | 22             | 4.5                                |
| LM9t175        | 183                            | -           | 11            | 36             | 5.4                                |

(b) Modified Frequentist significances expected for the different SUSY benchmark points and different amounts of integrated luminosity.

| LM-Point | $10 \text{ pb}^{-1}$ | $40 \text{ pb}^{-1}$ | $100 \text{ pb}^{-1}$ | $1 \text{ fb}^{-1}$ |
|----------|----------------------|----------------------|-----------------------|---------------------|
| LM1      | 2.7                  | 5.0                  | 6.5                   | 8.4                 |
| LM2      | 1.3                  | 2.2                  | 2.8                   | 3.3                 |
| LM4      | 2.5                  | 4.6                  | 5.5                   | 7.5                 |
| LM5      | 1.5                  | 2.4                  | 3.1                   | 4.1                 |
| LM6      | 1.4                  | 2.3                  | 3.0                   | 3.9                 |
| LM8      | 3.1                  | 5.7                  | 7.5                   | 10                  |
| LM9      | 1.8                  | 2.9                  | 4.2                   | 5.0                 |
| LM10     | 0.03                 | 0.1                  | 0.11                  | 0.17                |
| LM9p     | 1.6                  | 2.6                  | 3.9                   | 4.5                 |
| LM9t175  | 1.8                  | 3.1                  | 4.3                   | 5.4                 |

**Table C.7: Trained on LM9**

(a) Numbers of selected events for backgrounds and signals; scaled to an integrated luminosity of  $1 \text{ fb}^{-1}$ .

| Sample         | # Events @ $1 \text{ fb}^{-1}$ |             | $\sigma_{MC}$ | $\sigma_{sys}$ | Significance @ $1 \text{ fb}^{-1}$ |
|----------------|--------------------------------|-------------|---------------|----------------|------------------------------------|
|                |                                | upper limit |               |                |                                    |
| W+jets         | 11                             | 12          | 4.1           | 2.9            | -                                  |
| Z+jets         | 1.3                            | 1.3         | 1.1           | 0.6            | -                                  |
| $t\bar{t}$     | 72                             | 72          | 6.7           | 24             | -                                  |
| Diboson        | 0.37                           | 0.66        | 0.29          | 0.13           | -                                  |
| Drell-Yan      | 0.0                            | 0.073       | 0.064         | 0.017          | -                                  |
| QCD            | 0.61                           | 15          | 8.9           | 3.5            | -                                  |
| Background sum | 85                             | 101         | 12            | 30             | -                                  |
| LM1            | 250                            | -           | 14            | 39             | 3.2                                |
| LM2            | 83                             | -           | 3.5           | 8.9            | 1.5                                |
| LM4            | 218                            | -           | 9.5           | 29             | 3.2                                |
| LM5            | 100                            | -           | 3.7           | 7.1            | 1.8                                |
| LM6            | 78                             | -           | 2.6           | 5.9            | 1.4                                |
| LM8            | 371                            | -           | 8.4           | 44             | 4.8                                |
| LM9            | 310                            | -           | 15            | 46             | 3.9                                |
| LM10           | 3.2                            | -           | 0.1           | 0.59           | 0.06                               |
| LM9p           | 201                            | -           | 6.8           | 28             | 3.0                                |
| LM9t175        | 296                            | -           | 14            | 48             | 3.9                                |

(b) Modified Frequentist significances expected for the different SUSY benchmark points and different amounts of integrated luminosity.

| LM-Point | $10 \text{ pb}^{-1}$ | $40 \text{ pb}^{-1}$ | $100 \text{ pb}^{-1}$ | $1 \text{ fb}^{-1}$ |
|----------|----------------------|----------------------|-----------------------|---------------------|
| LM1      | 1.7                  | 2.6                  | 3.0                   | 3.2                 |
| LM2      | 0.68                 | 1.1                  | 1.3                   | 1.5                 |
| LM4      | 1.5                  | 2.3                  | 2.7                   | 3.2                 |
| LM5      | 0.79                 | 1.2                  | 1.5                   | 1.8                 |
| LM6      | 0.65                 | 1.0                  | 1.2                   | 1.4                 |
| LM8      | 2.3                  | 4.0                  | 4.5                   | 4.8                 |
| LM9      | 2.0                  | 3.0                  | 3.9                   | 3.9                 |
| LM10     | 0.03                 | 0.03                 | 0.06                  | 0.06                |
| LM9p     | 1.4                  | 2.2                  | 2.6                   | 3.0                 |
| LM9t175  | 1.9                  | 2.9                  | 3.9                   | 3.9                 |

**Table C.8:** Trained on LM10

(a) Numbers of selected events for backgrounds and signals; scaled to an integrated luminosity of  $1 \text{ fb}^{-1}$ .

| Sample         | # Events @ $1 \text{ fb}^{-1}$ |             | $\sigma_{MC}$ | $\sigma_{sys}$ | Significance @ $1 \text{ fb}^{-1}$ |
|----------------|--------------------------------|-------------|---------------|----------------|------------------------------------|
|                |                                | upper limit |               |                |                                    |
| W+jets         | 3.8                            | 4.4         | 1.6           | 2.2            | -                                  |
| Z+jets         | 0.31                           | 2.0         | 1.5           | 0.5            | -                                  |
| $t\bar{t}$     | 13                             | 13          | 2.7           | 3.8            | -                                  |
| Diboson        | 0.0                            | 0.43        | 0.23          | 0.093          | -                                  |
| Drell-Yan      | 0.003                          | 0.072       | 0.064         | 0.017          | -                                  |
| QCD            | 0.0                            | 15          | 8.9           | 3.4            | -                                  |
| Background sum | 17                             | 34          | 9.6           | 9.6            | -                                  |
| LM1            | 202                            | -           | 12            | 41             | 6.0                                |
| LM2            | 79                             | -           | 3.4           | 14             | 2.8                                |
| LM4            | 159                            | -           | 8.1           | 36             | 4.9                                |
| LM5            | 102                            | -           | 3.7           | 16             | 3.4                                |
| LM6            | 101                            | -           | 2.9           | 15             | 3.3                                |
| LM8            | 274                            | -           | 7.3           | 59             | 7.9                                |
| LM9            | 117                            | -           | 9.2           | 32             | 3.9                                |
| LM10           | 5.7                            | -           | 0.14          | 0.86           | 0.28                               |
| LM9p           | 139                            | -           | 5.6           | 25             | 4.3                                |
| LM9t175        | 129                            | -           | 9.5           | 39             | 4.4                                |

(b) Modified Frequentist significances expected for the different SUSY benchmark points and different amounts of integrated luminosity.

| LM-Point | $10 \text{ pb}^{-1}$ | $40 \text{ pb}^{-1}$ | $100 \text{ pb}^{-1}$ | $1 \text{ fb}^{-1}$ |
|----------|----------------------|----------------------|-----------------------|---------------------|
| LM1      | 2.0                  | 3.2                  | 4.6                   | 6.0                 |
| LM2      | 0.9                  | 1.7                  | 2.1                   | 2.8                 |
| LM4      | 1.7                  | 2.8                  | 4.1                   | 4.9                 |
| LM5      | 1.1                  | 2.1                  | 2.6                   | 3.4                 |
| LM6      | 1.1                  | 2.1                  | 2.6                   | 3.3                 |
| LM8      | 2.5                  | 4.8                  | 5.9                   | 7.9                 |
| LM9      | 1.3                  | 2.3                  | 2.9                   | 3.9                 |
| LM10     | 0.07                 | 0.17                 | 0.21                  | 0.28                |
| LM9p     | 1.6                  | 2.6                  | 3.3                   | 4.3                 |
| LM9t175  | 1.4                  | 2.4                  | 3.1                   | 4.4                 |



**Table C.9:** *Trained on LM9p*

(a) Numbers of selected events for backgrounds and signals; scaled to an integrated luminosity of  $1 \text{ fb}^{-1}$ .

| Sample         | # Events @ $1 \text{ fb}^{-1}$ |             | $\sigma_{MC}$ | $\sigma_{sys}$ | Significance @ $1 \text{ fb}^{-1}$ |
|----------------|--------------------------------|-------------|---------------|----------------|------------------------------------|
|                |                                | upper limit |               |                |                                    |
| W+jets         | 0.51                           | 3.3         | 2.0           | 0.89           | -                                  |
| Z+jets         | 0.06                           | 1.8         | 1.5           | 0.42           | -                                  |
| $t\bar{t}$     | 13                             | 13          | 2.6           | 6.4            | -                                  |
| Diboson        | 0.0                            | 0.43        | 0.23          | 0.093          | -                                  |
| Drell-Yan      | 0.0                            | 0.073       | 0.064         | 0.017          | -                                  |
| QCD            | 0.61                           | 15          | 8.9           | 4.0            | -                                  |
| Background sum | 14                             | 33          | 9.7           | 11             | -                                  |
| LM1            | 101                            | -           | 8.8           | 16             | 3.1                                |
| LM2            | 38                             | -           | 2.4           | 4.8            | 1.5                                |
| LM4            | 111                            | -           | 6.8           | 19             | 3.3                                |
| LM5            | 57                             | -           | 2.8           | 6.5            | 2.1                                |
| LM6            | 41                             | -           | 1.8           | 4.2            | 1.6                                |
| LM8            | 216                            | -           | 6.4           | 34             | 5.5                                |
| LM9            | 130                            | -           | 9.7           | 28             | 3.7                                |
| LM10           | 2.8                            | -           | 0.096         | 0.55           | 0.13                               |
| LM9p           | 115                            | -           | 5.1           | 19             | 3.4                                |
| LM9t175        | 136                            | -           | 9.8           | 27             | 3.8                                |

(b) Modified Frequentist significances expected for the different SUSY benchmark points and different amounts of integrated luminosity.

| LM-Point | $10 \text{ pb}^{-1}$ | $40 \text{ pb}^{-1}$ | $100 \text{ pb}^{-1}$ | $1 \text{ fb}^{-1}$ |
|----------|----------------------|----------------------|-----------------------|---------------------|
| LM1      | 1.1                  | 2.0                  | 2.5                   | 3.1                 |
| LM2      | 0.6                  | 0.9                  | 1.2                   | 1.5                 |
| LM4      | 1.2                  | 2.1                  | 2.7                   | 3.3                 |
| LM5      | 0.75                 | 1.3                  | 1.6                   | 2.1                 |
| LM6      | 0.6                  | 1.0                  | 1.2                   | 1.6                 |
| LM8      | 2.1                  | 4.0                  | 4.7                   | 5.5                 |
| LM9      | 1.4                  | 2.4                  | 2.9                   | 3.7                 |
| LM10     | 0.03                 | 0.07                 | 0.1                   | 0.13                |
| LM9p     | 1.3                  | 2.2                  | 2.7                   | 3.4                 |
| LM9t175  | 1.5                  | 2.5                  | 3.0                   | 3.8                 |

**Table C.10:** Trained on LM9t175

 (a) Numbers of selected events for backgrounds and signals; scaled to an integrated luminosity of  $1 \text{ fb}^{-1}$ .

| Sample         | # Events @ $1 \text{ fb}^{-1}$ |             | $\sigma_{MC}$ | $\sigma_{sys}$ | Significance @ $1 \text{ fb}^{-1}$ |
|----------------|--------------------------------|-------------|---------------|----------------|------------------------------------|
|                |                                | upper limit |               |                |                                    |
| W+jets         | 2.5                            | 3.1         | 1.6           | 0.85           | -                                  |
| Z+jets         | 0.09                           | 1.8         | 1.5           | 0.5            | -                                  |
| $t\bar{t}$     | 38                             | 38          | 4.9           | 14             | -                                  |
| Diboson        | 0.0                            | 0.43        | 0.23          | 0.093          | -                                  |
| Drell-Yan      | 0.0                            | 0.073       | 0.064         | 0.017          | -                                  |
| QCD            | 0.0                            | 15          | 8.9           | 3.4            | -                                  |
| Background sum | 41                             | 58          | 10            | 18             | -                                  |
| LM1            | 139                            | -           | 10            | 20             | 3.1                                |
| LM2            | 44                             | -           | 2.5           | 4.4            | 1.2                                |
| LM4            | 103                            | -           | 6.5           | 20             | 2.4                                |
| LM5            | 53                             | -           | 2.7           | 5.3            | 1.4                                |
| LM6            | 41                             | -           | 1.8           | 3.0            | 1.2                                |
| LM8            | 215                            | -           | 6.4           | 24             | 4.4                                |
| LM9            | 181                            | -           | 11            | 36             | 3.6                                |
| LM10           | 2.0                            | -           | 0.081         | 0.47           | 0.06                               |
| LM9p           | 120                            | -           | 5.2           | 16             | 2.8                                |
| LM9t175        | 167                            | -           | 11            | 24             | 3.5                                |

(b) Modified Frequentist significances expected for the different SUSY benchmark points and different amounts of integrated luminosity.

| LM-Point | $10 \text{ pb}^{-1}$ | $40 \text{ pb}^{-1}$ | $100 \text{ pb}^{-1}$ | $1 \text{ fb}^{-1}$ |
|----------|----------------------|----------------------|-----------------------|---------------------|
| LM1      | 1.3                  | 2.1                  | 2.5                   | 3.1                 |
| LM2      | 0.47                 | 0.8                  | 1.0                   | 1.2                 |
| LM4      | 1.0                  | 1.6                  | 2.0                   | 2.4                 |
| LM5      | 0.54                 | 0.95                 | 1.2                   | 1.4                 |
| LM6      | 0.44                 | 0.76                 | 0.96                  | 1.2                 |
| LM8      | 1.8                  | 2.9                  | 3.9                   | 4.4                 |
| LM9      | 1.6                  | 2.5                  | 3.1                   | 3.6                 |
| LM10     | 0.01                 | 0.04                 | 0.06                  | 0.06                |
| LM9p     | 1.1                  | 1.9                  | 2.3                   | 2.8                 |
| LM9t175  | 1.5                  | 2.4                  | 3.0                   | 3.5                 |

## Appendix D

### Parameters of low mass benchmark points

| LM Point            | LM1 | LM2 | LM4 | LM5 | LM6 | LM8  | LM9  | LM10 | LM9p | LM9t175 |
|---------------------|-----|-----|-----|-----|-----|------|------|------|------|---------|
| $m_0$               | 60  | 185 | 210 | 230 | 85  | 500  | 1450 | 3000 | 1450 | 1450    |
| $m_{1/2}$           | 250 | 350 | 285 | 360 | 400 | 300  | 175  | 500  | 230  | 175     |
| $\tan(\beta)$       | 10  | 35  | 10  | 10  | 10  | 10   | 50   | 10   | 50   | 50      |
| $\text{sign}(\mu)$  | 1   | 1   | 1   | 1   | 1   | 1    | 1    | 1    | 1    | 1       |
| $A_0$               | 0   | 0   | 0   | 0   | 0   | -300 | 0    | 0    | 0    | 0       |
| $\sigma_{LO}$ (pb)  | 46  | 7.8 | 21  | 6.4 | 4.3 | 9.4  | 32   | 0.16 | 10   | 31      |
| $\sigma_{NLO}$ (pb) | 61  | 11  | 28  | 8.7 | 5.7 | 13   | 52   | 0.23 | 16   | 51      |
| h                   | 109 | 113 | 110 | 112 | 113 | 113  | 114  | 119  | 114  | 115     |
| H                   | 372 | 434 | 466 | 567 | 579 | 689  | 488  | 2999 | 534  | 616     |
| A                   | 372 | 434 | 466 | 567 | 579 | 689  | 488  | 2999 | 534  | 616     |
| $H^\pm$             | 381 | 442 | 473 | 573 | 585 | 694  | 495  | 3001 | 540  | 622     |
| $\tilde{d}_L$       | 560 | 777 | 660 | 807 | 857 | 817  | 1478 | 3119 | 1510 | 1478    |
| $\tilde{d}_R$       | 536 | 746 | 635 | 776 | 820 | 796  | 1477 | 3112 | 1506 | 1477    |
| $\tilde{u}_L$       | 552 | 770 | 653 | 800 | 850 | 811  | 1474 | 3111 | 1506 | 1475    |
| $\tilde{u}_R$       | 540 | 752 | 640 | 782 | 828 | 800  | 1477 | 3114 | 1507 | 1477    |
| $\tilde{s}_L$       | 560 | 777 | 660 | 807 | 857 | 817  | 1478 | 3119 | 1510 | 1478    |
| $\tilde{s}_R$       | 536 | 746 | 635 | 776 | 820 | 796  | 1477 | 3112 | 1506 | 1477    |
| $\tilde{c}_L$       | 552 | 770 | 653 | 800 | 850 | 811  | 1474 | 3111 | 1506 | 1475    |
| $\tilde{c}_R$       | 540 | 752 | 640 | 782 | 828 | 800  | 1477 | 3114 | 1507 | 1477    |
| $\tilde{b}_1$       | 510 | 671 | 598 | 734 | 785 | 710  | 1008 | 2577 | 1052 | 1009    |
| $\tilde{b}_2$       | 536 | 724 | 632 | 771 | 816 | 789  | 1124 | 3087 | 1168 | 1148    |
| $\tilde{t}_1$       | 407 | 580 | 481 | 599 | 647 | 544  | 882  | 1918 | 918  | 859     |
| $\tilde{t}_2$       | 580 | 748 | 658 | 787 | 839 | 760  | 1024 | 2582 | 1070 | 1026    |
| $\tilde{e}_L$       | 186 | 304 | 289 | 338 | 287 | 539  | 1450 | 3009 | 1454 | 1451    |
| $\tilde{e}_R$       | 120 | 231 | 239 | 270 | 178 | 514  | 1450 | 3002 | 1451 | 1450    |
| $\tilde{\nu}_e$     | 167 | 292 | 276 | 327 | 275 | 533  | 1447 | 3006 | 1451 | 1447    |
| $\tilde{\mu}_L$     | 186 | 304 | 289 | 338 | 287 | 539  | 1450 | 3009 | 1454 | 1451    |
| $\tilde{\mu}_R$     | 120 | 231 | 239 | 270 | 178 | 514  | 1450 | 3002 | 1451 | 1450    |
| $\tilde{\nu}_\mu$   | 167 | 292 | 276 | 327 | 275 | 533  | 1447 | 3006 | 1451 | 1447    |
| $\tilde{\tau}_1$    | 111 | 156 | 233 | 264 | 171 | 506  | 1054 | 2978 | 1054 | 1055    |
| $\tilde{\tau}_2$    | 190 | 314 | 291 | 339 | 289 | 539  | 1267 | 2996 | 1270 | 1268    |
| $\tilde{\nu}_\tau$  | 167 | 279 | 275 | 326 | 274 | 530  | 1265 | 2994 | 1269 | 1266    |
| $\tilde{g}$         | 603 | 827 | 687 | 851 | 932 | 738  | 488  | 1260 | 618  | 488     |
| $\chi_1^0$          | 96  | 141 | 112 | 144 | 161 | 120  | 65   | 209  | 91   | 70      |
| $\chi_2^0$          | 178 | 264 | 208 | 271 | 303 | 228  | 110  | 359  | 159  | 133     |
| $\chi_3^0$          | 344 | 455 | 387 | 475 | 521 | 458  | 184  | 421  | 247  | 316     |
| $\chi_4^0$          | 363 | 468 | 405 | 490 | 535 | 470  | 225  | 481  | 281  | 328     |
| $\chi_{1\pm}$       | 179 | 267 | 210 | 273 | 305 | 230  | 107  | 360  | 158  | 134     |
| $\chi_{2\pm}$       | 360 | 465 | 402 | 487 | 531 | 467  | 223  | 479  | 279  | 328     |

**Table D.1:** Parameters, cross sections and sparticle masses of all used LM points. Mass spectra have been calculated by *SoftSusy*, cross sections by *Prospino2*. All masses and  $A_0$  in GeV.



# Appendix E

## Background samples

| Dataset | $p_T$ binning [GeV]        | LO Cross Section | # of Events |
|---------|----------------------------|------------------|-------------|
| W+0jets |                            | 51 nb            | 8.8M        |
| W+1jet  | $0 \leq p_T^W \leq 100$    | 10 nb            | 9.1M        |
|         | $100 \leq p_T^W \leq 300$  | 287 pb           | 247k        |
|         | $300 \leq p_T^W \leq 800$  | 3.3 pb           | 57k         |
|         | $800 \leq p_T^W \leq 1600$ | 17.8 fb          | 60k         |
| W+2jets | $0 \leq p_T^W \leq 100$    | 2.8 nb           | 2.4M        |
|         | $100 \leq p_T^W \leq 300$  | 252 pb           | 287k        |
|         | $300 \leq p_T^W \leq 800$  | 4.5 pb           | 25k         |
|         | $800 \leq p_T^W \leq 1600$ | 35 fb            | 54k         |
| W+3jets | $0 \leq p_T^W \leq 100$    | 659 pb           | 353k        |
|         | $100 \leq p_T^W \leq 300$  | 120 pb           | 118k        |
|         | $300 \leq p_T^W \leq 800$  | 3.4 pb           | 107k        |
|         | $800 \leq p_T^W \leq 1600$ | 34 fb            | 53k         |
| W+4jets | $0 \leq p_T^W \leq 100$    | 138 pb           | 126k        |
|         | $100 \leq p_T^W \leq 300$  | 42 pb            | 40k         |
|         | $300 \leq p_T^W \leq 800$  | 1.7 pb           | 29k         |
|         | $800 \leq p_T^W \leq 1600$ | 21 fb            | 55k         |
| W+5jets | $0 \leq p_T^W \leq 100$    | 84 pb            | 62k         |
|         | $100 \leq p_T^W \leq 300$  | 44 pb            | 44k         |
|         | $300 \leq p_T^W \leq 800$  | 3.4 pb           | 40k         |
|         | $800 \leq p_T^W \leq 1600$ | 66 fb            | 17k         |

**Table E.1:** *W boson standard model background datasets used in the analyses. Events and LO cross sections have been obtained with Alpgen; the NLO k-factor of 1.12 has been calculated with MCFM. The W+5jets samples are inclusive, containing also samples with more jets.*

| Dataset | $p_T$ binning [GeV]        | LO Cross Section | # of Events |
|---------|----------------------------|------------------|-------------|
| Z+0jets |                            | 5 nb             | 3.3M        |
| Z+1jet  | $0 \leq p_T^Z \leq 100$    | 1 nb             | 945k        |
|         | $100 \leq p_T^Z \leq 300$  | 34 pb            | 36k         |
|         | $300 \leq p_T^Z \leq 800$  | 403 fb           | 30k         |
|         | $800 \leq p_T^Z \leq 1600$ | 2.2 fb           | 13k         |
| Z+2jets | $0 \leq p_T^Z \leq 100$    | 302 pb           | 289k        |
|         | $100 \leq p_T^Z \leq 300$  | 32 pb            | 35k         |
|         | $300 \leq p_T^Z \leq 800$  | 616 fb           | 29k         |
|         | $800 \leq p_T^Z \leq 1600$ | 4.5 fb           | 22k         |
| Z+3jets | $0 \leq p_T^Z \leq 100$    | 77 pb            | 73k         |
|         | $100 \leq p_T^Z \leq 300$  | 14 pb            | 24k         |
|         | $300 \leq p_T^Z \leq 800$  | 448 fb           | 28k         |
|         | $800 \leq p_T^Z \leq 1600$ | 4.3 fb           | 16k         |
| Z+4jets | $0 \leq p_T^Z \leq 100$    | 15 pb            | 33k         |
|         | $100 \leq p_T^Z \leq 300$  | 4.7 pb           | 7k          |
|         | $300 \leq p_T^Z \leq 800$  | 224 fb           | 25k         |
|         | $800 \leq p_T^Z \leq 1600$ | 2.8 fb           | 12k         |
| Z+5jets | $0 \leq p_T^Z \leq 100$    | 9.7 pb           | 12k         |
|         | $100 \leq p_T^Z \leq 300$  | 5.7 pb           | 6k          |
|         | $300 \leq p_T^Z \leq 800$  | 504 fb           | 25k         |
|         | $800 \leq p_T^Z \leq 1600$ | 8.3 fb           | 37k         |

**Table E.2:**  $Z$  boson standard model background datasets used in the analyses. Events and LO cross sections have been obtained with Alpgen; the NLO  $k$ -factor of 1.12 has been calculated with MCFM. The Z+5jets samples are inclusive, containing also samples with more jets.

| Dataset           | LO Cross Section | # of Events |
|-------------------|------------------|-------------|
| $t\bar{t}$ +0jets | 619 pb           | 1.5M        |
| $t\bar{t}$ +1jet  | 176 pb           | 362k        |
| $t\bar{t}$ +2jets | 34 pb            | 81k         |
| $t\bar{t}$ +3jets | 5.9 pb           | 14k         |
| $t\bar{t}$ +4jets | 1.5 pb           | 5.3k        |

**Table E.3:**  $t\bar{t}$  standard model background datasets used in the analyses. Events and LO cross sections have been obtained with Alpgen; the NLO  $k$ -factor equals 1.85. The  $t\bar{t}$ +5jets sample is inclusive, containing also samples with more jets.

| Dataset | LO Cross Section | # of Events |
|---------|------------------|-------------|
| WW      | 70 pb            | 850k        |
| WZ      | 27 pb            | 360k        |
| ZZ      | 11 pb            | 140k        |

**Table E.4:** Di-boson standard model background datasets used in the analyses. Events and LO cross sections have been obtained with Phytia; No NLO  $k$ -factor is used for this background.

| Dataset                       | Mass binning [GeV]                 | LO Cross Section | # of Events |
|-------------------------------|------------------------------------|------------------|-------------|
| DrellYan $\rightarrow \mu\mu$ | $200 \leq m_{Z/\gamma} \leq 500$   | 1.7 pb           | 42k         |
|                               | $500 \leq m_{Z/\gamma} \leq 1000$  | 86 fb            | 42k         |
|                               | $1000 \leq m_{Z/\gamma} \leq 1500$ | 7.5 fb           | 13k         |
|                               | $1500 \leq m_{Z/\gamma}$           | 1.2 fb           | 14k         |

**Table E.5:** *Drell-Yan to muon pairs standard model background datasets used in the analyses. Events and LO cross sections obtained with Pythia; No NLO k-factor is used for this background.*

| Dataset | $\hat{p}_T$ binning [GeV]       | LO Cross Section | # of Events |
|---------|---------------------------------|------------------|-------------|
| QCD     | $0 \leq \hat{p}_T \leq 15$      | 53 mb            | 14M         |
| QCD     | $15 \leq \hat{p}_T \leq 20$     | 1.5 mb           | 1.7M        |
| QCD     | $20 \leq \hat{p}_T \leq 30$     | 630 $\mu$ b      | 2.7M        |
| QCD     | $30 \leq \hat{p}_T \leq 50$     | 163 $\mu$ b      | 2.5M        |
| QCD     | $50 \leq \hat{p}_T \leq 80$     | 22 $\mu$ b       | 2.5M        |
| QCD     | $80 \leq \hat{p}_T \leq 120$    | 3.1 $\mu$ b      | 1.2M        |
| QCD     | $120 \leq \hat{p}_T \leq 170$   | 494 nb           | 1.3M        |
| QCD     | $170 \leq \hat{p}_T \leq 230$   | 101 nb           | 1.2M        |
| QCD     | $230 \leq \hat{p}_T \leq 300$   | 25 nb            | 1.2M        |
| QCD     | $300 \leq \hat{p}_T \leq 380$   | 6.2 nb           | 1.2M        |
| QCD     | $380 \leq \hat{p}_T \leq 470$   | 1.8 nb           | 1.2M        |
| QCD     | $470 \leq \hat{p}_T \leq 600$   | 683 pb           | 1.2M        |
| QCD     | $600 \leq \hat{p}_T \leq 800$   | 204 pb           | 500k        |
| QCD     | $800 \leq \hat{p}_T \leq 1000$  | 35 pb            | 100k        |
| QCD     | $1000 \leq \hat{p}_T \leq 1400$ | 11 pb            | 30k         |
| QCD     | $1400 \leq \hat{p}_T \leq 1800$ | 1.6 pb           | 30k         |
| QCD     | $1800 \leq \hat{p}_T \leq 2200$ | 145 fb           | 20k         |
| QCD     | $2200 \leq \hat{p}_T \leq 2600$ | 24 fb            | 10k         |
| QCD     | $2600 \leq \hat{p}_T \leq 3000$ | 4.3 fb           | 10k         |
| QCD     | $3000 \leq \hat{p}_T \leq 3500$ | 0.84 fb          | 10k         |
| QCD     | $3500 \leq \hat{p}_T$           | 0.11 fb          | 10k         |

**Table E.6:** *QCD multijet standard model background datasets used in the analyses. Events and LO cross sections have been obtained with Pythia; No NLO k-factor is used for this background.*





## Bibliography

- [1] S. Weinberg. A Model of Leptons. *Phys. Rev. Lett.* *19*, 1264, 1967. [http://prola.aps.org/abstract/PRL/v19/i21/p1264\\_1](http://prola.aps.org/abstract/PRL/v19/i21/p1264_1).
- [2] S.L. Glashow, J. Iliopoulos, and L. Maiani. Weak Interactions with Lepton-Hadron Symmetry. *Phys. Rev. D* *2*, 1285, 1970. [http://prola.aps.org/abstract/PRD/v2/i7/p1285\\_1](http://prola.aps.org/abstract/PRD/v2/i7/p1285_1).
- [3] A. Salam and J.C. Ward. Gauge Theory of Elementary Interactions. *Phys. Rev.* *136*, B763, 1964. [http://prola.aps.org/abstract/PR/v136/i3B/pB763\\_1](http://prola.aps.org/abstract/PR/v136/i3B/pB763_1).
- [4] F. Halzen and A.D. Martin. *Quarks and Leptons: An introduction course in modern particle physics*. John Wiley & Sons, 1984. ISBN 0-471-88741-2.
- [5] S.L. Wu. e+e- physics at petra—the first five years. *Phys. Rep.* *107*, 2-5, 59, 1984. [http://dx.doi.org/10.1016/0370-1573\(84\)90033-4](http://dx.doi.org/10.1016/0370-1573(84)90033-4).
- [6] LEP working group for Higgs boson searches. Search for the Standard Model Higgs Boson at LEP. <http://arxiv.org/abs/hep-ex/0107029>, 2001.
- [7] D. Charlton. Experimental Tests of the Standard Model. <http://arxiv.org/abs/hep-ex/0110086>, 2001.
- [8] F. Zwicky. On the Masses of Nebulae and of Clusters of Nebulae. *ApJ*, *86*, 217, 1937. <http://dx.doi.org/10.1086/143864>.
- [9] B.W. Lee, C. Quigg, and H.B. Thacker. Weak interactions at very high energies: The role of the Higgs-boson mass. *Phys. Rev. D* *16*, 1519, 1977. <http://link.aps.org/abstract/PRD/v16/p1519>.
- [10] P. Binétruy. *Supersymmetry*. Oxford Graduate Texts, 2006. ISBN 0-19-850954-5.
- [11] G. Hinshaw et.al. Five-Year Wilkinson Microwave Anisotropy Probe (WMAP) Observations: Data Processing, Sky Maps, and Basic Results. *The Astrophysical Journal Supplement Series*, 2008. <http://arxiv.org/abs/0803.0732>.
- [12] W. de Boer. Comparison of grand unified theories with electroweak and strong coupling constants measured at LEP. *Phys. Lett. B*, *260*, 3-4, 447, 1991. [http://dx.doi.org/10.1016/0370-2693\(91\)91641-8](http://dx.doi.org/10.1016/0370-2693(91)91641-8).
- [13] J. Wess and B. Zumino. Supergauge transformations in four dimensions. *Nucl. Phys. B* *70*, 39, 1974. [http://dx.doi.org/10.1016/0550-3213\(74\)90355-1](http://dx.doi.org/10.1016/0550-3213(74)90355-1).
- [14] R. Haag, J.T. Lopuszanski, and M. Sohnius. All possible generators of supersymmetries of the S-matrix. *Nucl. Phys. B* *88*, 257, 1975. [http://dx.doi.org/10.1016/0550-3213\(75\)90279-5](http://dx.doi.org/10.1016/0550-3213(75)90279-5).
- [15] S. Coleman and J. Mandula. All Possible Symmetries of the S Matrix. *Phys. Rev.* *159*, 1251, 1967. [http://prola.aps.org/pdf/PR/v159/i5/p1251\\_1](http://prola.aps.org/pdf/PR/v159/i5/p1251_1).

- [16] T. Hebbeker. Can the sneutrino be the lightest super-symmetric particle? *Phys. Lett. B* 470, 259, 1999. [http://dx.doi.org/10.1016/S0370-2693\(99\)01313-1](http://dx.doi.org/10.1016/S0370-2693(99)01313-1).
- [17] S.P. Martin. A Supersymmetry Primer. <http://arxiv.org/abs/hep-ph/9709356>, 2006.
- [18] CMS Collaboration. CMS Physics Technical Design Report, Volume II: Physics Performance. *J. Phys. G* 34, 995, 2007. <http://dx.doi.org/10.1088/0954-3899/34/6/S01>.
- [19] <http://www.phys.ufl.edu/~jblender/isajet/isajet.html>.
- [20] <http://lepsusy.web.cern.ch/lepsusy/>.
- [21] <http://www-bdnew.fnal.gov/tevatron/>.
- [22] D0 Collaboration. Search for squarks and gluinos in events with jets and missing transverse energy using 2.1 fb<sup>-1</sup> of ppbar collision data at sqrt(s)=1.96 TeV. <http://arxiv.org/abs/0712.3805v2>, 2008.
- [23] The CDF Collaboration. Unified Search for Associated Production of Chargino-Neutralino using Leptons. [http://www-cdf.fnal.gov/physics/exotic/r2a/20080110.trilepton\\_dube/](http://www-cdf.fnal.gov/physics/exotic/r2a/20080110.trilepton_dube/), 2008.
- [24] D. Acosta et al. Potential to Discover Supersymmetry in Events with Muons, Jets and Missing Energy in pp Collisions at  $\sqrt{s} = 14$  TeV with the CMS Detector. CMS NOTE-2006/134, 2006.
- [25] <http://puhep1.princeton.edu/mumu/physics/>.
- [26] [http://cmsinfo.cern.ch/outreach/CMSdocuments/JimGIF/GIFVirdee1\\_index.html](http://cmsinfo.cern.ch/outreach/CMSdocuments/JimGIF/GIFVirdee1_index.html).
- [27] LHC Design Report, Volume 1. <http://doc.cern.ch/cernrep/2004/2004-003-v1/2004-003-v1.html>.
- [28] LHC Design Report, Volume 2. <http://doc.cern.ch/cernrep/2004/2004-003-v2/2004-003-v2.html>.
- [29] LHC Design Report, Volume 3. <http://doc.cern.ch/cernrep/2004/2004-003-v3/2004-003-v3.html>.
- [30] M. Pimiä et al. Compact muon solenoid. In D. Rein G. Jarlskog, editor, *Proc. ECFA Large Hadron Collider Workshop*, volume III, page 547, 1990. [http://doc.cern.ch/cernrep/1990/90-10/90-10\\_v3.html](http://doc.cern.ch/cernrep/1990/90-10/90-10_v3.html).
- [31] <http://fsp102-cms.de/>.
- [32] CMS collaboration. The CMS experiment at the CERN LHC. <http://dx.doi.org/10.1088/1748-0221/3/08/S08004>, 2008.
- [33] CMS collaboration. The Tracker Project - Technical Design Report. CERN/LHCC 98-6 - [http://cmsdoc.cern.ch/cms/TDR/TRACKER/tracker\\_tdr\\_files.html](http://cmsdoc.cern.ch/cms/TDR/TRACKER/tracker_tdr_files.html), 1998.
- [34] <http://abbaneo.web.cern.ch/abbaneo/cms/layout/whole.html>.

- 
- [35] CMS collaboration. The Electromagnetic Calorimeter - Technical Design Report. CERN/LHCC 97-33 - <http://cmsdoc.cern.ch/cms/TDR/ECAL/ecal.html>, 1997.
- [36] CMS collaboration. The Muon Project - Technical Design Report. CERN/LHCC 97-32 - <http://cmsdoc.cern.ch/cms/TDR/MUON/muon.html>, 1997.
- [37] CMS collaboration. The Hadron Calorimeter Project - Technical Design Report. CERN/LHCC 97-31 - <http://cmsdoc.cern.ch/cms/TDR/HCAL/hcal.html>, 1997.
- [38] Private communications with Hans Reithler.
- [39] CMS Collaboration. CMS Physics Technical Design Report, Volume I: Detector performance and software. <http://cdsweb.cern.ch/record/922757>, 2006.
- [40] <http://totem.web.cern.ch/Totem/>.
- [41] R. Frühwirth. Application of Kalman filtering to track and vertex fitting. *Nucl. Instrum. Meth. A* *262*, *444*, 1987. [http://dx.doi.org/10.1016/0168-9002\(87\)90887-4](http://dx.doi.org/10.1016/0168-9002(87)90887-4).
- [42] V. Innocente, M. Maire, and E. Nagy. GEANE: Average tracking and error propagation package. *Procs. MC91* *58*, 1991. <http://usparc.ihep.su/spires/find/hep/www?key=2767481>.
- [43] M. Spira, A. Djouadi, M. Muhlleitner. Decays of Supersymmetric Particles: the program SUSY-HIT. <http://arxiv.org/abs/hep-ph/0609292v1>, 2006.
- [44] B.C. Allanach. SOFTSUSY: a program for calculating supersymmetric spectra. *Comput.Phys.Commun.* *143*, *305*, 2002/2005. <http://arxiv.org/abs/hep-ph/0104145v12>.
- [45] M. Muhlleitner, A. Djouadi, and Y. Mambrini. SDECAY: a Fortran code for the decays of the supersymmetric particles in the MSSM. *Comput.Phys.Commun.* *168*, *46*, 2005. <http://arxiv.org/abs/hep-ph/0311167v1>.
- [46] A. Djouadi, J. Kalinowski, and M. Spira. HDECAY: a Program for Higgs Boson Decays in the Standard Model and its Supersymmetric Extension. *Comput.Phys.Commun.* *108*, *56*, 1998. <http://arxiv.org/abs/hep-ph/9704448v1>.
- [47] T. Sjostrand, S. Mrenna, and P. Skands. PYTHIA 6.4 Physics and Manual. <http://arxiv.org/abs/hep-ph/0603175v2> and <http://home.thep.lu.se/~torbjorn/Pythia.html>, 2006.
- [48] <http://www.ph.ed.ac.uk/~tplehn/prospino/>.
- [49] M. Mangano, M. Moretti, F. Piccinini, R. Pittau, and A. Polosa. ALPGEN, a generator for hard multiparton processes in hadronic collisions. *HEP* *0307*, *001*, 2003. <http://arxiv.org/abs/hep-ph/0206293v2>.
- [50] R. Bonciani, S. Catani, M. Mangano, and P. Nason. NLL resummation of the heavy-quark hadroproduction cross-section. *Nucl. Phys. B* *529*, *424*, 1998. [http://dx.doi.org/10.1016/S0550-3213\(98\)00335-6](http://dx.doi.org/10.1016/S0550-3213(98)00335-6).
- [51] <http://mcfm.fnal.gov/>.

- [52] <https://twiki.cern.ch/twiki/bin/view/CMS/AachenPdfUncertainties>.
- [53] Jet Energy Scale subgroup. Plans for Jet Energy Corrections at CMS. CMS AN-2007/055, 2007.
- [54] T. Junk. Confidence level computation for combining searches with small statistics. *Nucl. Instrum. Meth. A* 434, 435, 1999. <http://arxiv.org/abs/hep-ex/9902006>.
- [55] A.L. Read. Presentation of search results: the  $CL_s$  technique. *J. Phys. G: Nucl. Part. Phys.* 28, 2693, 2002. <http://dx.doi.org/10.1088/0954-3899/28/10/313>.
- [56] D0 Collaboration. Evidence for production of single top quarks. <http://arxiv.org/abs/0803.0739v2>, 2008.
- [57] R. Brun and F. Rademakers. ROOT: An object oriented data analysis framework. *Nucl. Instrum. Meth. A* 389, 81, 1997. <http://root.cern.ch/>.
- [58] A. Hocker et al. TMVA: Toolkit for multivariate data analysis. <http://arxiv.org/abs/physics/0703039v4>. <http://tmva.sourceforge.net/>.
- [59] Y. Freund and R.E. Schapire. A Decision-Theoretic Generalization of On-Line Learning and an Application to Boosting. *J. o. Comp. a. Syst. Sci.* 55, 119, 1997. <http://dx.doi.org/10.1006/jcss.1997.1504>.

# Selbständigkeitserklärung

Hiermit erkläre ich, diese Arbeit selbständig und nur unter Verwendung der angegebenen Hilfsmittel erstellt zu haben.